UNIVERSITÀ DEGLI STUDI DI PADOVA

Dipartimento di Fisica e Astronomia "Galileo Galilei"

MASTER DEGREE IN ASTROPHYSICS AND COSMOLOGY

FINAL DISSERTATION

TESTING NEW IDEAS REGARDING THE NATURE OF INTERSTELLAR EXTINCTION

Thesis supervisor

Prof./Dr. Giovanni CARRARO

Candidate

Vittorio CIBODDO

Academic Year 2022-2023

Per aspera sic itur ad astra

Contents

Introduction

The main goal of this thesis is to investigate the nature of interstellar extinction, a well-known phenomenon in the diffuse interstellar medium (ISM).
In particular, a specific focus on its historical description and on its parametric modelling will be provided. An analysis of the theoretical structure of its properties is needed in order to understand its implication on a cosmic scale.
In the end, a harsh comparison among different models is described; several final suggestions about alternative theories on the nature of interstellar extinction itself are listed.

The present work is organized under the following structure:

- Chapter 1 provides historical background about how the universe was studied in past centuries and how the scientific community has been able to reach the present knowledge about interstellar extinction;
- Chapter 2 goes into the details about the widely accepted physical explanation concerning interstellar extinction (a particular focus on extinction curves is highlighted in sec. 2.3);
- Chapter 3 displays the most used theoretical models about interstellar extinction and its parametrization. An application of extinction curve analyses based on Python is presented, alongside a comparison among the previous papers in literature (subsec. 3.2.2 and subsec. 3.2.5);
- Chapter 4 completes the description of the features within interstellar extinction, describing the so-called **D**iffuse **I**nterstellar **B**and**s** (**D**.**I**.**B**.**s**);
- Chapter 5 underlines all the critical issues concerning theoretical models in extinction and tries to provide an alternative view about how to overcome the aforementioned incongruencies;
- Chapter 6, finally, displays a summary of all the topics with some proposed suggestions about the nature of interstellar extinction.

Chapter 1

Historical background

The very first astronomical map (see fig. 1.1) about the distribution of stars in the Milky Way was provided by Herschel[1] in 1785 (see [Her85]).
The famous physicist and astronomer was able to perform such a measurement through the *star-gages* method (i.e. 'stellar counts' technique); this method was based on two fundamental assumptions:

1. Stars are distributed more or less uniformly within the Milky Way system and are not found beyond the boundaries[2] of that system;

2. The telescope[3] used for the *star-gages* can resolve all stars within the Milky Way system.

In this way, Herschel could perform the stellar counts of 683 regions in the sky, forming a circle running the galactic poles and crossing the plane of the Milky Way at right angles near the star Sirius (Alpha Canis Majoris) and again near the star Altair (Alpha Aquilae).
In regions where few stars were visible, an average regarding the number of stellar objects was computed over ten or more fields.

As one can see in fig. 1.1, the resulting cross-section of the Milky Way is roughly elliptical in shape, much more extended along the galactic plane (to the top and bottom in the figure) than toward the poles (the galactic North Pole is toward the left side of the map).
A great cleft in the system appears in the lower part, in the direction of the Aquila constellation, where a dark streak in the Milky Way is also visible to the naked eye: most likely, this is the so-called **Great Rift** (also known as **Dark Rift**), i.e. a famous dark band caused by interstellar clouds of cosmic dust that significantly obscure -or better, extinguish- the centre and most radial sectors of Milky Way from Earth's perspective.
In the neighbourhood of Aquila constellation, this structure is also known as **Aquila Rift**: we are dealing with a system of molecular clouds, which are a phase of the interstellar medium with enough high densities and enough low temperatures to allow the formation of molecules (e.g. molecular hydrogen H_2).

[1] Sir Frederick William Herschel (1738-1822), mostly known as the discoverer of the planet Uranus in 1781.

[2] Until the first decades of last century, the universe edges were thought to be coincident with Milky Way dimensions.

[3] We are dealing with a Newtonian reflector, with a focal length of 20 feet ($\sim$ 6 meters) and an aperture of 19 inches ($\sim$ 0.5 meters).

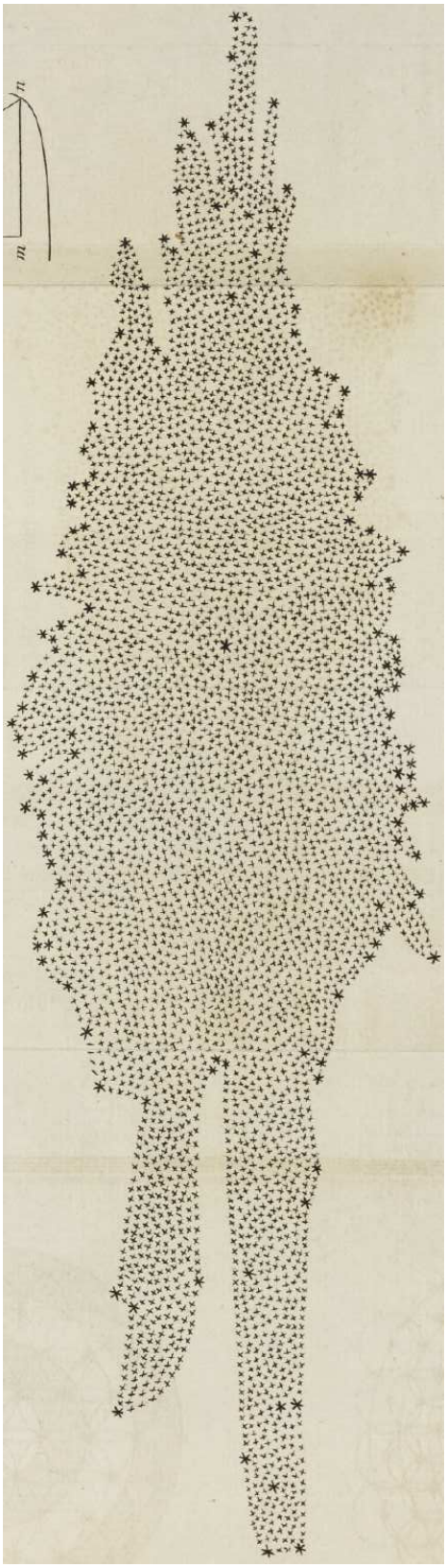

Figure 1.1: The so-called Herschel's map (here turned 90° counterclockwise). It is the very first mapping of stellar distribution in our Galaxy in astronomical history. The method used to achieve such a result is called *star-gages*, which nowadays we can refer to as 'star counts'. Sun's position is highlighted by the larger star in the interior of the map. Details in the text. Fig. from [Her85].

These clouds are opaque to light in the optical part of the spectrum due to the presence of interstellar dust grains mixed with the diffuse gaseous component.

It is worth noting that the latter considerations were inaccessible to Herschel, above all because of the lack of sufficiently sophisticated technological instruments and, as a consequence, of a theoretical base about physical processes.

Despite the map in fig. 1.1 being a remarkable result and having a profound historical meaning, a clearer picture of the physical features of our Galaxy would have been provided only at the beginning of the XX century.
The turning point, in this sense, can be summarised in the following question: is interstellar space completely transparent, or does light suffer an appreciable modification or loss of intensity when passing through the enormous spaces which separate us from the more remote celestial objects? Technically, any effect of this kind is referred to as *absorption of light in space*, whatever the peculiar physical process assumed for its cause. Several hypotheses have been proposed; the older view attributed such absorbing properties to the supposed existence of ether itself. At the beginning of 1900, thanks to the observational discovery of the diffuse interstellar gas by J. F. Hartmann (1904), astronomers started to hold the idea that interstellar medium was not an 'empty' system but composed by a `much rarefied invisible material medium and admit that the latter is not necessarily of uniform distribution throughout all space` ([Tru30]). According to prevailing physical theories at that time, light passing through such a material medium may be absorbed by free atoms or molecules; it may be scattered by free electrons, atoms, molecules or by solid particles of extremely small size; finally, it may be obstructed by larger bodies (e.g. meteorites). So, up until 1920s the observable phenomena useful in this discussion were:

1. *General absorption*, i.e. the loss of starlight on its passage from the star to the observer. In this case, the apparent brightness of a star will decrease more rapidly than a simple inverse square law with its distance ($I \propto r^{-2}$);

2. *Selective absorption*, i.e. the loss of starlight heavily depends on wavelength. In this case, any observational property of the star based on photometric assumptions will change with its distance from the observer;

3. *Monochromatic absorption*, i.e. interstellar absorption lines in stellar spectra. In this case, some absorption features may be produced not in the stellar atmosphere but by atoms contained in the space between the star and the observer;

4. *Obscuration effects*, i.e. the existence of **dark nebulae**. They are noticed either as well-defined nearly starless patches in the middle of rich Milky Way star fields, or as dark passages apparently projected on bright diffuse nebulae. In addition, there is the well-known fact that basically no globular clusters or spiral nebulae are visible near the galactic equator: this suggests the presence of an absorbing medium in our Milky Way system which is strongly concentrated to the galactic plane;

5. *Dispersion of light*, i.e. the velocity of light varies with the wavelength through a material medium. If an effect of this kind is present, the light variation of a distant eclipsing binary should not be observed simultaneously in all colours. This is called the Nordmann-Tikhoff phenomenon.

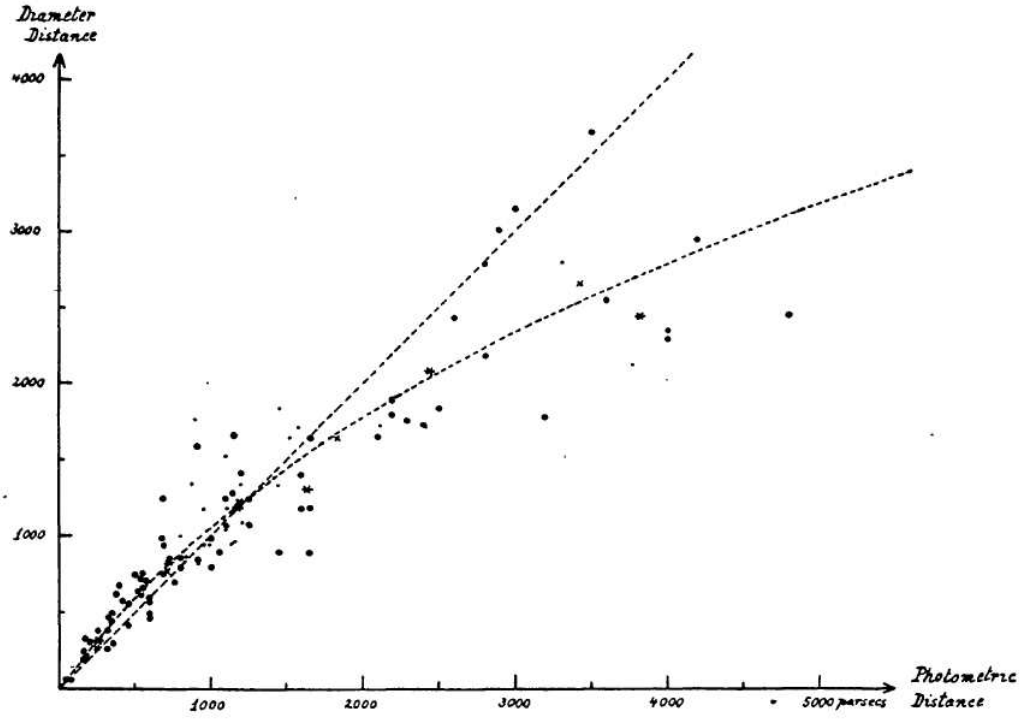

Figure 1.2: Comparison of the distances of 100 open star clusters determined from apparent magnitudes and spectral types (x-axis) with those determined from angular diameters (y-axis). The large dots refer to clusters with well-determined photometric distances, the small dots to clusters with less certain data.
The asterisks and crosses represent group means. If no general space absorption were present, the clusters should fall along the dotted straight line; the dotted curve gives the relation between the two distance measures for a general absorption of $0^m.7$ per 1 000 parsecs. Details in text. Fig. from [Tru30].

Thanks to the study of open star clusters, Trumpler (1930) could bring to light new results about the existence of a general and selective absorption due to a diffuse interstellar material. Fig. 1.2 shows the results of his work.

Some comments about the graphic.
So, if no absorption of light were present, the two distance scales should be in agreement, and the clusters should be scattered along the dotted straight line.
It is, however, evident that the clusters deviate systematically from this straight line. In particular, it can be noted that for the nearer (distant) clusters the diameter distances are larger (smaller) than the photometric distances. This discrepancy is not due to a systematic error in the estimates of angular diameters: in fact, it persists even if we select only clusters which are nearly of the same angular diameter but at different distances. Therefore, unless it can be admitted that the dimensions of open clusters depend on their distance from the Sun, the only acceptable physical explanation is that the inverse square law on which the photometric distances are based does not hold and that a general absorption is taking place within our stellar system. Assuming that this absorption is approximately uniform within the region occupied by these clusters, Trumpler found out its numerical value equal to $0^m.7$ per 1 000 parsecs. The relation between the diameter distances and the photometric distances which we should expect for an

absorption of this amount is represented by the dotted curve in fig. 1.2: it can be noted a better fit (better than the straight line). Comparing some other observational work of that time (Shapley, van Rhijn, Kapteyn), Trumpler classified this particular absorption feature with a *selective absorption* phenomenon.
From his original paper:

> The space absorption decreases rapidly with increasing wavelength, similar to the extinction in the Earth's atmosphere. This suggests its interpretation as Rayleigh scattering, i.e., scattering of light by particles which are small compared with the wavelength of light. According to Rayleigh such scattering is inversely proportional to the fourth power of the wave-length. This law, however, is not exactly fulfilled by our figures. If we determine its numerical coefficient so as to fit the selective absorption, which is the more accurate of the two, we have a small non-selective residual effect left which, if real, must be explained by other causes (electron scattering, obstruction by larger meteoric particles).

Moreover:

> [...] find that the average mass of the particles would have to be of the order of 2×10^{-19} grams (~ 3400 calcium atoms). Such extremely fine solid dust particles with a diameter of about one-hundredth of the wavelength of visual light would still be small enough to produce Rayleigh scattering. We see, thus, that our numerical results for the selective absorption cannot be traced to Rayleigh scattering by free atoms in interstellar space; they admit, however, interpretation as scattering by fine cosmic dust.

Nowadays it is known that interstellar dust is the main responsible for the interaction with starlight in the interstellar medium. The particular behaviour found out observationally by Trumpler in open star clusters can be explained by a combination of physical processes, overall known as **extinction**. Chapter 2 shows a detailed description of this subject, while section 2.5 will provide an insight into dust properties.

Chapter 2

Extinction

Extinction occurs when electromagnetic radiation passes through a medium containing small particles. In the case of the interstellar medium, this population is mainly constituted by dust grains and a diffuse gaseous component.

The fundamental interaction among these three agents is expressed by two physical processes: absorption and scattering. So, as first approach, extinction can be seen as the sum of the previous phenomena. It represents a powerful indirect method to infer some properties about stars and the interstellar medium itself all over the surroundings.

There are different techniques to take into account the extinction and to manage observational data in this sense; we can group them into two main categories:

- Theoretical method;
- Observational method.

In the following sections a complete description of both of them is provided.

2.1 Theoretical method

Let's consider a system with a population of spherical particles. In this framework, this is the abstraction of the interstellar medium with dust grains[1].
So let's consider dust grains as spheroids of average constant radius a and number density (per unit volume) n_d; let's evaluate the journey of a light beam through the settled medium.
This path can be visualized as a cylinder of length L and unit cross-sectional area (along the line of sight from a distant star, the source of the beam).
The interaction between the light and the population of spheroids produces extinction of light itself, so an observer along the line of sight will detect a decrease in light intensity I such as

$$\frac{dI}{I} = -n_d \, C_{ext} \, dL \tag{2.1}$$

where C_{ext} is *extinction coefficient*.

[1] That is just an idealization: considering dust grains as spheres do not take into account, for instance, polarization. However, this is a (mathematically) convenient starting point.

Integrating eq. (2.1) over the entire pathlength gives

$$I = I_0\, e^{-\tau} \tag{2.2}$$

where I_0 is the initial value of light intensity (computed at $L = 0$, so it is the intensity of the beam as emitted by the star without any "medium interference") and

$$\tau = \int n_d\, dL\, C_{ext} = N_d\, C_{ext} \tag{2.3}$$

is the *optical depth* of extinction caused by the dust.
Here another quantity has been introduced: N_d is the **column density** of the dust, i.e. the total number of dust grains in the unit column met by the beam along its path.
To express these considerations in astronomical units, it is useful to "convert" the intensity reduction due to extinction in magnitudes.
So a combination of eq. (2.2) and eq. (2.3) gives:

$$A_\lambda = -2.5\, log\left(\frac{I}{I_0}\right) = 1.086\, N_d\, C_{ext} \tag{2.4}$$

where A_λ is the total extinction coefficient at some wavelength λ.
More often A_λ is expressed in terms of the so-called **extinction effiency factor** $\boldsymbol{Q_{ext}}$, which is the ratio between the extinction cross-section and geometric cross-section:

$$Q_{ext} = \frac{C_{ext}}{\pi a^2} \tag{2.5}$$

Therefore eq. (2.4) can be written in the following form:

$$A_\lambda = 1.086\, N_d\, \pi\, a^2\, Q_{ext} \tag{2.6}$$

As mentioned before, considering dust grains as a population of spherical particles with average radius is an idealization; a more realistic situation is represented by a size distribution.

Let's evaluate extinction caused by a grain population where $n(a)\, da$ defines the number of grains per unit volume in the line of sight with radii in the range a to $a + da$. The previous equation can be replaced by:

$$A_\lambda = 1.086\, \pi\, L \int a^2\, Q_{ext}\,(a)\, n(a)\, da \tag{2.7}$$

The key point here is that the problem of evaluating A_λ, i.e. the expected spectral dependence in extinction, is reduced to compute Q_{ext}.
This is true if a composition and size distribution of grains is assumed *a priori*.

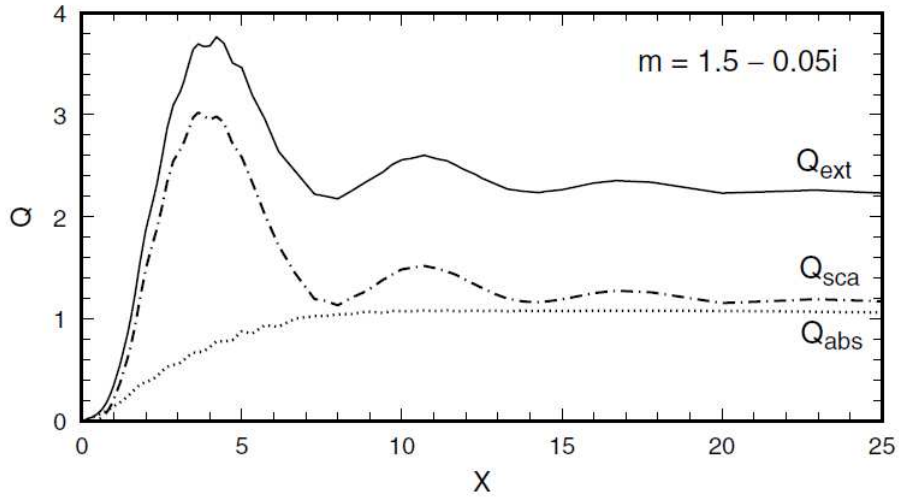

Figure 2.1: An example: results of Mie theory calculations for spherical grains of refractive index $m = 1.5 - 0.05i$. Fig. from [Whi18], pag. 69.

Modeling speaking, the extinction can be seen as the sum of absorption and scattering; using this simplified approach, we are allowed to write:

$$Q_{ext} = Q_{abs} + Q_{scat} \tag{2.8}$$

These efficiencies are functions of two quantities (see [Whi18], ch.3):

- A dimensionless size parameter:

$$X = \frac{2\pi a}{\lambda} \tag{2.9}$$

- A composition parameter, which depends on the complex refractive index of the grain material ([Dra10]):

$$m = n - ik \tag{2.10}$$

To clarify, Q_{abs} and Q_{scat} may be calculated for any assumed grain model and then the results be compared with observational data. The main effort here is to solve Maxwell's equations with appropriate boundary conditions at the grain surface. A solution was first formulated by Mie (1908) and later on by Debye (1909) in an independent way, resulting in what is now known as the **Mie theory**.
Fig. 2.1 shows an example of this framework.

It is helpful analyzing the plot in terms of the variation in extinction with respect to λ^{-1} (remember that the dimensionless size parameter X is closely dependent on the incident wavelength in the form $X \propto \lambda^{-1}$).
For instance, Q_{ext} increases monotonically with X in the range $0 < X < 4$: in this domain, extinction is dominated by scattering term (for the chosen refractive index). More precisely, for $1 < X < 3$, Q_{ext} increases almost linearly with X. As long as X becomes large, Q_{ext} becomes pretty constant, indicating that the extinction is neutral (i.e. it is wavelength independent) for grains much larger than λ.

2.1.1 Small-particle approximation

When $X \ll 1$, useful approximations can be applied to give simple expressions[2] for the efficiency factors:

$$Q_{scat} \simeq \frac{8}{3}\left(\frac{2\pi a}{\lambda}\right)^4 \left|\frac{m^2-1}{m^2+2}\right|^2 \tag{2.11}$$

and

$$Q_{abs} \simeq \frac{8\pi a}{\lambda} Im\left\{\frac{m^2-1}{m^2+2}\right\} \tag{2.12}$$

In the assumption of grains made out of pure dielectrics, m is a real number ($m \in \mathbb{R}$) and almost constant with respect to wavelength.
If this is the case, we have $Q_{scat} \propto \lambda^{-4}$ and $Q_{abs} = 0$: a situation which reminds the so-called *Rayleigh scattering*.

Generally speaking, the quantity $(m^2-1)/(m^2+2)$ is often only weakly dependent on wavelength for materials that are not strongly absorbing, in which case $Q_{scat} \propto \lambda^{-4}$ and $Q_{abs} \propto \lambda^{-1}$ are still good approximations.

2.2 Observational method

Theoretical methods imply different models and approximations about the environment and the interaction between electromagnetic radiation and the medium itself. This brings a lot of uncertainties and several issues about the physical coherence of the results. For these reasons, it is widely advisable to use comparative techniques directly with observational data.

The idea is the following: we consider the 'pairing' of stars of identical spectral type and luminosity class but unequal reddening and determine their colour difference. Let's denote with subscript 1 the 'reddened' star and with subscript 2 the 'comparison' star. Therefore the apparent magnitude of each star as a function of wavelength may be written as:

$$\begin{aligned} m_1(\lambda) &= M_1(\lambda) + 5log\, d_1 + A_1(\lambda) \\ m_2(\lambda) &= M_2(\lambda) + 5log\, d_2 + A_2(\lambda) \end{aligned} \tag{2.13}$$

where M, d and A represent absolute magnitude, distance and total extinction, respectively.
According to our initial assumptions, the quantity $M(\lambda)$ is expected to be very similar (or almost identical) for stars of the same spectral classification, so we may assume $M_1(\lambda) = M_2(\lambda)$.
Moreover, if we assume the statement $A(\lambda) = A_1(\lambda) \gg A_2(\lambda)$ (i.e. the extinction toward star 2 is negligible compared with that toward star 1), then the magnitude difference $\Delta m(\lambda) = m_1(\lambda) - m_2(\lambda)$ reduces to

$$\Delta m(\lambda) = 5log\left(\frac{d_1}{d_2}\right) + A(\lambda) \tag{2.14}$$

[2] See [BH83], chapter 5.

Let's focus on the right-hand side of eq. (2.14); here, the first term is independent of λ and it is constant for a given pair of stars. Therefore, in this context, the quantity $\Delta m(\lambda)$ may be used to represent $A(\lambda)$.

If we previously choose two standard wavelengths, λ_1 and λ_2, it is possible to define the normalized extinction E_{norm}:

$$\begin{aligned} E_{norm} &= \frac{\Delta m(\lambda) - \Delta m(\lambda_2)}{\Delta m(\lambda_1) - \Delta m(\lambda_2)} \\ &= \frac{A(\lambda) - A(\lambda_2)}{A(\lambda_1) - A(\lambda_2)} \\ &= \frac{E(\lambda - \lambda_2)}{E(\lambda_1 - \lambda_2)} \end{aligned} \tag{2.15}$$

where $E(\lambda_1 - \lambda_2)$, the difference in extinction between the specified wavelengths, is equal to the colour excess[3].
In practical terms, normalization is helpful because it allows extinction curves[4] for different reddened stars to be superimposed and compared.
Generally speaking, theoretical extinction curves (such that inferred from eq. (2.7)) for a given grain model may be normalized in the same way to allow direct comparison between observations and theory, in order to reduce uncertainties and calibrate free parameters in a more suitable way.

Observational data used to build the interstellar extinction curve typically come from broadband photometry and low-resolution spectrometry.
In particular, this *modus operandi* is straightforward if it is applied within standard passbands, such as the Johnson system. Indeed, extinction curves are commonly normalized with respect to the B and V passbands; hence, E_{norm} can be exploited in the form $E_{\lambda-V}/E_{B-V}$.
Actually, broadband photometry alone can not be always sufficient because it provides little information on the structure of the curve. That's why low-resolution spectrometry is needed, in particular at wavebands in the range $\Delta\lambda < 50\,\text{Å}$: at this level, the matching of individual stellar spectral lines in the reddened and comparison stars becomes important. Early-type stars (spectral classes O -A0) are often used for such investigations because they have several positive aspects:

1. Their spectra are simpler and then easier to match (with respect to late-type stars);

2. Their high intrinsic luminosity is most suitable for probing interstellar extinction at optical and UV wavelengths.

Fig. 2.2 shows an example of this kind of observational extinction curve (with pair method), based on data from a matching pair of stars observed by the **I**nternational **U**ltraviolet **E**xplorer (**IUE**) satellite.

It can be noted a broad absorption feature centred near $\lambda \approx 4.6\,\mu\text{m}^{-1}$ in the reddened star and weak or absent in the comparison star, resulting in a prominent peak in extinction.

[3] See [Tru30] for details.
[4] Plots where it is shown A_λ with respect to incident wavelength (or better λ^{-1}).

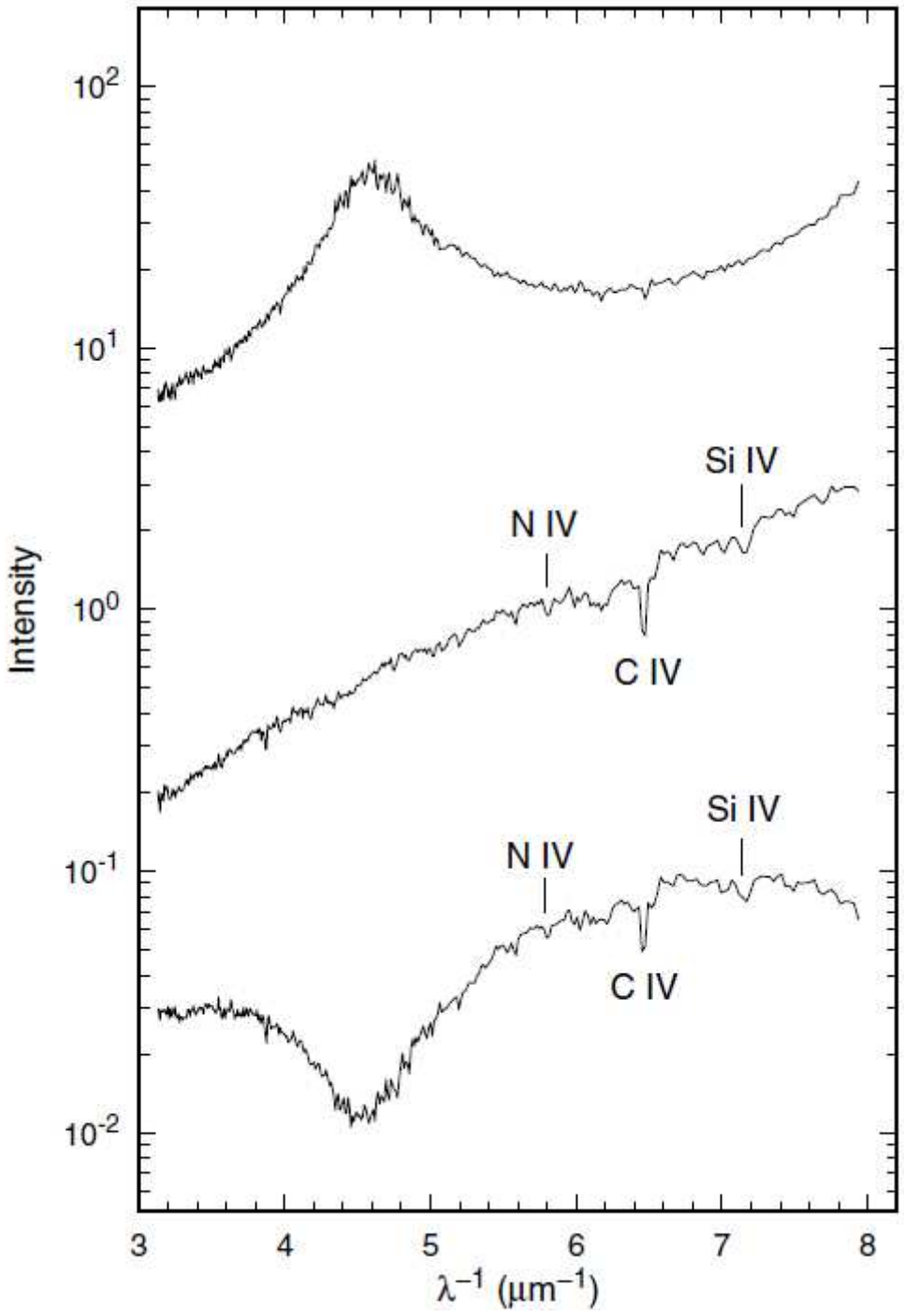

Figure 2.2: An illustration of the pair method for determining interstellar extinction curves. The lower curve is the UV-spectrum of a reddened star (HD 34078, spectral type O 9.5 V, $E_{B-V} = 0.54$), the middle curve is the corresponding spectrum of an almost unreddened star of the same spectral type (HD 38666, $E_{B-V} = 0.03$). Finally, the upper curve is the resulting extinction curve, obtained by taking the intensity ratio of the two spectra. Some specific spectral lines are highlighted. Based on data from the IUE satellite.
Figure from [Whi18], pag.74.

Just like the theoretical techniques, two difficulties associated with the pair method should be noted:

1. There are not so many suitable companion stars for detailed spectrophotometry, in particular OB stars that are close enough to the Sun or at high galactic latitude to have negligible reddening. Clearly, this problem is highlighted when we deal with supergiants: the main reason why these kinds of stars are often excluded from studies of extinction in the UV is that mismatches in their spectral lines can be troublesome;

2. Many early-type stars have infrared excess emission, due to thermal radiation caused by the presence of circumstellar dust or free-free emission caused by ionized gas. So an extinction curve built from these samples of stars could be heavily distorted in the spectral bands at which significant emission occurs (if compared with a normal star or with normal intrinsic colours).

2.3 The average extinction curve: the R_V parameter

It is possible to build an average extinction curve for a quite large sample of stars. Reliable data in the literature[5] have shown that extinction curves take the same general form in many lines of sight: this observational fact provides a valuable benchmark for comparison with curves deduced for individual stars and a basis for modelling. The stars included in these works are reddened predominantly by diffuse clouds in the solar neighbourhood of the Milky Way, within 2-3 kpc from the Sun; moreover, the associated values of extinction come out through the use of standard normalizations.

According to eq. (2.15), within Johnson's passbands notation, we have:

$$\begin{aligned} \frac{E_{\lambda-V}}{E_{B-V}} &= \frac{A_\lambda - A_V}{E_{B-V}} \\ &= R_V \left\{ \frac{A_\lambda}{A_V} - 1 \right\} \end{aligned} \tag{2.16}$$

where

$$R_V \equiv \frac{A_V}{E_{B-V}} \tag{2.17}$$

is the ratio of total-to-selective extinction.
If this parameter is known, it is possible to infer the *absolute extinction* A_λ/A_V (which is the real target). How R_V can be practically computed is shown in the next section; fig. 2.3 shows the typical structure of an average extinction curve (data are based on the aforementioned works in previous literature).

It can be noted that the functional behaviour is almost linear in the visible range (between 1 and $2\,\mu\mathrm{m}^{-1}$), with changes in slope approaching the blue domain near $2.2\,\mu\mathrm{m}^{-1}$ (the so-labelled *knee*) and in the infrared near $0.8\,\mu\mathrm{m}^{-1}$ (the *toe*). This section of the curve is well explained by the dependence $Q_{ext} \propto \lambda^{-1}$, in which according to Mie theory a population of dust grains of radius $a \simeq 0.2\,\mu\mathrm{m}^{-1}$ can roughly reproduces its form (with a refractive index $m \simeq 1.5 - 0.05i$).

[5] See [SM79], [Sea79] and [Whi88].

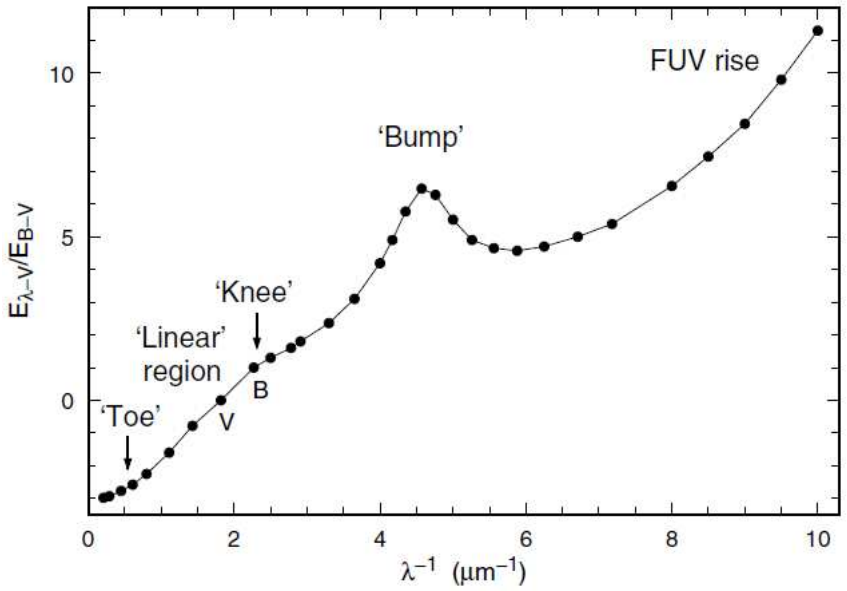

Figure 2.3: The average interstellar extinction curve in the spectral range 0.2-10 μm^{-1}. Data come from previous literature, as discussed in the text.
Figure from [Whi18], pag.77.

At shorter wavelengths this comparison breaks down and the most prominent feature in the observed curve is a broad, symmetric peak in the mid-UV centred at $\sim 4.6\,\mu m^{-1}$: this is known as the **2175 Å bump**, which will be discussed in detail section 2.4. Beyond the 'bump' we note a trough near $\sim 6\,\mu m^{-1}$, followed by a steep rise into the far-UV.

2.3.1 Long-wavelength extinction and evaluation of R_V

In the absence of neutral[6] extinction, the parameter R_V is formally related to the normalized relative extinction by the limit

$$R_V = -\left[\frac{E_{\lambda-V}}{E_{B-V}}\right]_{\lambda\to\infty} \tag{2.18}$$

and may be quite easily deduced by extrapolation of the observed extinction curve with reference to some model. For instance, assuming that *small-particle approximation* applies at sufficiently long wavelengths, an inverse power law of the form $Q_{ext} \propto \lambda^{-\beta}$ appears to be a reasonable model.

As already discussed in previuos sections (see eq. (2.11)), a limiting value for the index ($\beta = 4$) arises for scattering by pure dielectrics; on the other hand, indexes close to unity are predicted for absorption-dominated extinction (see eq. (2.12), where $\beta = 1$ if m is independent of λ).

[6]It is defined 'neutral' that extinction which occurs when particles larger than the longest observed wavelength are present.

More precisely, in the infrared range the observed extinction is very well parametrized by an inverse power law in the form of

$$\frac{E_{\lambda-V}}{E_{B-V}} = \varepsilon\lambda^{-\beta} - R_V \tag{2.19}$$

where ε is a constant.
According to previous literature (see [MW90] for more details), a consistent fit to average data in the ISM yields values of $\varepsilon = 1.19$, $\beta = 1.84$ and $R_V = 3.05$ (with errors around 1%). This predicted idealization is not holding for longer wavelengths ($\lambda \gtrsim 5\,\mu\mathrm{m}^{-1}$): here the absorption term should dominate over scattering and so extinction (as an overall process) will strictly depend on the nature of the grain material.

Keeping our analysis within the aforementioned limits in λ, it is possible to give an average (and conventional) expression for R_V:

$$R_V = 3.05 \pm 0.15 \tag{2.20}$$

This is the most likely average value of R_V in diffuse clouds.
A useful approximation may be applied to link R_V to the relative extinction in an infrared passband[7] such as K:

$$R_V \simeq 1.1\,\frac{E_{V-K}}{E_{B-V}} \tag{2.21}$$

2.3.2 The blue-ultraviolet section

At shorter wavelengths, average extinction curves show several regional variations; this particular feature is very likely linked to the optical properties of interstellar dust: Baade and Minkowski ([BM37], 1937) were the first to find out that, for instance, extinction curves for stars in the Orion Nebula (M42) differ from the mean curve in a way consistent with the selective removal of small particles in the size distribution.
This "depletion" effect can be due to several processes, for example grain growth by coagulation, removal by radiation pressure in stellar winds or size-dependent destruction. These observed properties are most conspicuous at UV range and quite remarkable from star to star, hinting that it is the smallest grains that are most subject to change.

There exist an empirical model ([FM86], [FM88] and [FM90]) which allow us to characterize this variations in the following form:

$$\frac{E_{\lambda-V}}{E_{B-V}} = (c_1 + c_2 x) + c_3 D(x) + c_4 F(x) \tag{2.22}$$

where $x = \lambda^{-1}$ and c_1, c_2, c_3 and c_4 are constants for a given line of sight.

[7] In principle there are several equivalent versions of eq. (2.21) for different passbands and different scaling constants. However, K is the preferred one for this purpose as it has the longest wavelength in the 'non-thermal' infrared.

Let's focus on the right-hand side. It can be divide in three components:

1. a linear term, $\boldsymbol{c_1 + c_2 x}$;

2. a 'bump' term, $\boldsymbol{c_3 D(x)}$ (where $D(x)$ is the mathematical parametrization of the 2175 Å feature. See eq. (2.24) for a complete expression);

3. a far-UV term, $\boldsymbol{c_4 F(x)}$ (where $F(x)$ is an empirical function for the model itself).

Each of these components can vary more or less independently from one line of sight to another. These variations are easily detectable in associated extinction curves as changes in slope between $2\,\mu\mathrm{m}^{-1}$ and $3\,\mu\mathrm{m}^{-1}$, i.e. between the knee and the bump (see fig. 2.3 for a reminder). Naturally, these changes are accompanied by variations in R_V; from a physical point of view, this means that there are fluctuations in the size distribution of the grains responsible for continuum extinction in the visible to near ultraviolet: here the slope declines as the mean grain size increases. Fig. 2.4 shows star-to-star variations in the 2175 Å feature. The sample includes stars that represent a quite wide range of environments: from dense clouds (such as HD 147889 in the ρ Oph complex) to H II regions and diffuse clouds. As one can see by the graphic, a variety of morphologies is evident. The 2175 Å feature shows variations in strength and width independent of changes in far-UV extinction. A deeper discussion about the bump is provided in the next section.

Finally, it is helpful to compare the results shown until now (data on extinction within Milky Way) with those of other galaxies. In literature there exist two best studied cases, the Large (LMC) and Small Magellanic (SMC) Clouds .

Figure 2.5 and figure 2.6 show graphically what it is going to be explained in the following. The Magellanic complex is composed by two irregular galaxies, each of them is deficient in heavy elements by factors of about 2.5 (LMC) and 7 (SMC) compared with the solar standard and it seems likely that this could affect the quality as well as the quantity of dust in their interstellar media.

- In the case of LMC, two distinct curves of extinction can be appreciated. One refers to stars in the vicinity of the 30 Doradus complex, the other describes properties of the environment more widely diffuse in the galaxy. The former displays a weaker bump and a stronger far-UV rise. Actually, what is more remarkable is that the form of the general extinction in the LMC is pretty similar to that of the Milky Way: this fact suggests that the composition and the distribution of dust grains between the two galaxies have to be quite comparable, at least in proportion;

- On the other hand, SMC seems radically different. In this case, extinction curve displays a steep continuum and extremely weak or absent bump absorption. Empirical fits through eq. (2.22) suggest that the continuum extinction has a dominant linear component. These differences might be related to the low metallicity of the SMC and its effect on grain production. Gordon *et al.* ([GCW97]) found out a similarity in optical properties for dust in starburst galaxies with respect to that in the SMC, so the radiative environment may play an important role as well.

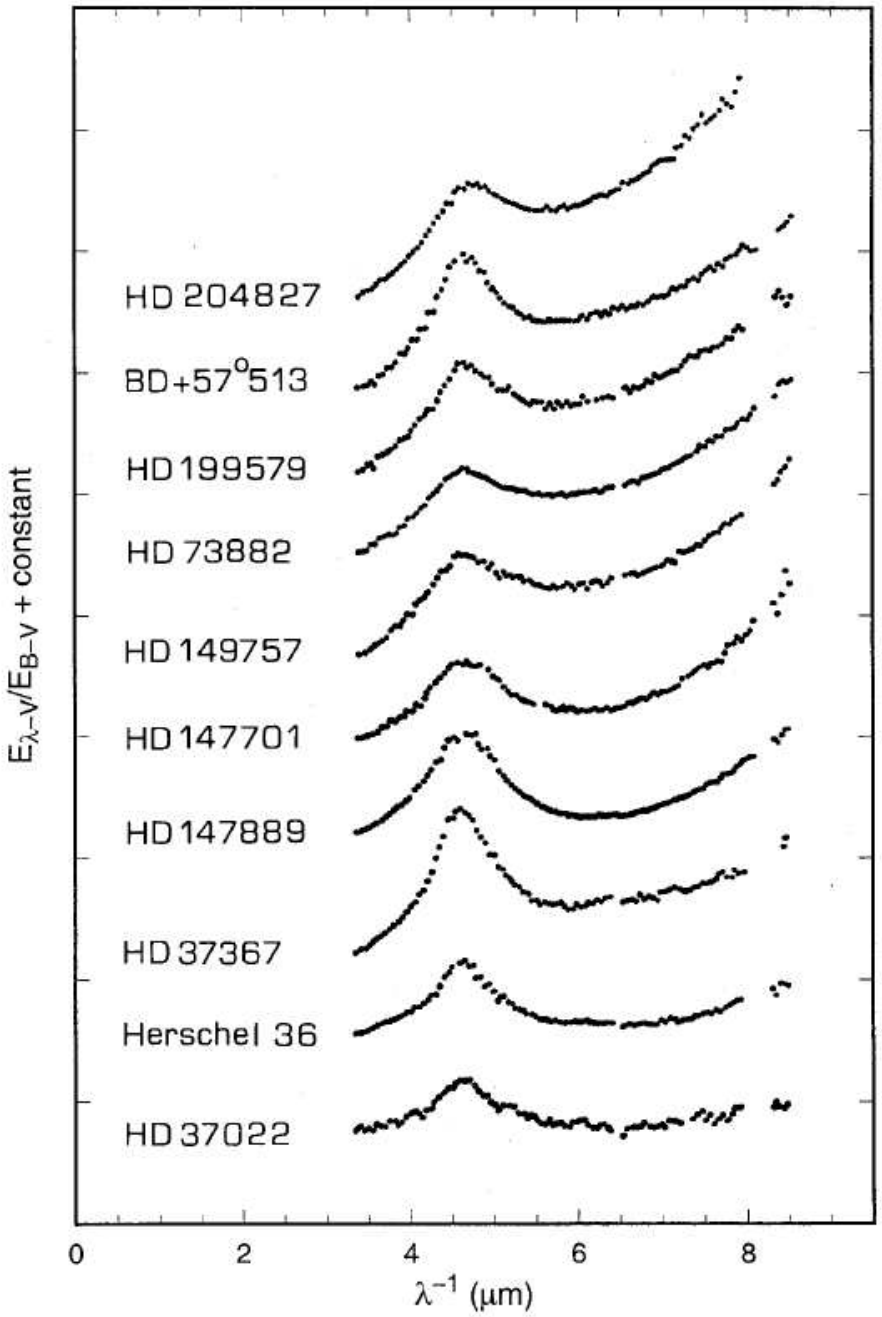

Figure 2.4: Comparison of the ultraviolet extinction curves of 10 stars (labelled in the plot) observed with the International Ultraviolet Explorer satellite. Individual curves have been displaced vertically for display. Figure from [Whi18], pag.86.

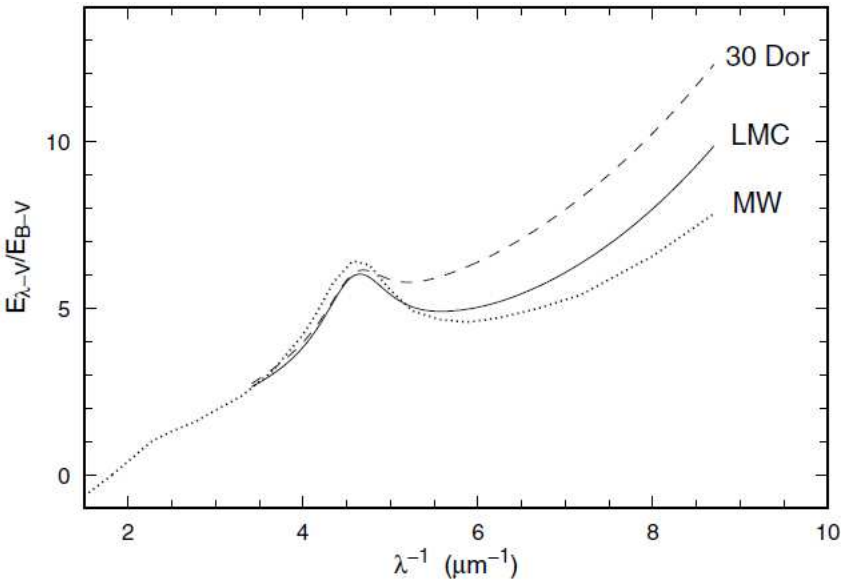

Figure 2.5: Ultraviolet extinction curves for the Large Magellanic Cloud (LMC). The average for stars widely distributed in the LMC (full curve) is compared with that for the 30 Doradus region of the LMC (broken curve) and the solar neighbourhood of the Milky Way (dotted curve). [FM86] (1986) as data benchmark. Figure from [Whi18], pag.88.

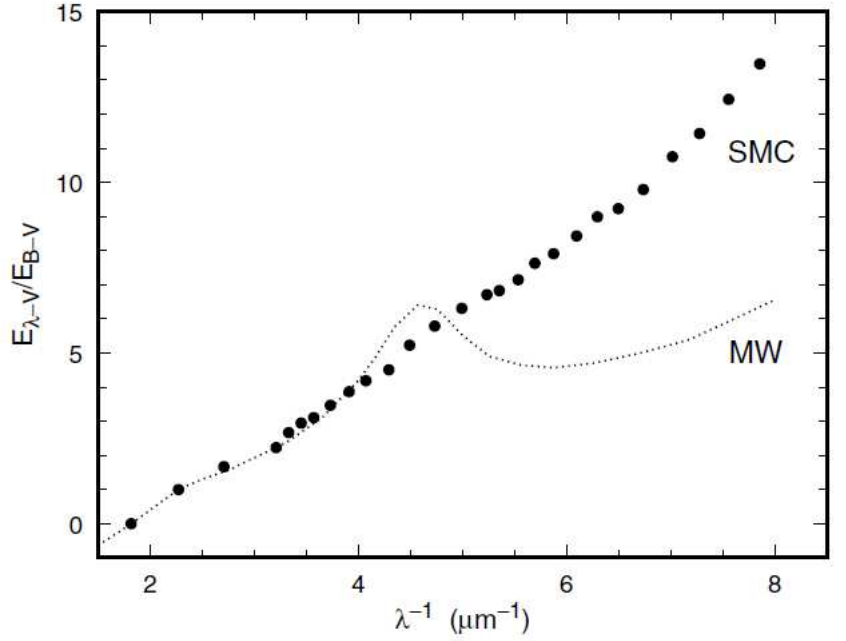

Figure 2.6: The ultraviolet extinction curve for the Small Magellanic Cloud (SMC, points). The average for the Milky Way is also shown for comparison (dotted curve). Prévot *et al* ([Pre+84], 1984) as data benchmark.
Figure from [Whi18], pag.89.

2.4 The 2175 Å absorption feature

The most peculiar observed property in extinction curves deserves a specific section. The bump has an associated central wavelength λ_0 (the peak wavelength), whose mean value is

$$\langle \lambda_0 \rangle = 2175 \pm 10 \,\text{Å} \tag{2.23}$$

A mathematical representation of the overall profile shape may be very helpful to provide physical insight. To a good approximation, the feature is Lorentzian; however, Fitzpatrick and Massa ([FM86]) demonstrated that a better fit can achieved through the so-called Drude profile:

$$D(x) = \frac{x^2}{(x^2 - x_0^2)^2 + \gamma^2 x^2} \tag{2.24}$$

where $x = \lambda^{-1}$ (and so $x_0 = \lambda_0^{-1}$).
Statistically, x_0 and γ are related to the position and width (i.e. FWHM) of the feature, respectively. Another parameter associated with the bump profile is its strenght. Traditionally this is expressed by the quantity A_{bump}:

$$A_{bump} = c_3 \int_0^\infty D(x)\, dx = \frac{\pi\, c_3}{2\gamma} \tag{2.25}$$

Mathematically it is the area under the 2175 Å profile in the normalized extinction curve and is thus a measure of strength per unit E_{B-V}.
The position, width and strength parameters λ_0, γ and A_{bump} have been evaluated for many lines of sight; fig. 2.7 lists results for a selection of individual stars that sample diverse environments, together with mean values for the Milky Way and the Large Magellanic Cloud.

One of the most remarkable observational properties of the 2175 Å profile is the occurrence of variations in width that are unaccompanied by changes in position. This behaviour seems to go against Mie theory, which predicts a strong correlation between x_0 and γ for particles involved with sizes comparable with the incident wavelength. At least three trends can be discerned by fig. 2.7:

1. Stars in the diffuse ISM tend to have relatively strong bumps of average width;

2. Stars associated with H II regions and/or OB star clusters generally have narrow, weak bumps;

3. Stars from dense clouds tend to have broad bumps (but with wide dispersion in both width and strength).

2.4.1 Implications for the identity of the carrier

The 2175 Å bump remains unchallenged as the dominant feature in the extinction curve, therefore it must be caused by a very strong absorber.
This carrier has to be cosmologically abundant, sufficiently robust to survive in a variety of interstellar environments and capable of producing absorption at the specific observed profile position (and not at other wavelengths, where there are no notable structures).

Star	Environment	λ_0^{-1}	γ	$A_{\rm bump}$
HD 29647	DC	4.70	1.62	3.35
θ^1 Ori C	H II	4.63	0.84	2.43
HD 37061	H II	4.57	1.00	2.69
HD 37367	DISM	4.60	0.91	7.04
HD 38087	RN	4.56	1.00	6.68
HD 62542	DC	4.74	1.29	3.11
HD 93028	OB	4.63	0.79	2.62
HD 93222	OB	4.58	0.81	3.33
ρ Oph	DC	4.60	0.99	5.57
HD 147889	DC	4.63	1.16	7.14
ζ Oph	DC	4.58	1.25	5.71
Herschel 36	H II	4.62	0.88	3.51
HD 197512	DISM	4.58	0.96	6.83
HD 204827	OB/DC	4.63	1.12	4.98
HD 210121	HLC	4.60	1.09	3.48
Mean ISM (45 stars)		4.60	0.99	5.17
General LMC (13 stars)		4.60	0.99	4.03
30 Dor LMC (12 stars)		4.61	0.89	2.62

Figure 2.7: Representative values of the 2175 Å bump parameters in units of μm^{-1}. Here the notation used: DC (dark clouds), DISM (diffuse ISM), H II (compact H II region), HLC (high latitude cloud), OB (OB star cluster) and RN (reflection nebula). Figure from [Whi18], pag.94.

Let's first write down some constraints that this element may have to match.
The equivalent width of the bump is related to the strength parameter A_{bump} by the expression:

$$W_\nu = c\, A_{bump}\, E_{B-V} \tag{2.26}$$

Using $A_{bump} \simeq 5.2 \times 10^6$ m^{-1} (fig. 2.7) and expliciting W_ν in terms of column density, the abundance relative to hydrogen of the carrier (X) is

$$\frac{N_X}{N_H} \simeq \frac{10^{-5}}{f} \tag{2.27}$$

where f is the oscillator strength per absorber.
The strongest permitted transitions typically have $f \leq 1$ and so the abundance of the carrier must be $N_X/N_H \geq 10^{-5}$.

Which are the chemical elements whose abundances can match the constraint? X has likely to contain one or more from the set [C, N, O, Ne, Mg, Si, S, Fe]. However:

- Ne is a noble gas, so it can be ruled out;
- S shows a weak depletion in ISM so it can not suit the constrain;
- N and O are excluded, too, because they are electron acceptors.

Therefore the carrier must contain one or more elements from the updated set [C, Mg, Si, Fe].

Graphitic carbon is by far the most widely discussed material amongst candidates for the bump and this choice has gained a measure of acceptance. That's because theoretical models involving small graphite grains well match the average profile of observed features; in addition, being a form of solid carbon, it can satisfy abundance constraints quite easily and from an optical point of view it is able to survive for long periods in the diffuse ISM.
Nevertheless, there are two specific problems with graphite identification.

1. *Origin and formation.* Observations of circumstellar dust suggest that solid material injected into ISM by carbon stars is in the non-graphitic form, so a mechanism for graphite formation in the interstellar medium must be formulated to strengthen the case for its inclusion in grain models;

2. *Bump constraints.* Properties of the 2175 Å feature force to put very tight (and often unrealistic) boundaries on the nature of the particles involved, for instance about size, shape, the presence of surface coatings, etc.

For these reasons, the debate is still ongoing and some other alternatives have been presented in the literature.
Further carbon-based materials have been suggested as carriers of the bump (Sakata *et al.*[8] 1977, 1983), as well as **P**olycyclic **A**romatics **H**ydrocarbons (**PAHs**). The latter, in particular, is a known molecular complex in the ISM due to the associated infrared emission; therefore, these molecules may be contributing to the UV extinction at some level. Indeed, PAHs show absorptions near 2200 Å (although the associated spectral profile is broader than the observed one in extinction curves), but also in the range 2400-4000 Å ; here no extinctional features have been observed in the ISM.
O-rich materials have also been proposed but none are now thought to be viable. A dielectric such as a silicate could be enough strong to absorb at very high photon energies (nearby the UV bump position); the problem here would be the extreme sensitivity with particle radius variations: the feature position and shape would require unreasonable fine-tuning of the size distribution.

To summarize, graphite or partly graphitized carbon grains remain the most likely identification of the 2175 Å bump. The particles responsible must be small, with dimensions $\sim 0.01\,\mu$m or less and the position of the feature is then independent of size but dependent on shape.

[8] See [Sak+77] and [Sak+83] for further details.

2.5 Dust density and dust-to-gas ratio

As widely mentioned in the previous sections, extinction is strictly linked to the dust grains population[9], both in optical properties and size distribution.
To produce the observed mean rate of extinction, an estimate of the amount of grain material is required. If we assume a population of spherical particles with average radius a and refractive index m, the Kramers-Krönig relationship gives

$$\int_0^\infty Q_{ext}\, d\lambda = 4\,\pi^2\, a \left\{ \frac{m^2-1}{m^2+2} \right\} \tag{2.28}$$

The mass density of dust in a column of length L is

$$\rho_d = \frac{N_d\, m_d}{L} \tag{2.29}$$

where N_d is the column density (as presented in eq. (2.3)) and

$$m_d = \frac{4}{3}\pi\, a^3\, s \tag{2.30}$$

is the mass of a spherical dust grain composed of material of specific density s. Using eq. (2.6) to relate A_λ to Q_{ext}, previous expressions can be rearranged in the form

$$\rho_d \propto s \left\{ \frac{m^2+2}{m^2-1} \right\} \int_0^\infty \frac{A_\lambda}{L}\, d\lambda \tag{2.31}$$

Observationally (see [Spi78], pag. 153), ρ_d may be expressed in terms of $\langle A_V/L \rangle$ in mag kpc^{-1}:

$$\rho_d \simeq 1.2 \times 10^{-27} s \left\{ \frac{m^2+2}{m^2-1} \right\} \left\langle \frac{A_V}{L} \right\rangle \tag{2.32}$$

For instance, if we assume a population of grains made out mostly of low-density silicates, then eq. (2.32) gives the approximate value

$$\rho_d \simeq 18 \times 10^{-24}\,\mathrm{kg\,m^{-3}} \tag{2.33}$$

The dust-to-gas ratio, if we suppose the presence of helium in the gaseous component of ISM, is

$$Z_d = 0.71 \frac{\rho_d}{\rho_H} \simeq 0.007 \tag{2.34}$$

where $\rho_H \simeq 1.8 \times 10^{-21}$ kg m^{-3}.
This result is consistent with estimates of Z_d based on abundance and depletion data. A similar calculation for reddened stars in the Large Magellanic Cloud yields $Z_d \sim 0.002$, a significant difference which is qualitatively consistent with the low metallicity of that galaxy compared with the Milky Way.

[9] For further details, see [Car+21] chapter 10.

2.6 Summary

Interstellar extinction curves display a wide diversity in morphological structure (e.g. figures 2.4, 2.5 e 2.6), but there are some features that seems in common despite different environments. For instance, the infrared domain is well predictable through an inverse power law (see eq. (2.19)); on the other hand, the UV section is characterized by the famous 2175 Å bump: it is ubiquitous and seems quite stable in position and profile shape, whilst displaying variations in amplitude and width (see section 2.4).
It is possible to parametrize the extinction curve at these short wavelengths, too, in terms of a quite manageable mathematical formula (eq. (2.22)).
During the past decades a lot of effort was put into the attempt to build a unique mathematical description of extinction curves. In this sense, Cardelli *et al.*[10] (1989) is considered a pioneeristic work in the field. In the mentioned paper the entire extinction curve is represented by the equation

$$\frac{A_\lambda}{A_V} = a(x) + \frac{b(x)}{R_V} \tag{2.35}$$

where $a(x)$ and $b(x)$ are coefficients that have unique values at a given wavenumber $x = \lambda^{-1}$.
The eq. (2.35) is often referred to as the **CCM extinction law**. The aforementioned coefficients are determined empirically by the slope and the intercept of the correlation of A_λ/A_V with R_V^{-1}. Figure 2.8 show R_V-dependent extinction. According to original data from Cardelli, R_V tends to be higher in dense clouds, where grains grow by coagulation, compared with the average value of around 3.1 (eq. (2.20)). The curves converge in the infrared ($\lambda < 1\,\mu\mathrm{m}^{-1}$) and diverge in the ultraviolet ($\lambda > 2\,\mu\mathrm{m}^{-1}$).

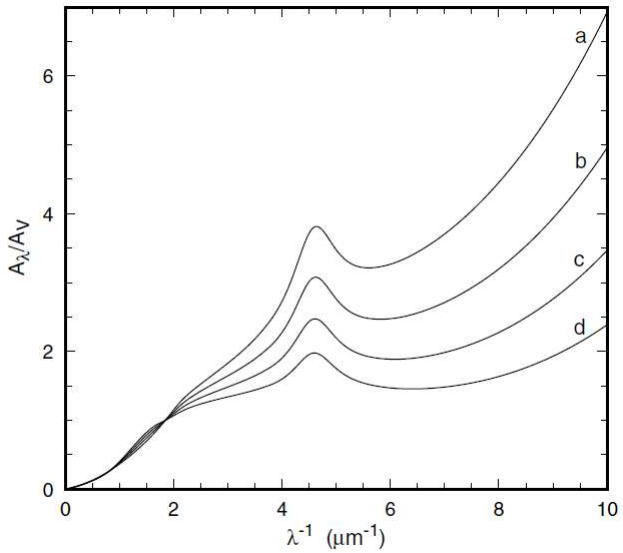

Figure 2.8: R_V-dependent variations in the extinction curve. Curve *a*: $R_V = 2.5$; curve *b*: $R_V = 3.1$; curve *c*: $R_V = 4.0$; curve *d*: $R_V = 5.5$. Empirical fits based on original data from Cardelli ([CCM89]) and elaborated by Fitzpatrick ([Fit99]). Figure from [Whi18], pag.89.

[10] See [CCM89] for references.

Chapter 3

Modelization of interstellar extinction

3.1 CCM model

Interstellar extinction can show a large range of variability from one line of sight to another. In the previous chapter, we have seen how extinction curves provide specific features according to the energy in the electromagnetic spectrum, from IR to UV domain. Nevertheless, it is possible to compare the shapes of different extinction curves to infer common properties and build up an average extinction curve, which models the physical phenomenon behind the graphic representation.

Cardelli, Clayton and Mathis (1989, hereafter **C.C.M.**) developed a pioneering work to model the behaviour of interstellar extinction.
As mentioned in section 2.6, there exists a convenient way to build up this kind of parametrization, that is trying to express $A(\lambda)$, the absolute extinction at any wavelength, in terms of $A(\lambda_{ref})$, i.e. the absolute extinction at a chosen reference wavelength. Logically, the easiest choice for λ_{ref} is a wavelength for which variability in the shape of the extinction at higher energies is small or negligible (e.g. $\lambda_{ref} > 0.7\,\mu$m); however, since so many observations exist for the yellow portion of the spectrum, the visual extinction $A(\lambda_{ref} = V)$ is used as a reference for historical reasons.

Conventionally, extinction has often been analyzed using a two-colour normalization of the form $E(\lambda - V)/E(B - V)$ (see section 2.3); however, the true nature of the variability of observed extinction may be hidden by the choice of normalization. For this reason, the quantity $A(\lambda)/A(V)$ is a more fundamental extinction parameter than the colour excess because the absolute extinction is expressed directly, rather than by comparing one colour with another.

Precedent studies (see [FM86] and [FM88], FM86 and FM88 from now on respectively) have encouraged the study of the relationship between the optical and UV portions of the extinction law, in particular because the UV domain was accurately determined and conveniently parametrized by simple analytic expressions; by combining these results with optical and (near)IR photometry, Cardelli *et al.* ([CCM89]) showed that there is a strong relationship between the shape of absolute optical and UV extinction laws (based on the same line of sights of

FM86 and FM88); this connection is expressed by the parameter:

$$R_V \equiv \frac{A(V)}{E(B-V)} \tag{3.1}$$

Cardelli, Clayton and Mathis model is also known as **CCM-model** and it is a R_V-dependent parametrization because its algebraic expression is strictly linked to the value of R_V; for instance, extinction laws computed by this model show large systematic differences in extinction for lines of sight with considerably different values of R_V.
Given the definition of this parameter, clearly it hides some important environmental properties from a physical point of view: for instance, $R_V = 5$ is a typical value found along the line of sight of some dense clouds, which suggests the abundant presence of some interstellar molecules. Generally, this argument is valid within CCM-model whenever R_V has a value larger than the one conventionally accepted for the standard diffuse ISM, which is $R_V = 3.1$.
These aspects are going to be deeply analyzed in section 3.2; in the following discussion, a more detailed vision of the model is provided.

3.1.1 Algebraic expression for CCM extinction curves

Extinction curves based on CCM-model are basically plots of $A(\lambda)/A(V)$ against R_V^{-1}; it can be seen that, in the range $0.12\,\mu\text{m} < \lambda < 0.32\,\mu\text{m}$, the behaviour is pretty much linear, so an analytic expression is of the form:

$$\frac{A(\lambda)}{A(V)} = a(\mathrm{x}) + \frac{b(\mathrm{x})}{R_V} \tag{3.2}$$

where $\mathrm{x} = \lambda^{-1}$.

There is also a similar linear relationship between $A(\lambda)/A(V)$ and R_V^{-1} for extinction in the visual-(near)IR domain. In the following, the explicit expression of equation (3.2) for the different spectral ranges.

- **Infrared** ($0.3\,\mu\text{m}^{-1} \leq \mathrm{x} \leq 1.1\,\mu\text{m}^{-1}$)

$$a(\mathrm{x}) = 0.574\,\mathrm{x}^{1.61} \tag{3.3}$$

$$b(\mathrm{x}) = -0.527\,\mathrm{x}^{1.61} \tag{3.4}$$

- **Optical/(near)IR** ($1.1\,\mu\text{m}^{-1} \leq \mathrm{x} \leq 3.3\,\mu\text{m}^{-1}$ and $\mathrm{y} = (\mathrm{x} - 1.82)$)

$$a(\mathrm{x}) = 1 + 0.17699\mathrm{y} - 0.50447\mathrm{y}^2 - 0.02427\mathrm{y}^3 + 0.72085\mathrm{y}^4 + 0.01979\mathrm{y}^5 - 0.77530\mathrm{y}^6 + 0.32999\mathrm{y}^7 \tag{3.5}$$

$$b(\mathrm{x}) = 1.41338\mathrm{y} + 2.28305\mathrm{y}^2 + 1.07233\mathrm{y}^3 - 5.38434\mathrm{y}^4 - 0.62251\mathrm{y}^5 + 5.30260\mathrm{y}^6 - 2.09002\mathrm{y}^7 \tag{3.6}$$

- **Ultraviolet** ($3.3\,\mu\text{m}^{-1} \leq \mathrm{x} \leq 8\,\mu\text{m}^{-1}$)

$$a(\mathrm{x}) = 1.752 - 0.316\mathrm{x} - \frac{0.104}{[(\mathrm{x}-4.67)^2 + 0.341]} + F_a(\mathrm{x}) \tag{3.7}$$

$$b(\mathrm{x}) = -3.090 + 1.825\mathrm{x} + \frac{1.206}{[(\mathrm{x}-4.62)^2 + 0.263]} + F_b(\mathrm{x}) \tag{3.8}$$

where:

$$F_a(\mathrm{x}) = -0.04473(\mathrm{x}-5.9)^2 - 0.009779(\mathrm{x}-5.9)^3 \qquad (5.9 \leq \mathrm{x} \leq 8)$$
$$F_b(\mathrm{x}) = 0.2130(\mathrm{x}-5.9)^2 + 0.1207(\mathrm{x}-5.9)^3 \qquad (5.9 \leq \mathrm{x} \leq 8)$$
$$F_a(\mathrm{x}) = F_b(\mathrm{x}) = 0 \qquad (\mathrm{x} < 5.9)$$

Fig. 3.1 shows a comparison between the computed optical/(near)IR portion of the extinction curve (based on previous equations) and the observed one with data for three lines of sight with widely separated values of R_V.

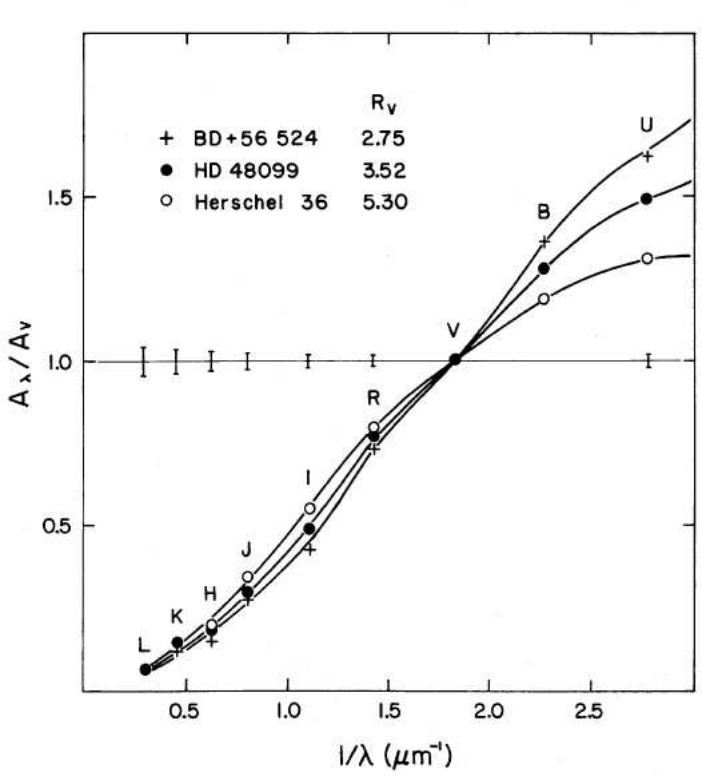

Figure 3.1: Comparison between the mean optical/(near)IR R_V-dependent extinction law from CCM parametrization and three lines of sight with largely separated R_V values. The wavelength position of the various broad-band filters from which the data were obtained is labelled. The 'error' bars represent the computed standard deviation of the data about the best fit of $A(\lambda)/A(V)$ vs R_V^{-1} with $a(\mathrm{x}) + b(\mathrm{x})/R_V$, where $\mathrm{x} \equiv \lambda^{-1}$. Figure from [CCM89], pag.5.

As one can note, the effect of varying R_V on the shape of the extinction curves is quite apparent, particularly at the shorter wavelengths; the fit is quite good for all three lines of sight.
The equation for the segment $1.1\,\mu\mathrm{m}^{-1} \leq \mathrm{x} \leq 3.3\,\mu\mathrm{m}^{-1}$ was found by fitting a 7^{th}-order polynomial to $a(\mathrm{x})$ and $b(\mathrm{x})$ derived from $A(\lambda)/A(V)$ vs R_V^{-1} at the passband I through U and the UV point at $\mathrm{x} = 3.3\,\mu\mathrm{m}^{-1}$.
The 'error' bars shown in the figure are the standard deviations of the data at each passband about the best fit; therefore they do not represent *true* errors but the real deviations of various lines of sight from the mean.

The polynomial expression (up to 7^{th}-order) is needed to allow the mean extinction to be directly calculated at all wavelengths (the split into three segments, i.e. infrared, optical and UV, is due to computational requirements).
Therefore, the R_V-dependent model can be compared to standard average curves if the extinction parameter has a constant value, conventionally $R_V = 3.1$.
Moreover, CCM polynomial functions have the advantage of joining smoothly onto the UV domain, with a better fit with respect to (for instance) the well-known Whitford extinction law (1958): it can be more accurate for the diffuse ISM near $x \approx 2.25\,\mu m^{-1}$, but it shows an abrupt change in slope between optical and near-UV.

Fig. 3.2 displays a comparison of CCM-model for the same three lines of sight shown in fig. 3.1, but for the UV spectral regime. Because the curves are closely spaced, only the optical data at U, B and V have been provided.
The agreement is generally quite good.

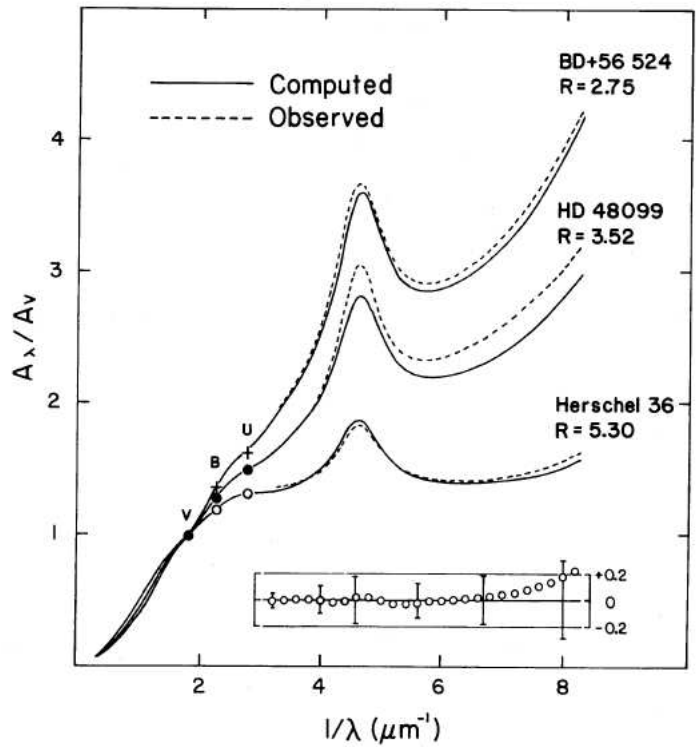

Figure 3.2: Same as fig.3.1 except for the UV portion of the mean R_V-dependent extinction law. Again, the 'error' bars represent the computed standard deviation of the data about the best fit of $A(\lambda)/A(V)$ vs R_V^{-1} with $a(x) + b(x)/R_V$.
The only serious deviation occurs for $x > 7\,\mu m^{-1}$ (see text for details).
Figure from [CCM89], pag.6.

As with the optical/(near)IR, one test of the consistency of the UV-parametrized equations is to compare reddening corrections produced using eq. (3.7) with existing average curves, the most quoted of which are those in Seaton's (see [Sea79]).
In this case, too, the appropriate R_V value is adopted to be 3.1-3.2.
Differences between CCM parametrization and Seaton's work (hereafter S79) are shown in the lower inset in fig. 3.2.

The following is noted:

- For $x < 7\,\mu m^{-1}$, discrepancies are less than $\pm 4\%$;
- For $x > 6.7\,\mu m^{-1}$, the deviation becomes increasingly larger.

These discrepancies are meant to be due to how the extinction curves have been built. For instance, S79 curves were derived by averaging extinction curves for which individual values of R_V were not known but were presumably not significantly different than 3.2; CCM equations, on the other hand, were determined by considering extinction at all R_V values (e.g., $2.5 < R_V < 6$) for a single data set representing the entire UV spectral domain.

In conclusion, the most important result of CCM-model is that the entire mean extinction law, from the near-IR through the optical and accessible UV, can be well represented by a mean relationship which depends upon a single parameter. By convenience, this parameter is R_V, but it has no particular physical significance.
On the other hand, the meaning of the one-parameter nature of the mean extinction law is that it shows that the processes which produce changes in extinction operate effectively and rather continuously over most or all of the range of grain sizes and compositions; the deviations of the observations from mean relation are impressively small. Even though there are rather different physical conditions in the ISM along the various lines of sight to stars which have the same values of R_V, the extinction law is characterized quite well by R_V alone.
Generally speaking, this would not be the case: in fact, one can easily imagine that if diverse types of grains provide most of the extinction at various wavelengths, we would expect that some processes would modify a particular component (e.g. the far-UV rise) and leave others unchanged.
However, in the real ISM the processes which modify the extinction at one wavelength also seem to modify the entire mean extinction law in a regular way.
The processes for modifying grains must be general and stochastic in nature, so that grains of all but the largest sizes participate to an appreciate extent.
Since it is not clear whether the extinction law at the longest wavelengths varies among the various lines of sight, we reserve judgment as to the modifications of the largest grains.

3.2 Application: study of extinction curves in Python

3.2.1 Description of the project

Using the well-known software Python, it is possible to compute and perform several calculations about interstellar extinction. There exists an 'extinction' package, indeed, which allows us to take advantage of the most known theoretical model about this subject.
More in detail, through this coding package we are able to:

- Get E_{B-V} for a set of coordinates (or list of coordinates) from different
  - distant sources (e.g. using N.E.D.[1] and I.R.S.A.[2] archives);
  - local dust maps (see [SFD98], [Sch+14], [Abe+14], [Gre+15]).
- Compute the ISM transmission for different extinction laws:
  - Cardelli, Clayton and Mathis, i.e. CCM-model ([CCM89]);
  - O'Donnell parametrization (see [ODo94]);
  - Fitzpatrick & Massa (see [Fit99]);
  - Goobar's work (see [Goo08]).

According to the spirit of the present work, it is clear that CCM model represents a milestone in modelling interstellar extinction; therefore, historically and conventionally, Cardelli *et al.* work will be the object of discussion. Nevertheless, it is useful to describe some of the characteristics of these models in a numerical way.

- *Cardelli et al.*
  In Cardelli, Clayton & Mathis (1989) the mean R_V-dependent extinction law, is parameterized as
  $$\left\langle \frac{A(\lambda)}{A_V} \right\rangle = a(\mathrm{x}) + \frac{b(\mathrm{x})}{R_V}$$
  where the coefficients $a(\mathrm{x})$ and $b(\mathrm{x})$ are functions of wavelength. At a wavelength of approximately 5494.5 Å (a characteristic wavelength for the V band), $a(\mathrm{x}) = 1$ and $b(\mathrm{x}) = 0$, so that $A(\lambda = 5494.5\,\text{Å}) = A_V$.
  This function returns
  $$A(\lambda) = A_V \left(a(\mathrm{x}) + \frac{b(\mathrm{x})}{R_V} \right)$$
- *O'Donnell.*
  O'Donnell's paper (1994) is basically based on Cardelli *et al.* parametrization but on different spectrum ranges. In fact, the former is valid between 3030 Å and 9091 Å; the latter is valid between 1250 Å and 3.3 μm.
- *Fitzpatrick & Massa.*
  This model relies on the parametrization of Fitzpatrick & Massa 1990 ([FM90]), with validity in the UV (below 2700 Å) and spline fitting in the optical and in the infrared. This function is defined from 910 Å to 6 μm, but the claimed validity goes down only to 1150 Å.

[1] **N**ASA **E**xtragalactic **D**atabase, available at https://ned.ipac.caltech.edu/.
[2] **I**nfra**R**ed **S**cience **A**rchive, available at https://irsa.ipac.caltech.edu/frontpage/.

3.2.2 Interstellar extinction models in Python

According to previous sections (in particular, see subsec. 3.1.1), it has been possible to write a Python code which shows proper features of interstellar extinction based on theoretical models. The following figures display the results. At the end of the present section, the code[3] itself will be provided.

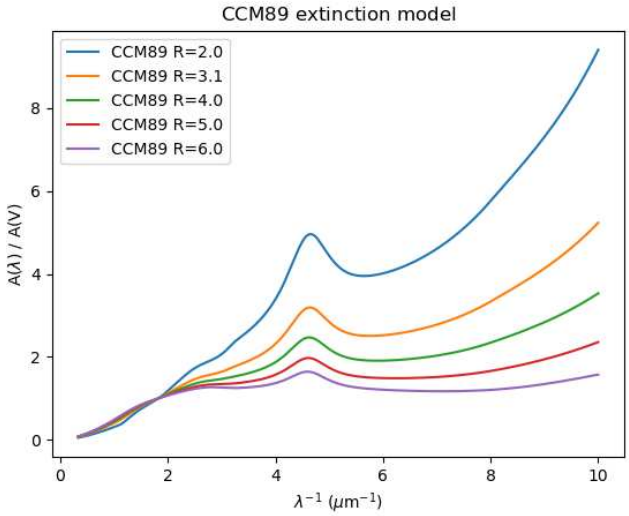

Figure 3.3: Extinction curve based on Cardelli *et al.* model (sec.3.1.1) at different values of R_V. It can be noted how the steepness of extinction behaviour changes within the same λ^{-1} interval; for reference purposes, it is highlighted the standard $R_V = 3.1$ value. Plot made according to Python code in subsec. 3.2.4

3.2.3 Python codes for interstellar extinction curves

```
import matplotlib as mpl
import pylab
import numpy as N
from scipy import interpolate


# *Indicative* Bessel filter central wavelengths [A]
BesselFilters = dict(U=3590.,
                     B=4320.,
                     V=5410.,
                     R=6360.,
                     I=8000.)


def ccm_extinction_parameters(lbda, odonnell=True):
    def cardelli_ir(x):
        """A/Av in InfraRed: 0.3-1.1 micron^-1."""
```

[3] For details: https://github.com/nicolaschotard/extinctions/blob/master/extinctions/extinction.py

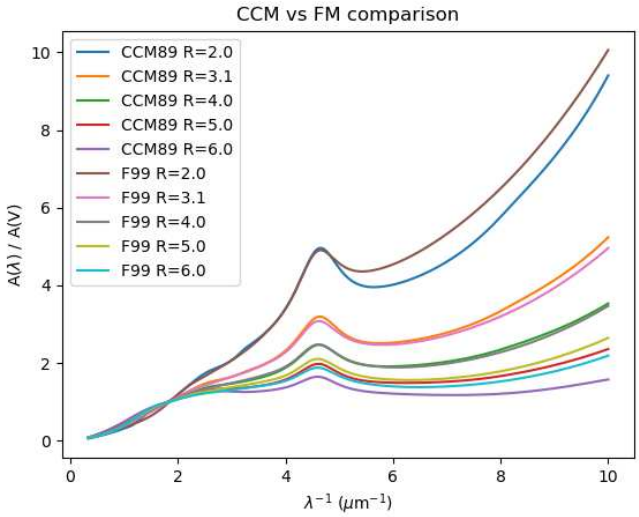

Figure 3.4: Comparison between two different extinction models: Cardelli *et al.* (CCM89) and Fitzpatrick & Massa (F99); each extinction curve is computed accordingly with the same different R_V values of fig.3.3. Plot made according to Python code in subsec. 3.2.4

```
        assert ((x >= 0.3) & (x <= 1.1)).all()
        a = +0.574 * x ** 1.61
        b = -0.527 * x ** 1.61
        return a, b

    def cardelli_opt(x):
        """A/Av in Optical/Near IR: 1.1-3.3 micron^-1."""
        assert ((x >= 1.1) & (x <= 3.3)).all()
        y = x - 1.82
        pa = [+0.32999, -0.77530, +0.01979, +
              0.72085, -0.02427, -0.50447, +0.17699, 1]
        pb = [-2.09002, +5.30260, -0.62251, -
              5.38434, +1.07233, +2.28305, +1.41338, 0]
        a = N.polyval(pa, y)
        b = N.polyval(pb, y)
        return a, b

    def cardelli_uv(x):
        """A/Av in UV: 3.3-8 micron^-1."""
        assert ((x >= 3.3) & (x <= 8)).all()
        y = x - 5.9
        fa = N.where(x >= 5.9, (-0.04473 - 0.009779 * y) * y ** 2, 0)
        fb = N.where(x >= 5.9, (+0.2130 + 0.1207 * y) * y ** 2, 0)
        a = +1.752 - 0.316 * x - 0.104 / ((x - 4.67) ** 2 + 0.341) + fa
        b = -3.090 + 1.825 * x + 1.206 / ((x - 4.62) ** 2 + 0.263) + fb
        return a, b

    def cardelli_fuv(x):
```

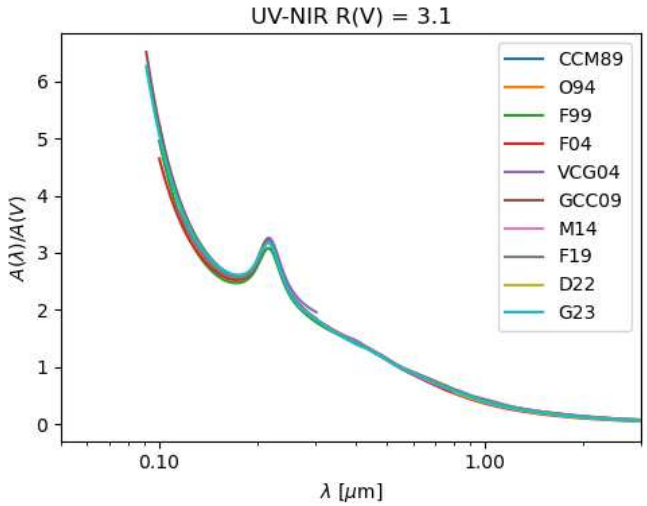

(a) *UV-NIR ($R_V = 3.1$)*

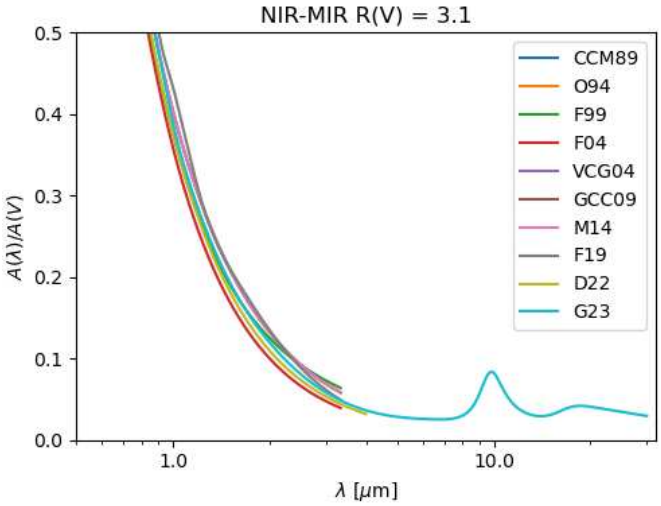

(b) *NIR-MIR ($R_V = 3.1$)*

Figure 3.5: Wide comparison of the most known theoretical models for interstellar extinction parametrization, keeping fixed R_V to the standard value of 3.1 in the Galaxy. Upper diagram: comparison from UV-domain to near-infrared range. Lower diagram: comparison from near-infrared to mid-infrared. For computational reasons, these extinction curves are displayed with a λ-behaviour in the x-axis. Plots made according to Python code in subsec. 3.2.4.

```
    """A/Av in Far UV: 8-10 micron^-1."""
    assert ((x >= 8) & (x <= 10)).all()
    y = x - 8.
    a = N.polyval([-0.070, +0.137, -0.628, -1.073], y)
    b = N.polyval([+0.374, -0.420, +4.257, +13.67], y)
    return a, b

x = 1e4 / N.atleast_1d(lbda)           # [micron^-1]
i_ir = (x >= 0.3) & (x < 1.1)           # IR
```

```
    i_opt = (x >= 1.1) & (x < 3.3)         # Opt/Near IR
    i_uv = (x >= 3.3) & (x < 8)            # UV
    i_fuv = (x >= 8) & (x <= 10)           # Far UV

    a = N.zeros(len(x), 'd') * N.nan
    b = N.zeros(len(x), 'd') * N.nan
    a[i_ir], b[i_ir] = cardelli_ir(x[i_ir])
    if odonnell:
        a[i_opt], b[i_opt] = odonnell_opt(x[i_opt])  # Updated O'Donnell expression
    else:
        a[i_opt], b[i_opt] = cardelli_opt(x[i_opt])  # Original CCM89 expression
    a[i_uv], b[i_uv] = cardelli_uv(x[i_uv])
    a[i_fuv], b[i_fuv] = cardelli_fuv(x[i_fuv])

    return a, b


def odonnell_opt(x):
    if N.min(x) >= 3000:
        x = 10000. / N.array(x)  # Transform into micron^-1
    assert ((x >= 1.1) & (x <= 3.3)).all()
    y = x - 1.82
    pa = [-0.505, +1.647, -0.827, -1.718, +1.137, +0.701, -0.609, +0.104, 1]
    pb = [+3.347, -10.805, +5.491, +11.102, -7.985, -3.989, +2.908, +1.952, 0]
    a = N.polyval(pa, y)
    b = N.polyval(pb, y)
    return a, b


def extinction_law(lbda, law='OD94', rv=3.1):
    if law == 'CCM89':
        a, b = extinctionParameters(lbda, odonnell=False)
    elif law == 'OD94':
        a, b = extinctionParameters(lbda, odonnell=True)
    elif law == 'FM98':
        a, b = fm99_extinction(lbda, rv=rv), 0
    else:
        raise ValueError("'law' has to be either CCM89, OD94 or FM98.")
    return a + b / rv


def extinction_factor(lbda, ebmv, law='OD94', rv=3.1):
    a = extinction_law(lbda, law=law, rv=rv)      # A(lambda)/A_V
    return 10 ** (-0.4 * a * rv * ebmv)   # A_V := R_V * E(B-V)


def fm99_extinction(lbda, rv=3.1, lmc2=False, avglmc=False, params=None,
                    k=5, s=None, ccmstyle=True):

    if isinstance(lbda, (int, float)):
```

```
    lbda = [lbda]

def fmuv(x, rv):
    """Extinction in the ultra-violet."""
    xuv = (x - 5.9) * N.array((x - 5.9) > 0, dtype=int)
    yuv = (params['c1'] + params['c2'] * x + params['c3'] * x ** 2 /
           ((x ** 2 - params['x0'] ** 2) ** 2 + (x * params['gamma']) ** 2) +
           params['c4'] * (0.5392 * xuv ** 2 + 0.05644 * xuv ** 3) + rv)
    return yuv

def fmop(rv):
    """Extinction in the optical."""
    xop = N.array([1.66667, 1.82815, 2.14132, 2.43309])
    yop = [N.polyval([2.13572e-04, 1.00270, -4.22809e-01], rv),
           N.polyval([-7.35778e-05, 1.00216, -5.13540e-02], rv),
           N.polyval([-3.32598e-05, 1.00184, 7.00127e-01], rv),
           N.polyval([-4.45636e-05, 7.97809e-04, -5.46959e-03,
                      1.01707, 1.19456], rv)]
    return xop, yop

def fmir(rv):
    """Extinction in the infra-red."""
    xir = N.array([0.37736, 0.81967])
    yir = N.array([0.26469, 0.82925]) * rv / 3.1
    return xir, yir

# Define parameters for the differentes cases
if params is not None:
    keys = ['gamma', 'x0', 'c4', 'c3', 'c2', 'c1']
    if not all([key in params for key in keys]):
        raise KeyError(
            "params dictionary must have the following keys: %s" % keys)
    else:
        print("Use the given set of parameters:")
elif lmc2:
    params = {'gamma': 1.05, 'x0': 4.626, 'c4': 0.42,
              'c3': 1.92, 'c2': 1.31, 'c1': -2.16}
    print("Use the lmc2 set of parameters:")
elif avglmc:
    params = {'gamma': 0.91, 'x0': 4.596, 'c4': 0.64,
              'c3': 2.73, 'c2': 1.11, 'c1': -1.28}
    print("Use the avglmc set of parameters:")
else:
    c2 = -0.824 + 4.717 / rv
    params = {'gamma': 0.99, 'x0': 4.596, 'c4': 0.41,
              'c3': 3.23, 'c2': c2, 'c1': 2.030 - 3.007 * c2}
    print("Use the standard set of parameters for MW:")
print('; '.join(["%s=%.2f" % (p, params[p]) for p in params]))

# Make sure that the law is constructed over a fair range of wavelength
```

```
    rlbda = N.arange(2000, 10000, 1)

    # Convert to inverse microns
    x = 10000. / N.array(rlbda)

    # Initialize the extinction curve array
    extcurve = x * 0.

    # Set the limits
    xcutuv = 3.704
    iuv, n_uv = x >= xcutuv, x < xcutuv
    iopir, nopir = x < xcutuv, x >= xcutuv

    # Compute the NUV extinction
    if len(x[n_uv]) > 0:
        extcurve[iuv] = fmuv(x[iuv], rv)

    # Compute the OP/IR extinction
    if len(x[nopir]) >= 0:
        # For the UV (ref)
        xspluv = N.array([3.704, 3.846])
        yspluv = fmuv(xspluv, rv)

        # For OP
        xsplop, ysplop = fmop(rv)

        # For IR
        xsplir, ysplir = fmir(rv)

        # Make a spline
        spline = interpolate.UnivariateSpline(N.concatenate([[0], xsplir,
                                                             xsplop, xspluv]),
                                              N.concatenate(
                                                  [[0], ysplir, ysplop, yspluv]),
                                              k=k, s=s)

        # Save only OP/IR
        extcurve[iopir] = spline(x[iopir])

    if ccmstyle:
        # normalization to a CCM law (=1 at lbd=5494.5)
        sp = interpolate.UnivariateSpline(rlbda, extcurve / rv, k=k, s=s)
        return sp(lbda) / sp(5494.5)
    else:
        sp = interpolate.UnivariateSpline(rlbda, extcurve - rv, k=k, s=s)
        return sp(lbda)


def fm_unreddened(lbda, flux, ebmv, rv=3.1, lmc2=False,
                  avglmc=False, k=5, s=None):
```

```
    extcurve = fm99_extinction(lbda, rv=rv, lmc2=lmc2, avglmc=avglmc, k=k, s=s)
    return flux * 10. ** (0.4 * ebmv * extcurve * rv)


# Goobar08 extinction law
def goobar08_law(lbd, lbdref, a, p):

    return 1. - a + a * (lbd / lbdref) ** p


def ap_to_rv(a, p, r=0.8):

    return 1. / (a * (r ** p - 1.))


class ExtinctionsPlots(object):

    def __init__(self, dpi=100, wmin=3000, wmax=10000):
        """Extinction laws figures."""
        # Set the different parameters used to create the figures
        self.dpi = dpi
        self.wavelength = N.linspace(wmin, wmax, wmax - wmin)

        # Set the reference wavelength to the one of the CCM law (i.e. 5494.5 A)
        self.ref_wavelengths = {'B': 4394.43, 'V': 5494.51}
        self.cmap = pylab.cm.RdYlBu
        self.num = 100
        self.Rvs = N.linspace(1.1, 4.1, self.num)
        self.Ebmvs = [0.05, 0.2, 0.6]

    def plot_all_figures(self):
        f = [m for m in dir(self)
             if m.startswith('plot')
             and m != 'plot_all_figures']
        for m in f:
            getattr(self, m)()

    def plot_extinction_laws(self):
        fig = pylab.figure(dpi=100)
        print(("Figure %i: Extinction laws" % (fig.number)).center(80, '='))
        print("""
        Avalaible extinction laws from extinction.py
        """)
        gl = "Goobar law".center(30, '-')

        # Compute the goobar extinction law
        a, p = 0.9, -1.5  # Set the values for the MW dust
        goob_ext = goobar08_law(self.wavelength, self.ref_wavelengths['V'], a, p)
        print("""
```

```
%s
Set the values for the MW dust:
a = %.2f ; p = %.2f
Corresponding: Rv =%.2f
""" % (gl, a, p, ap_to_rv(a, p)))

# Compute the CCM extinction law
cl = "CCM law".center(30, '-')
print("""
%s
CCM law for Rv = 3.1
CCM law for Rv = %.1f
""" % (cl, ap_to_rv(a, p)))
ccm_ext = extinction_law(self.wavelength, law='CCM89')
ccm_goob = extinction_law(self.wavelength,
                          rv=ap_to_rv(a, p), law='CCM89')

# Compute the FM extinction law
fl = "Fitzpatrick law".center(30, '-')
print("""
%s
Fitzpatrick law for Rv = 3.1
""" % fl)
fm_ext = fm99_extinction(self.wavelength)

# Compute the O'Donnel extinction law
ol = "O'Donnel 94 law".center(30, '-')
print("""
%s
O'Donnel 94 law for Rv = 3.1\n
""" % ol)
od_ext = extinction_law(self.wavelength, law='OD94')

# Make a figure
ax = fig.add_axes([0.08, 0.09, 0.88, 0.86],
                  xlabel=r'wavelength [$\AA$]',
                  ylabel=r'$A_{\lambda}$/$A_{V}$',
                  title='Extinction laws')
ax.plot(self.wavelength, ccm_ext, '-k',
        lw=3, label='CCM 89, Rv=3.1')
ax.plot(self.wavelength, od_ext, '--r',
        lw=3, label="O'Donnel 94, Rv=3.1")
ax.plot(self.wavelength, fm_ext, '-r',
        lw=3, label='Fitzpatrick 99, Rv=3.1')
ax.plot(self.wavelength, goob_ext, '-.g',
        lw=3, label="Goobar 08 (MW), 'Rv'=%.2f" % ap_to_rv(a, p))
ax.plot(self.wavelength, ccm_goob, '-.k',
        lw=3, label='CCM 89, Rv=%.2f' % ap_to_rv(a, p))
ax.legend(loc='best').draw_frame(False)
ax.set_ylim(ymin=0.3, ymax=2.4)
```

```
        fig.savefig('extinction_laws.png')

    def plot_cardelli_law(self, rv=3.1, ebmv=0.3):
        fig = pylab.figure(dpi=self.dpi)
        print(("Figure %i: Cardelli extinction law" %
               (fig.number)).center(80, '='))
        print("""
        Top panel: Cardelli extinction law parammeters a and b (top pannel).
        Bottom panel:
        - CCM extinction law as A(lbd)/Av = a+b/Rv for Rv = %.2f
        - Interstellar medium transmission for Rv = %.2f and E(B-V) = %.2f.\n
        """ % (rv, rv, ebmv))

        # Create the figure and axes
        ax1 = fig.add_axes([0.06, 0.51, 0.92, 0.42],
                           title='CCM extinction law '
                           '($R_V=%.1f, E(B-V)=%.1f$)' % (rv, ebmv))
        ax2 = fig.add_axes([0.06, 0.09, 0.92, 0.42],
                           xlabel=r'$\lambda$ [$\AA$]')

        # Get the extinction parameters, law and factor (transmission)
        a, b = extinctionParameters(self.wavelength)
        ext_law = extinction_law(self.wavelength, rv=rv)
        ext_factor = extinction_factor(self.wavelength, ebmv, rv=rv)

        # Plot them, adn set the labels
        ax1.plot(self.wavelength, a, 'y', lw=1.5, label=r'$a_{\lambda}$')
        ax1.plot(self.wavelength, b, '-.g', lw=1.5, label=r'$b_{\lambda}$')
        ax2.plot(self.wavelength, ext_law, '--b', lw=1.5,
                 label=r'$A_{\lambda}/A_{V}$ ($=a_{\lambda}+b_{\lambda}/R_V$)')
        ax2.plot(self.wavelength, ext_factor, 'r', lw=1.5,
                 label=r'$T_{\lambda}$ ($=10^{-0.4 \times R_V \times '
                 r'E(B-V) \times A_{\lambda}/A_V }$)')

        # Add lines and annotations about reference filter postions
        ax1.axvline(self.ref_wavelengths['B'], ls=':', color='k', lw=0.8)
        ax1.axvline(self.ref_wavelengths['V'], ls=':', color='k', lw=0.8)
        ax2.axvline(self.ref_wavelengths['B'], ls=':', color='k', lw=0.8)
        ax2.axvline(self.ref_wavelengths['V'], ls=':', color='k', lw=0.8)
        ax1.axhline(0, ls=':', color='k', lw=0.8)
        ax1.axhline(1, ls=':', color='k', lw=0.8)
        ax2.axhline(1, ls=':', color='k', lw=0.8)
        ax1.annotate(r'$\lambda_{B}$',
                     xy=(self.ref_wavelengths['B'] + 10, 3.3),
                     xycoords='data', color='k',
                     horizontalalignment='left', size='large')
        ax1.annotate(r'$\lambda_{V}$', xy=(self.ref_wavelengths['V'] + 10, 3.3),
                     xycoords='data', color='k',
                     horizontalalignment='left', size='large')
```

```
        # Set axes limits to clean the figures
        ax1.set_ylim(ymin=-0.9, ymax=3.8)
        ax1.set_xticklabels([])
        ax1.set_yticks(ax1.get_yticks()[1:-1])
        ax2.set_ylim(ymin=0, ymax=2)
        ax2.set_xticks(ax2.get_xticks()[1:-1])
        ax2.set_yticks(ax2.get_yticks()[1:-1])

        # Set the legends on the two axes
        ax1.legend(loc='best').draw_frame(False)
        ax2.legend(loc='best').draw_frame(False)

        fig.savefig('ccm_law.png')

    def plot_cardelli_law_variability(self):
        fig = pylab.figure(dpi=self.dpi)
        print(("Figure %i: CCM law variability (A(lbd)/Av)"
               % (fig.number)).center(80, '='))
        print("""
        Cardelli extinction law for several values of Rv. This figure express
        the extinction law variability as a function af Rv.\n""")

        ax = fig.add_axes([0.10, 0.09, 0.9, 0.89],
                          xlabel=r'$\lambda$ [$\AA$]',
                          ylabel=r'$A_{\lambda}/A_V$')

        ext = []
        colors = self.cmap(N.linspace(0, 1, len(self.Rvs)))
        for i, rv in enumerate(self.Rvs):
            ext_law = extinction_law(self.wavelength, rv=rv)
            ax.plot(self.wavelength, ext_law, color=colors[i])
            ext.append(ext_law[0])
        scat = ax.scatter([self.wavelength[0]] * self.num,
                          ext, c=self.Rvs, cmap=(self.cmap),
                          visible=False, label='__nolgend__')
        cb = fig.colorbar(scat, format='%.2f')
        cb.set_label(r'$R_{V}$')
        ax.axvline(self.ref_wavelengths['V'], ls=':', color='k', lw=0.8)
        ax.axhline(1, ls=':', color='k', lw=0.8)

        ax.annotate(r'$\lambda_{V}$',
                    xy=(self.ref_wavelengths['V'] + 10, 3),
                    xycoords='data', color='k',
                    horizontalalignment='left', size='large')
        ax.annotate(r'$\frac{A_{\lambda}}{A_{V}} = '
                    r'a_{\lambda} + \frac{b_{\lambda}}{R_V}$',
                    xy=(6400, 1.85), xycoords='data',
                    color='k', horizontalalignment='left', size='xx-large')
        ax.set_ylim(ymin=0.05, ymax=4)
```

```
        ax.set_xlim(xmin=self.wavelength.min(), xmax=self.wavelength.max())

        fig.savefig('ccm_law_variability.png')
```

3.2.4 Plotting specific models in Python

```
import matplotlib.pyplot as plt
import numpy as np
import astropy.units as u
from astropy.table import Table
from dust_extinction.parameter_averages import CCM89, F99
from synphot import units, config
from synphot import SourceSpectrum,SpectralElement,Observation,ExtinctionModel1D
from synphot.spectrum import BaseUnitlessSpectrum
from synphot.reddening import ExtinctionCurve
import astropy.visualization
```

Cardelli, Claython & Mathis interstellar extinction model ([CCM89]).

```
    # Create wavelengths array.
wav = np.arange(0.1, 3.0, 0.001)*u.micron

for model in [CCM89]:
    for R in (2.0,3.1,4.0,5.0,6.0):
        # Initialize the extinction model
        ext = model(Rv=R)
        plt.plot(1/wav, ext(wav), label=model.name+' R='+str(R))

plt.xlabel('$\lambda^{-1}$ ($\mu$m$^{-1}$)')
plt.ylabel('A($\lambda$) / A(V)')
plt.legend(loc='best')
plt.title('CCM89 extinction model')
plt.show()
```

Comparison between CCM model and Fitzpatrick & Massa ([Fit99]) parametrization.

```
        # Create wavelengths array.
wav = np.arange(0.1, 3.0, 0.001)*u.micron

for model in [CCM89,F99]:
    for R in (2.0,3.1,4.0,5.0,6.0):
        # Initialize the extinction model
        ext = model(Rv=R)
        plt.plot(1/wav, ext(wav), label=model.name+' R='+str(R))

plt.xlabel('$\lambda^{-1}$ ($\mu$m$^{-1}$)')
plt.ylabel('A($\lambda$) / A(V)')
plt.legend(loc='best')
plt.title('CCM vs FM comparison')
plt.show()
```

A wide comparative overview of the most known extinction models in the literature.

```
import numpy as np
import matplotlib.pyplot as plt
from matplotlib.ticker import ScalarFormatter
import astropy.units as u

from dust_extinction.parameter_averages import (CCM89, O94, F99, F04,
                                                VCG04, GCC09, M14, F19, D22,
                                                G23)

fig, ax = plt.subplots(ncols=2, figsize=(10, 4))

# generate the curves and plot them
x = np.arange(1./30., 1./0.0912, 0.001)/u.micron

Rv = 3.1

models = [CCM89, O94, F99, F04, VCG04, GCC09, M14, F19, D22, G23]

for cmodel in models:
   ext_model = cmodel(Rv=Rv)
   indxs, = np.where(np.logical_and(
      x.value >= ext_model.x_range[0],
      x.value <= ext_model.x_range[1]))
   yvals = ext_model(x[indxs])
   ax[0].plot(1./x[indxs], yvals, label=ext_model.__class__.__name__)
   ax[1].plot(1./x[indxs], yvals, label=ext_model.__class__.__name__)

for iax in ax:
   iax.set_xscale('log')
   iax.xaxis.set_major_formatter(ScalarFormatter())

   iax.set_xlabel(r'$\lambda$ [$\mu$m]')
   iax.set_ylabel(r'$A(\lambda)/A(V)$')

ax[0].set_title(f'UV-NIR R(V) = {Rv}')
ax[0].set_xlim(0.08, 3.0)
ax[1].set_title(f'NIR-MIR R(V) = {Rv}')
ax[1].set_xlim(1.0, 32.0)
ax[1].set_ylim(0.0, 0.50)

ax[0].legend(loc='best')
ax[1].legend(loc='best')
plt.tight_layout()
plt.show()
```

3.2.5 Analyses and comparisons with the literature

'Standard' theoretical model of Cardelli, Claython & Mathis (CCM89 in the previous plots) shows proper behaviour, well discussed in sec. 3.1.
As fig. 3.3 displays, extinction curves of this kind have the classical structure: a (quasi)linear trend in the infrared and in the visible, with the characteristic UV bump at $\sim 2200\,\text{Å}$ and the UV-rise in the far ultraviolet domain. The noticeable aspect here is how curves change their steepness at different values of R_V: it is evident that the more the value of this parameter the 'lower' the effect of extinction (at the same wavelength), i.e. the analytical behaviour becomes more and more (quasi)linear. Recalling the operative definition of R_V (eq. (2.17)), this can be described as an anti-correlate effect of $E(B-V)$ ($R_V \propto E(B-V)^{-1}$).

It is interesting the comparison between CCM89 and Fitzpatrick & Massa parametrization shown in fig. 3.4. FM99 is based on the consideration reported in [Fit99]: it is very similar to Cardelli *et al.* paper with a proper focus on UV range. In fact, with the same R_V values, one can denote slight differences at shorter wavelengths: this is due to analytic discrepancy on parametric expression in this domain. As reported by several articles in the literature, both CCM89 and FM99 meet very good fits with observational data. Fig. 3.6 displays this aspect.

Similarly, Cardelli *et al.* model describes a good match with observations (see fig. 3.1 and fig. 3.2)

A further confirmation in this sense is emphasized in fig. 3.7: from a sample of 80 Galactic extinction curves computed from IUE satellite data, it is possible to denote the goodness of the aforementioned parametric fit, even if the UV range continues to remain really hard to be described with a proper behaviour (this might be due to the nature of UV bump and the physical properties of its carrier; see chapter 6 for a summary).

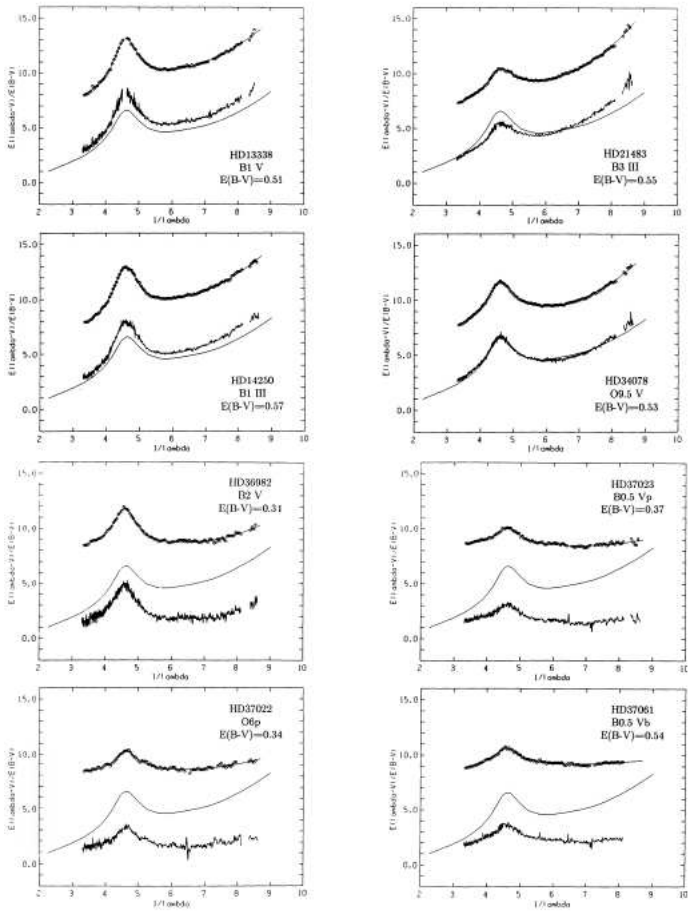

Figure 3.6: Extinction curves for a sample of O-B stars with different reddening. The lower portion of each plot shows the un-binned data, along with the parametric model (solid black line). Displaced by five units (typically) above these curves are the binned data, represented as discrete points. The star's name, spectral type and colour excess are included. Further details on the cited paper.
Figure from [FM90], pag.10.

3.3 Incongruencies within CCM-model

Cardelli *et al.* (1989) is a pioneering work considering light extinction in the interstellar medium; this model is now a benchmark in this field. Nevertheless, it presents some nasty points which can create unwanted results.
First, a brief recap.

3.3.1 Introductory overview

Trumpler (see [Tru30]) demonstrated that extinction of starlight must exist, amounting to $\sim 50\%$ (0.7 magnitude in astronomical brightness) for every 100 parsec of distance in the Galactic plane, otherwise open cluster diameters would increase systematically with distance, a most unlikely situation.
Historically, there were observations which seemed to not confirm Trumpler's extinction value, depending on the chosen line of sight (and so distance).
For example, earlier in the century, Kapteyn ([Kap09]) inferred 1.0 magnitude of

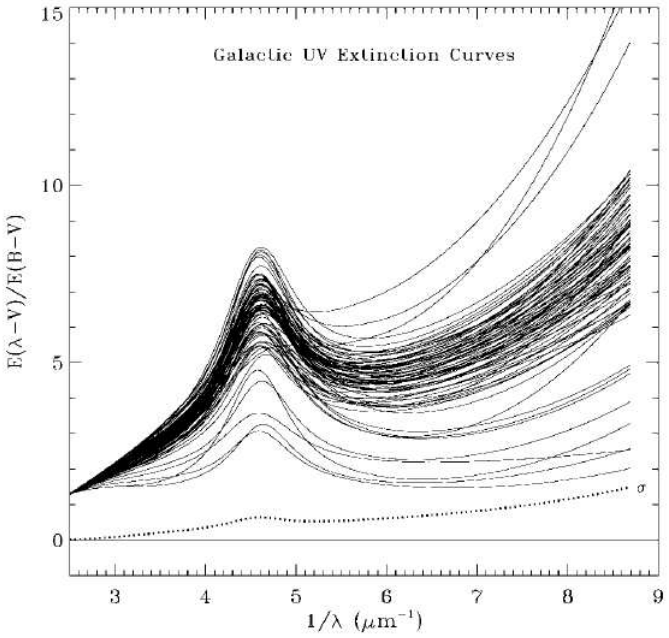

Figure 3.7: Examples of 80 Galactic UV extinction curves derived from IUE satellite observations. Analytical fits to the curves are shown, based on Cardelli *et al.* parametrization and on the work of Fitzpatrick & Massa (1990). The curves are taken from the Fitzpatrick & Massa catalogue. This figure demonstrates the enormous range of properties exhibited by UV extinction in the Milky Way. The dotted line, labelled "σ", shows the standard deviation of the sample scaled to the value $\sigma(1500)\,\text{Å} = 0.74$, as derived from ANS satellite data (see the cited paper for details). Figure from [Fit99], pag.3.

extinction per kpc from star counts in the direction of the Galactic centre; on the other hand, NGC 1893 towards the anticentre contains stars displaying extinction of only ~ 1.2 magnitudes at a distance of ~ 4 kpc.
Trumpler's work, in addition, is important also because in the process it revealed the nature of yet another component of the Galaxy: interstellar dust.

Today is better known a correlation between interstellar extinction and wavelength (λ) dependence through spectrophotometry of hot stars (spectral types O, B, A); cooler stars (spectral types F, G, K) show a lot of contaminations and other abundances in their spectra which make extinction hard to detect.
Therefore, at visible and near-infrared wavelengths, interstellar extinction depresses stellar continua in magnitude units in nearly linear fashion as a function of λ^{-1} (as it can be easily seen in fig. 3.8).

It is convenient to graph the effects of interstellar extinction on stellar continua using a colour difference diagram, which plots continuum depression in stellar magnitudes (i.e., interstellar extinction along the y-axis) as a function of inverse wavelength (λ^{-1}, along the x-axis).
It can be noted that the extinction is nearly linear as a function of λ^{-1} from $0.8\,\mu\text{m}^{-1}$ ($\lambda = 1.2\,\mu$m) to $2.3\,\mu\text{m}^{-1}$ ($\lambda = 0.435\,\mu$m). Deviations from a linear law occur at shorter wavelengths, namely at $\lambda < 0.435\,\mu$m ($= 4350\,$Å), where the ultraviolet interstellar extinction normally displays some curvature. At such wavelengths, the amount of extinction appears to be less than that expected from

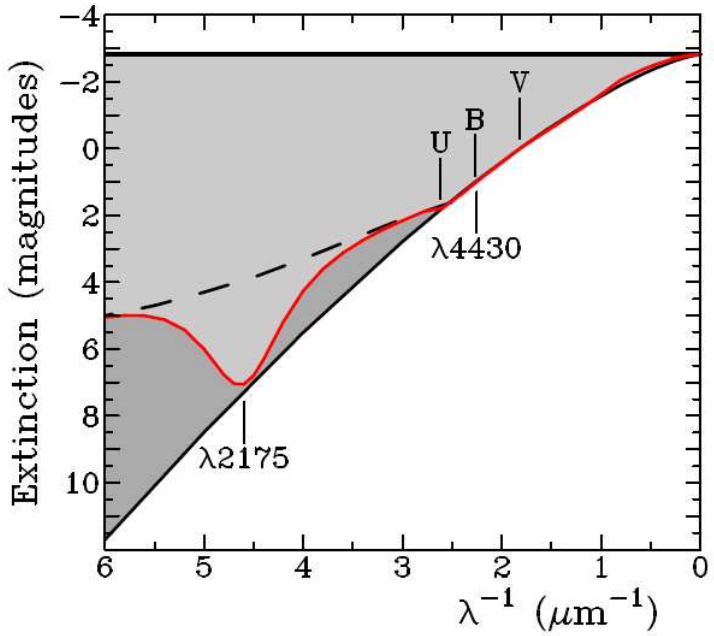

Figure 3.8: A schematic colour difference diagram illustrating a simple $\lambda^{-1.375}$ extinction law, normalized to $A_V = 0$ for $E_{B-V} = 1.0$ and $R_V = 2.82$, shown as the black curve relative to the stellar continuum (horizontal line). The standard Cardelli *et al.* extinction law is shown by the red curve for the same value of R_V, the grey area representing the depression of the stellar continuum by the effects of interstellar extinction for that law. The dashed line lying above the solid curve in the ultraviolet region represents forward scattering starlight (the dark grey area) by Raleigh scattering according to Zagury ([Zag13]; see chapter 5 for details). Vertical lines denote the location of diffuse interstellar bands at 2175 Å and 4430 Å, as well as the U, B and V bands for Johnson system photometry.
Figure from [TMB14], pag.2.

a simple continuation of the linear law at visible and infrared wavelengths.
It is also expected, by induction, no extinction at infinitely long wavelengths.

3.3.2 Extinction as scattering process: alternative parametrizations to CCM-model

In the UBV photometric Johnson system, the degree of linearity of the extinction curve can be assessed using the parameter E_{U-B}/E_{B-V}, i.e. the ratio of the reddening E_{U-B} (seen as the difference in magnitudes between U and B bands) with respect to the similar amount E_{B-V} (same as before but between B and V bands). This ratio can also be written as

$$\frac{E_{U-B}}{E_{B-V}} = X + Y \times E_{B-V}$$

where:

- Y is the *curvature term*, arising from the changing wavelength sensitivity of broadband filters on stellar continua as reddening increases.

A mean value is of the form:

$$Y = 0.021 \pm 0.006$$

- X is the *slope of the reddening line*, which varies with position along the Galactic plane. A linear extinction law implies (see [Nan64]):

$$X = 0.83$$

Clearly, correcting for the effects of interstellar reddening and extinction is essential for nearly all studies in Galactic astronomy tied to observations at optical wavelengths. Extinction corrections (e.g. A_V in the visual domain) are made from a star's measured reddening E_{B-V}, using the ratio of total-to-selective extinction $R_V = A_V/E_{B-V}$ applicable to dust extinction towards the object.
Observed values of R_V are found to vary with Galactic location, as also noted by Cardelli *et al.*. CCM extinction law, predicts, among other features, that variations in X and R_V should be linearly related (see fig. 3.9); for this reason, it is common the usage of mean reddening laws with a value of $R_V = 3.1$ by convention.

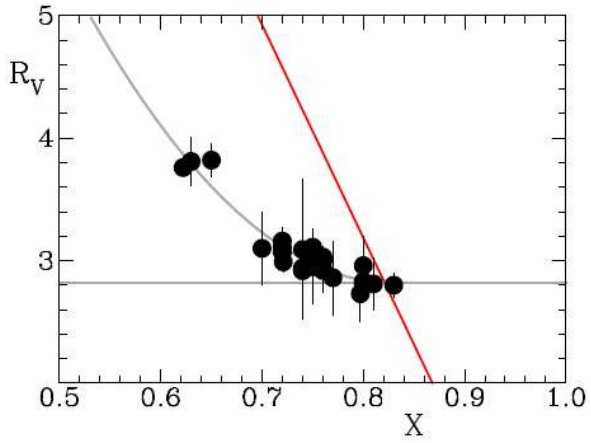

Figure 3.9: The variation of R_V (observed) with reddening slope X.
The illustrated quadratic fit reaches a minimum at $R_V = 2.82$ for $X = 0.83$. Shown for comparison is the linear trend (red line) expected from the formulae of Cardelli *et al.* (see subsec. 3.1.1). Figure from [TMB14], pag.3.

As seen in the previous section, the CCM-model ([CCM89]) established that interstellar extinction, from the infrared to the far-UV, can be parametrized using empirical polynomial functions with a dependence on only one parameter, R_V, in addition to reddening E_{B-V}. On the other hand, these formulae are tied to complex polynomial fits (with up to 7^{th}-order terms) that have no particular physical meaning. In some cases the cited fits to observations are not particularly accurate (e.g., reddened stars with no 2175 Å bump) and may be considerably improved if a dependence of the bump itself on E_{B-V} is introduced. Therefore, the decision by Cardelli *et al.* that R_V is the free parameter of interstellar extinction does not appear to be an accurate choice.

An alternative approach to the extinction law has been developed by Zagury (2013): he suggests that the existence of linear extinction over the entire infrared, through the optical region, and the one-parameter dependence of the CCM-model normalized extinction curves in the UV and far-UV are incompatible with potential variations in three independent types of particles from one interstellar dust cloud to another.
As it will be clearer in chapter 5, Zagury supposes that the lack of extinction relative to a simple λ^{-1} relation observed in the near UV does not result from a change in the properties of interstellar grains, but is the consequence of forward scattered starlight by interstellar gas clouds along the line of sight to the observer enhancing the observed amount of radiation from a star. As yet it is the only alternative to classical interstellar grain models.
This view requires that the scattered light be coherent scattering by hydrogen in the forward direction; in such a situation, true interstellar extinction becomes a simple case of Mie scattering over the entire infrared to far-UV wavelength region, with an extinction law described by

$$A(\lambda) \propto \lambda^{-p} \tag{3.9}$$

where p is related to the size distribution of the dust grains responsible.
A value of $p = 1$ (the simplest situation) would imply an invariant value of $R_V = 4$ throughout the Galaxy, whereas observed values of $R_V \simeq 3$ are typical of most Galactic fields. Associated values of p for interstellar extinction must therefore lie in the range 1.3-1.4, which is similar to what is observed for atmospheric aerosols. By implication, the size distributions of atmospheric and interstellar dust particles must be governed by similar physical mechanisms.

An important aspect of the Zagury description of interstellar extinction is how it affects the interpretation of observations in the UV. For Cardelli formulation, all extinction originates from interstellar dust particles in accordance with their size distribution, in conjunction with the spectroscopic properties of the constituents, which contribute specific absorption dips via atomic and molecular transitions, such as that observed at 2175 Å; on the other hand, according to Zagury's proposal, the extinction rise in the UV that generates the pseudo-continuum (on which the 2175 Å feature is superimposed) is an artefact of a separate process, namely forward scattered starlight that varies as λ^{-4} (depicted schematically by the dashed line in fig. 3.8). In this alternative scheme, interstellar extinction alone closely follows the already displayed $\lambda^{-1.375}$ relation.

Forward scattering of starlight can be a relatively efficient process for particles with small dimensions relative to wavelengths of light being scattered.
According to [Zag13], the origin of this phenomenon in the far-UV arises when light from a star passes through a distant cloud of hydrogen; depending upon the relative distances of the star, cloud and observer, a relatively thin cloud of hydrogen sufficiently distant from both a reddened star and Earth will redirect starlight along the line of sight to the star. In this way, the proportion of forward scattered light can be more than an order of magnitude greater than the incident starlight in the forward direction, thereby accounting for an artificial λ^{-4} continuum in the far-UV.

In this context, the 2175 Å bump is naturally seen as an interruption of the scattered starlight, although its physical origin is unclear. One possible alternative explanation is related to resonance processes linked to coherent scattering: it

may be related to the strong diffuse interstellar band (see chapter 4 for details) at 4430 Å and perhaps to the weaker DIB at 6614 Å (about twice and three times the bump's wavelength, respectively). This is due to the fact that the strength of the DIB at 4430 Å is known to correlate quite closely with the strength of the 2175 Å bump, so a similar origin[4] of both features is expected.

This alternative interpretation of interstellar extinction solves a number of anomalies left unexplained by interstellar grain models and CCM formulation, in particular the existence of clearly reddened ($E_{B-V} > 0$) stars that display no far-UV rise or 2175 Å absorption. Such stars show UV extinction that varies roughly as $\lambda^{-1.375}$, so the lack of a far-UV rise or 2175 Å absorption must be attributed to the lack of a hydrogen cloud sufficiently distant from the reddened star and Earth to generate forward-scattered starlight.

In addition, Zagury's idea of seeing extinction as a scattering-related phenomenon leads to interesting predictions regarding the optical reddening law and observed values of R_V.
If scattered starlight is strong enough in the UV, it will gradually become more important in the optical wavelength region, first in the standard U band and then in the blue B band; it might even contribute a very minor component in the visual V band. The effect is to decrease the colour excesses E_{U-B} and E_{B-V} for a star systematically from their true values, more so for E_{U-B}, with a related effect on the observed reddening slope X.
So, if we consider extinction behaviour as $A(\lambda) \propto \lambda^{-1.375}$, the true value for the ratio of total-to-selective extinction is $R_V = 2.82$: in this framework, also the value of R_V has to increase. Observed values of X should therefore decrease under such conditions; finally, the minimum of observed R_V values should correspond to the true value for interstellar extinction without a scattered light component, producing the best p-value that fits the interstellar grain extinction law of Zagury.

It is consequential now to infer that the relationship between X and R_V has to be more complex than linearity, namely it has to be at least quadratic in reddening ($\propto E^2_{B-V}$).

3.3.3 Dependence of R_V (observed) on X

Establishing an estimate of reddening slope X for any star field is a challenging task that requires high-quality photometry and spectral types for stars in the field. The Cardelli *et al.* formulation in the optical and infrared is tied mainly to colour difference data for stars, which can introduce unwanted systematic effects. Therefore, the use of high-quality data for stars in restricted star fields is just as effective and helped to generate the observational correlation between R_V (observed) and X: this study was completed and improved by Turner ([TMB14]), involving data of open clusters containing Cepheid variables and globular clusters such as M14 (in this last case with some adjustment due to the particular nature of the source: M14, indeed, is one of only a few clusters in the well-studied field of Upper Scorpius affected by differential reddening).
A compilation of the results of this study is given in fig. 3.10, whose data have been already displayed in fig. 3.9.

[4]Several studies (see [Zim82] and [SG06]) have pointed out the origin as two-photon absorption process from molecular hydrogen (H_2) under conditions of induced resonance Rayleigh scattering.

Region	X	R_V	±s.e.
Berkeley 58	0.750	2.95	±0.30
Berkeley 59	0.800	2.81	±0.09
NGC 129	0.760	3.01	±0.07
NGC 654	0.760	2.92	±0.16
IC 1805	0.760	3.01	±0.06
Alessi 95	0.830	2.80	±0.10
Pleiades	0.750	3.11	±0.15
NGC 1647	0.770	2.86	±0.30
CV Mon	0.760	3.03	±0.07
NGC 2439	0.760	3.00	±0.10
Westerlund 2	0.630	3.81	±0.20
Ruprecht 91	0.650	3.82	±0.13
Lyngå 2	0.720	3.16	±0.10
NGC 5617	0.720	3.07	±0.11
Pismis 20	0.740	2.92	±0.16
NGC 6193	0.760	2.93	±0.19
Messier 4	0.622	3.76	±0.07
NGC 6611	0.721	2.99	±0.08
Trumpler 35	0.740	2.92	±0.10
Collinder 394	0.700	3.10	±0.10
NGC 6830	0.720	3.11	±0.16
NGC 6834	0.750	2.96	±0.13
SU Cyg	0.740	2.94	±0.38
P Cyg	0.797	2.73	±0.23
NGC 7062	0.810	2.81	±0.21
Trumpler 37	0.800	2.83	±0.12
NGC 7128	0.800	2.96	±0.24
NGC 7654	0.750	3.03	±0.15
NGC 7790	0.740	3.09	±0.57

Figure 3.10: Reddening and extinction data for galactic fields.
Figure from [TMB14], pag.4.

As anticipated in previous sections, the observational trend shown in fig. 3.9 appear to follow a quadratic behaviour rather than the linear relation expected by CCM-model. A least square quadratic solution to the data has a minimum at R_V (observed) and consequently a value for X of:

$$R_V = 2.82 \pm 0.06 \Longleftrightarrow X = 0.83 \pm 0.01$$

By implication, the true value of R_V for interstellar extinction is 2.82 and is associated with an interstellar reddening law of slope $X = 0.83$.
Smaller reddening slopes X and larger values of R_V (observed) must be artefacts of enhanced forward scattered starlight in the UV permeating disproportionately into the optical wavelength bands. The provided data show a specific range in value for the extinction parameter, with $2.8 \lesssim R_V \lesssim 4$; a similar domain can be set for the reddening slope, with $0.62 \lesssim X \lesssim 0.83$. These numbers may represent the maximum variation possible for apparent extinction in the Milky

Way by interstellar dust clouds intermingled with clouds of hydrogen. Therefore, the large values of R_V (observed) $\simeq 5$ cited for stars in some H II regions must represent unique circumstances associated with neutral extinction that enhances the overall extinction towards an object with minimum influence on the reddening slope X.

In conclusion, reliance on [CCM89] results for correcting for the effects of interstellar extinction in the Galaxy can no longer be supported according to fig. 3.9: CCM model, in fact, predicts variations in both reddening slope X and ratio of total-to-selective absorption R_V (observed) that exceed the range of observed values (fig. 3.10). The tendency seems to suggest the use of relationships more suitable to the specific regions under investigation and not of general value in correcting interstellar extinction.

3.3.4 Summary

The nature of interstellar extinction in the Galaxy was tested by Turner *et al.* using empirical observational data related to variations in reddening slope X ($= E_{U-B}/E_{B-V}$ for small reddening) and observed ratio of total-to-selective extinction R_V, for stars in well-studied galactic fields, typically regions of open clusters where the properties of the extinction do not vary appreciably from one star to another. The derived quadratic variation of R_V (observed) with X is presumably related to increasing amounts of forward-scattered starlight in the UV, affecting the optical colour excesses E_{U-B} and E_{B-V}, as well as R_V (observed), in a systematic fashion, the effect increasing in direct proportion to the amount of forward-scattered starlight in the ultraviolet. The observed dependence differs markedly from expectations predicted by the Cardelli *at al.* relationship for interstellar extinction.

A major repercussion of the present findings is that the use of the CCM formulae to correct for interstellar extinction is no longer justified. Although total extinctions for dust obscuration are made from observations over the visual and infrared *V*-*R*-*I* bands in order to minimize potential variations from the Galactic mean, it should be noted that dust extinction described by a $A(\lambda) \propto \lambda^{-1.375}$ absorption model predicts different intrinsic infrared colours from those usually adopted, as well as less total extinction A_V. The differences might appear to be small, but tests indicate that they are significant: for example, the 2175 Å feature observed towards galaxies at high Galactic latitude is generally weak or absent, despite non-zero reddenings for the galaxies, implying that a value of $R_V = 2.82$ is applicable for them.

Chapter 4

Diffuse Interstellar Bands

Superimposed on the extinction curves are a huge number of absorption lines, the so-called **Diffuse Interstellar Bands** (**D.I.Bs.**). The identification of the DIB carriers remains an important problem in astronomy; the current number of $\sim$ 200 DIBs ([Tua+00]) is still increasing, suggesting that more absorption lines of this kind could be detected in the interstellar medium. The development of DIB research in recent years indicates that most DIB carriers could be large carbon-bearing molecules which reside ubiquitously in the interstellar gas.

4.1 Historical overview

The first mention of the DIBs was published by Heger in 1922, who pointed out the *stationary* (i.e. 'interstellar') nature of the absorption features at 5780 Å and 5797 Å. The first paper making an issue of the features (and reporting the existence of several others) came some years later and it is often cited as the true beginning of the DIB problem: it is Merrill's work, in 1934 (see [Mer34]).
Soon after the publication of the aforementioned paper, several astronomers started to speculate on the origin of the DIBs, with initial suggestions regarding molecules, although no specific species were initially mentioned (e.g. Russell 1935, Swings 1937, Saha 1937). In the meantime, observational research identified a few more bands; in the 1950s, speculations about their origins turned to solid-state transitions (McKellar *et al.* 1955), while the molecular hypothesis continued to remain in the background (Herzberg 1958).

The quality data at that time was generally poor by today's standards, either because the spectra were photographic and/or were low-dispersion (including some photoelectric surveys done with filters providing virtually no spectral information). The possibility of molecular carriers was widely disregarded during these middle years, largely because ion-molecule reaction schemes were generally unknown to astronomers who, therefore, thought there were no sufficiently rapid mechanisms for forming molecules in significant quantities in the diffuse interstellar medium. This began to change in the 1960s and 1970s, as millimetre-wave observers began to find copious quantities of molecules in dense clouds, and at the same astronomers became aware of the potential of ion-molecule reactions to efficiently produce complex species. The entire scientific community was beginning a laborious turn back toward the molecular hypothesis for the DIBs.

4.2 Properties of the diffuse bands

The most recent era in diffuse band research has been advancement on two fronts:

1. The development of better observational tools and the accompanying improvement in data quality;

2. The involvement of traditional chemists in research on the problem.

The most significant instrumental advance has been in the area of electronic detectors, particularly CCDs and other linear devices such as reticons.
These detectors allow the possibility of obtaining spectra with signal-to-noise ratios in the hundreds, rendering unambiguous several previously disputed characteristics of the DIBs. For example, it became possible in short order to rule out the existence of either emission wings or subtle band profile variations that might have been expected from solid-state absorbers. High-quality spectra have also yielded clear evidence for multiple band carriers and for many very weak features.
The interest in DIBs on the part of chemists, on the other hand, has brought new data to bear on the problem. Laboratory studies are being conducted on candidate species and theoretical analyses are being used to constrain the properties of the carriers. Today $\sim$ 200 DIBs have been reported, ranging from the blue (near 4000 Å) to the near-infrared (out to nearly 9000 Å).

As already mentioned, the DIBs are broader than atomic lines, so their interstellar character is not immediately obvious. They were originally identified as *interstellar* on the basis of their 'stationary' nature (i.e. they do not share the periodic Doppler shifts in binary stars, thus ruling out a stellar origin).
Further evidence comes from the fact that they generally correlate with other interstellar parameters such as extinction, gas column densities and distance. Another observational property is their complete absence in stars that have little or no extinction or reddening due to dust, and their lack of any dependence on stellar spectral type (this tends to argue against a circumstellar origin as well).

Detecting and measuring the DIBs can be difficult, especially for the broader and weaker among them. For these bands, it is often necessary to compare reddened and unreddened stars of similar spectral type, dividing one by the other in order to remove stellar lines. This is the case shown in fig. 4.1, where the provided DIBs have been obtained with this type of spectral computation. It is worth noting the low quality of the presented spectrum: this is due to the poor technology available at that time and the consequent techniques used.

This may not always be necessary for the stronger and narrower DIBs, so long as there are no blends with stellar lines.
Widths of the DIBs vary from something less than 1 Å FWHM (e.g. the 6613 Å band) to nearly 30 Å (the well-studied 4430 Å feature). Some of the very weak bands recently recognized may be considerably narrower than 1 Å, and it is always possible that weak bands bigger than $\lambda = 4430$ Å may have escaped detection. Band depths are usually only a few percent of the continuum, which can make the broad features difficult to detect or measure accurately, particularly when blended with stellar photospheric lines.

The profiles of the DIBs come in many forms, including symmetric bands as well as asymmetries toward either the blue or the red. Perhaps the most

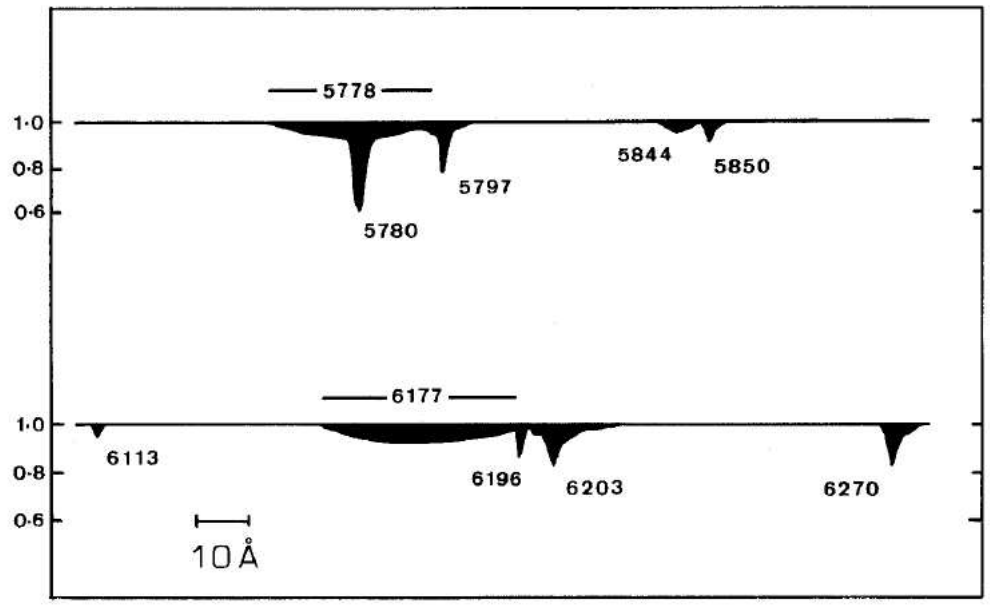

Figure 4.1: A schematic representation of diffuse bands in the yellow-red region of the spectrum, based on intensity traces for the reddened star HD 183143 (data from Herbig 1975). Interstellar absorptions are shown in the wavelength range 5730-5900 Å (top) and 6110-6280 Å (bottom). Photospheric and telluric features in the spectra are eliminated with reference to corresponding data for a comparison star (β Orioni) of similar spectral type and low reddening.
Figure from [Whi18], pag.105.

significant finding about DIB profiles is their apparent invariance: despite early claims (based on photographic spectra) that profile variations were seen in some of the bands, modern data have failed to reveal any discrepancies from star to star that could not be attributed to Doppler components in discrete interstellar clouds.
An example of a high-quality DIB spectrum is reported in fig. 4.2, a detail of which is better provided in fig. 4.3.

Another outstanding characteristic of the DIBs is the relative lack of features in the blue and near-UV. Until recently, no sign of a diffuse band at wavelengths below 4430 Å was reported, and even now only a few very weak features have been seen, between 3900 Å and 4200 Å. The major limitations on the sensitivity for detecting features were imposed by the fact that:

- Hot stars have very crowded photospheric spectra at these wavelengths, creating much 'noise' in the continuum due to stellar lines;
- The extinction is so high in the UV that stars reddened enough to have strong diffuse bands are hopelessly faint.

As a result, the UV observations are confined to stars with rather weak optical DIBs. Nevertheless, this particular observational property can be used to make some strict constraints on the nature of DIB carriers.

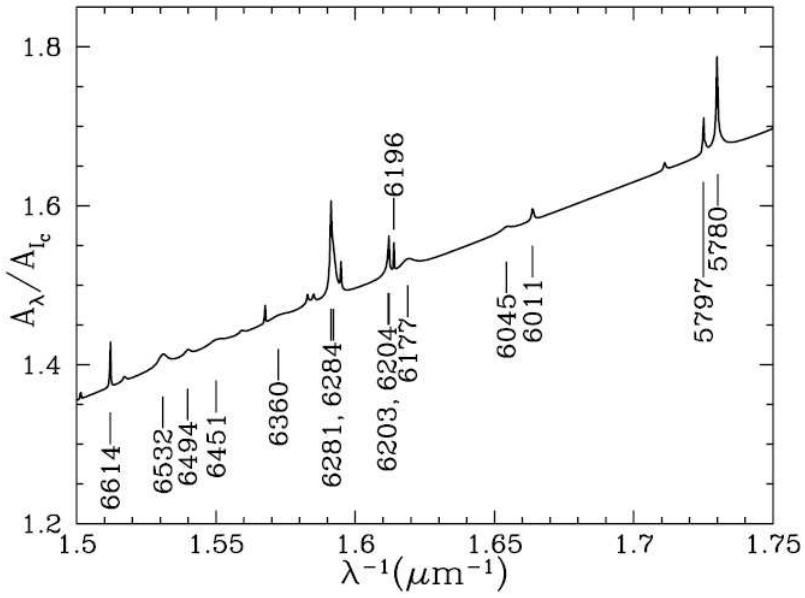

Figure 4.2: Extinction at wavelength λ (relative to the extinction at $I_C = 8020\,\text{Å}$) for $5714\,\text{Å} < \lambda < 6667\,\text{Å}$, showing some of the diffuse interstellar bands, based on the compilation by Jennisken & Desert (1994). Figure from [Dra10], pag.270.

4.3 Constraints on diffuse band carriers

There are a number of observational constraints which must be satisfied.

- *Ability of a proposed carrier to form and survive under interstellar conditions.*
  A DIB model must involve chemical-physical elements that are diffuse in the interstellar medium and can survive in those conditions, according to observational features in spectra. For instance, in the 1950s and 1960s, it was not even considered a molecular origin for the DIBs because it seemed clear that molecules could not form and survive under the harsh conditions of the diffuse interstellar medium;

- *Invariance of wavelengths and profiles.*
  The observed DIBs appear to be constant from star to star in terms of central wavelengths and band profile, even though regions known to have variable properties such as dust grain size are sampled. This constraint poses a serious challenge to any solid-state absorber model for the DIBs, because in such models there should be profile variations and possibly emission wings, which are not seen;

- *Narrow widths of some DIBs.*
  It is significant that some of the DIBs are too narrow to be solid-state absorption features (e.g., the well-known 6614 Å band, which has a FWHM of less than 1 Å);

- *General correlation with other interstellar quantities.*
  This is not a very stringent constraint but it is useful to discriminate against circumstellar models for the DIBs, for which no correlation with interstellar reddening (for example) would be expected;

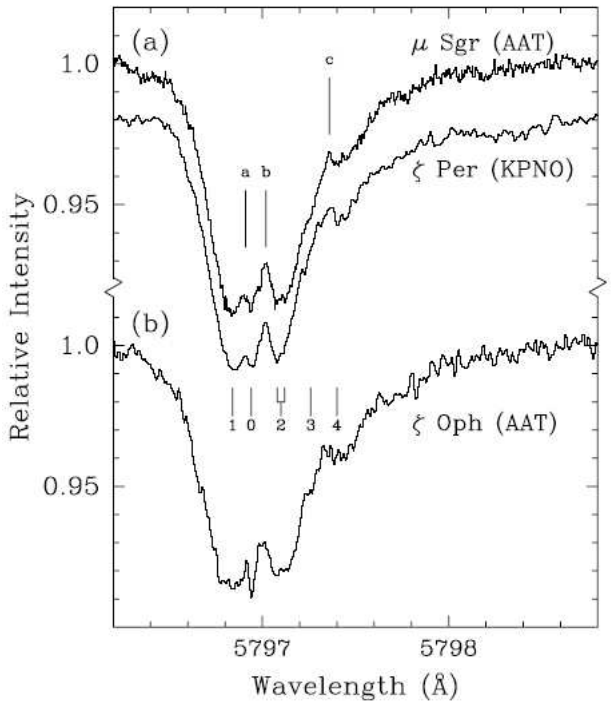

Figure 4.3: Fine structure, possibly due to molecular rotation, in the $\lambda = 5797$ Å DIB, on 3 different lines of sight. This and similar structure seen in other bands strongly suggests that at least some DIBs arise in large free-flying molecules (i.e. ultrasmall dust grains). Data from Kerr *et al.*, 1998.
Figure from [Dra10], pag.270.

- *Correlations among the bands ('families' of DIBs).*
  Observationally speaking, if there are groups of DIBs which share common features they could have the same origin. However, the reality or significance of these groupings is not clear, as different samplings of stars appear to yield different groupings of DIBS. One possible turn-around in the grouping of DIBs is that several sets of these features could have originated by different carriers, suggesting how many elements are involved in the process and they can help to discriminate against models that try to unify DIBs (which are clearly unrelated on the basis of correlation studies);

- *Environmental constraints.*
  It seems that DIBs are weak or absent in dense clouds, suggesting that their carriers are modified or destroyed (or simply not formed) in these regions. Unlikely this evidence may be counter-intuitive and go against the molecular hypothesis, the constraint is very useful to deduce which kinds of molecules are viable and which are not. For instance, the weakness of the DIBs in dark clouds could support mechanisms involving molecular cations or other species that require UV radiation for their existence; similarly, the absence (or weakness) of diffuse bands in circumstellar environments appears to rule out species that form in the close environs of stars having circumstellar shells, suggesting that long-term exposure to interstellar conditions or some other kind of processing is required before material can acquire its DIB-absorbing properties;

- *Lack of ultraviolet DIBs.*
  Sensitive research for DIBs at ultraviolet wavelengths has not yet been carried out, but it seems likely that the number and intensity of DIBs diminishes below 4430 Å. This is something that has to be explained by any successful DIB model;

- *Emission in the Red Rectangle.*
  The Red Rectangle is a unique patch of nebulosity with a hot star embedded within it, which gives rise to a wide variety of optical emission lines. Many have been identified as molecular, with the appearance of several clear molecular band series;

- *Fine structure in DIB profiles.*
  One of the perplexing challenges to the molecular hypothesis for the DIBs has been the difficulty in finding any hint of rotational-vibration band structure in any of the profiles. But recent observations have begun to reveal a structure that is very likely of molecular nature (see fig. 4.3), i.e. details that are not due to Doppler components along the lines of sight but intrinsic;

- *Cosmic abundance constraints.*
  Finally, the ingredients for making DIB carriers must be quite abundant. The total absorption due to all of the known DIBs is enormous, requiring substantial quantities of raw materials. Clearly, these elements must be cosmically quite diffuse and a deeper focus is needed in the following section.

4.3.1 Cosmic abundance constraints

According to the previous paragraphs, it is quite accepted nowadays the molecular nature of DIBs because only these kinds of compounds can satisfy all the constraints just listed. The challenge regards finding out which molecules can be the carriers for these spectral features. Most current speculation, based on observational evidence (for details, see sec. 4.4), is focused on *organic* molecules, i.e. carbon-based compounds. There are two main reasons for thinking in this way:

1. *All (or most of) the complex molecules known or suspected to exist in the interstellar medium are organic.*
   For instance, the majority of the species identified through millimetre-wave emission lines in dark clouds are **carbon chains** and related species, or in the infrared domain there are a lot of spectral features that are almost certainly caused by C-C and C-H bonds (popularly thought to be in the form of PAHs, i.e. Polycyclic Aromatic Hydrocarbons);

2. *Specific types of organic molecules have been shown to have appropriate spectra.*
   This means that candidate species or families of molecules have been demonstrated to have the required general spectroscopic properties. For instance, carbon chains are found to have numerous visible-wavelength transitions falling within the range where DIBs are common (see [Ful+93]).

Therefore, within the molecular hypothesis, there is particular evidence that DIBs are produced by organic molecules, i.e. carbon-based compounds.

However, according to Snow & Witt (see [SW95]) there is not as much carbon available for the formation of interstellar molecules as expected.
C-atom abundances in the solar system are enhanced with respect to other stars in the galactic disk; this has the corollary that studies of the interstellar carbon abundance, which are normally based on the assumption that the galactic carbon budget is the same as the solar one, have been overestimating the quantity of carbon available to make interstellar dust and other carbon-based species. Reviews of stellar composition studies show very clearly that the solar system is overabundant in carbon and several other heavy elements. Young stars have substantially less carbon than the Sun, indicating that the overall abundance of carbon in the ISM is less (by nearly a factor of ~ 2) than normally thought.

To have a quantitative idea of what has been discussed until this point, it is possible to assess how much carbon is available in the ISM for the DIBs.
With reference to Snow & Witt aforementioned paper, we consider a typical line of sight having strong diffuse bands (e.g. HD 183143); it is found that the total equivalent width of all the DIBs in the spectrum of this star is about 22 Å.
Assuming the DIBs are unsaturated, this implies a total absorbing column density:

$$N = \frac{10^{14}}{f} \ \mathrm{cm}^{-2}$$

where f is the representative oscillator strength of the diffuse band transitions.
If each carrier contains m-carbon atoms, then the column density of carbon atoms required to produce the DIB spectrum toward this star is about

$$N_C = \frac{10^{14}\, m}{f}$$

The total column density of carbon in the line of sight toward HD 183143 is approximately 10^{18} cm^{-2} or less (based on the revised galactic C/H ratio in [SW95]); if a typical oscillator strength for the molecular electronic transitions is of order $f = 0.01$ then we find that the number of C-atoms in a DIB carrier is about

$$m = f\, N_C\, 10^{-14} \Longrightarrow m \leq 100$$

Fig. 4.4 summarises all the DIB carrier candidates for each observed spectral feature.

This result is not a serious limitation and indeed it can be seen as a consistency check for the hypothesis that the DIBs are formed by large organic molecules.
A carbon budget of up to about 100 C-atoms per molecule is quite satisfactory for carbon chains or ionized PAHs.

4.4 New observations of diffuse interstellar bands

One of the most recent studies about DIBs has provided a new survey of interstellar diffuse bands. Tuairisg *et al.* (see [Tua+00]) produced a deep survey between 3906 Å and 6812 Å under consistent observing conditions toward three very reddened and five unreddened stars, among which they have registered one of the strongest DIBs in this field.

Feature	Assumed carrier	Carbon abundance (C atoms per 10^6 H atoms)
UIR emission	Hot gas-phase PAH ions	4
		4 to 15
		65
	Hot solid PAH (anthracene)	26
3.4-μm absorption	Amorphous carbon on grains	290
	Aliphatic hydrocarbon on grains	96
		11 to 154
3.3-μm absorption	Cold PAHs in diffuse ISM	15 to 20
4.67-μm absorption	Solid CO	9
DIBs (all)	PAHs in HAC; $f = 10^{-2}$	$0.3m$
DIB λ4430	Ionized pyrene	<1
DIB λ7141	Ionized naphthalene	<2
DIB λ4430	Ionized methyl pyrene	<1
DIBs λλ9577, 9632	C_{60}^+	<1
2175 Å bump	Amorphous carbon	70
	Small graphite grains	60
	Anthracite (coal)	106

Figure 4.4: Carbon required for observed spectral features. In this model, m represents the average number of carbon atoms per DIB carrier. For moderate-sized PAHs, m would be in the vicinity of 20. The acronym 'U.I.R.' stands for 'Unidentified InfraRed'. Figure from [SW95], pag. 1458.

Fig. 4.5 shows this enhancement along the line of sight of the star BD +63° 1964; we are dealing with a B0 II star and it has therefore relatively few stellar lines. Nevertheless, the spectrum has, especially towards the blue, some prominent stellar lines which hamper the detection and measurement of possible new DIBs. Few stellar lines appear above 4800 Å where most of the diffuse interstellar bands are concentrated. To distinguish DIBs from stellar lines the spectrum of BD+63° 1964 was divided by the stellar standard HD 37128, which is a very good match in spectral type and rotational velocity. The resulting spectrum is characterised mostly by interstellar features, with a few residual stellar lines.

In addition, some corrections were adopted to consider telluric contaminations[1], especially due to oxygen lines, mostly around the diffuse band at 6284 Å and water lines above 5800 Å. To remove these contaminations, the bright star HD 32630 was chosen for subtraction; is valid the following relation:

$$I_{TC} = \frac{I}{I_t^{\frac{z}{z_t}}}$$

where:

- I and I_t are the object spectrum and the telluric standard spectrum, respectively;
- $\frac{z}{z_t}$ is the ratio of the respective airmasses.

[1] Generally speaking, they are interferences in astronomical spectra due to Earth's atmosphere (so typical of ground-based observations).

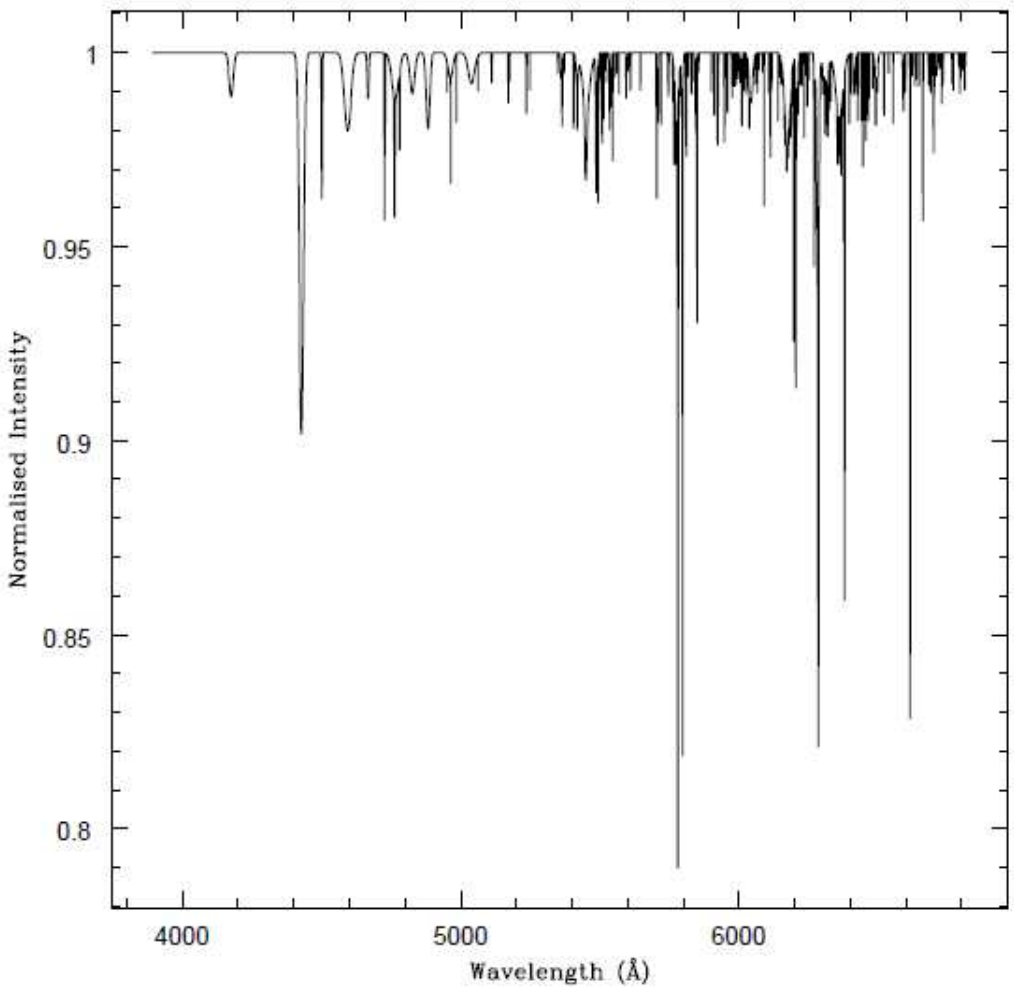

Figure 4.5: A synthetic spectrum of all 226 DIBs confirmed towards BD+63° 1964 between 3906 Å and 6812 Å. Figure from [Tua+00], pag.227.

The reddened star HD 183143 (a B7 star, $E_{(B-V)} = 1.28$), up to now the reference star for studies of DIB behaviour, was used to add confirmation to the newly detected DIBs. However, a synthetic spectrum (i.e. a spectrum produced by modelling software) was produced in order to have a more accurate vision of the DIBs structure, just as one can see in fig. 4.5.

What is very important in this survey by Tuairisg *et al.* is the confirmation of the molecular nature of DIBs, with some particular features of the work's target. The line of sight along the star BD +63° 1964, in fact, shows a unique nature in this sense: at 3933 Å and 3968 Å there are absorption lines of Ca II, as well as the CH band at 4300 Å, which seem to indicate at least two clouds of different velocities. In order to understand the DIB behaviour, models of diffuse clouds have been performed using information on various atomic and molecular species residing along the aforementioned line of sight, confirming the probable presence of a cloud edge where UV radiation may trigger the ionization of DIB carriers ([Tua+00]).

Chapter 5

Extinction: an alternative view

The 2200 Å bump is a major figure of interstellar extinction; however, extinction curves with no bump exist and are, with no exception, linear[1] from the near-infrared down to 2500 Å at least, often over all the visible-UV spectrum. Therefore, the possibility that the classical description (by Cardelli *et al.*, Fitzpatrick & Massa, etc) is somehow not so satisfying in covering all the observational evidence lies somewhere in the research field.

The duality linear vs bump-like extinction curves can be used to re-investigate the relationship between the bump and the continuum of interstellar extinction, and answer questions such as:

- Why do we observe two different kinds of extinction (linear or with a bump) in interstellar clouds?
- How are they related?
- How does the existence of two different extinction laws fits with the requirement that extinction curves depend exclusively on the reddening $E(B-V)$ and on a single additional parameter?
- What is this free parameter?

The most prominent alternative view on the nature of interstellar extinction was provided by Zagury (2013, see [Zag13]), as already anticipated in subsec. refTurner$_i$$ntroduction-to-Zagury.Inthenextparagraphs, wearegoingtoexploitwithmoredetailsthisp$

[1] Here and farther in the text, along the whole chapter, *'linear'* means that the extinction law is actually **quasi-linear**: this means it follows a $1/\lambda^p$ law, with p close to 1.

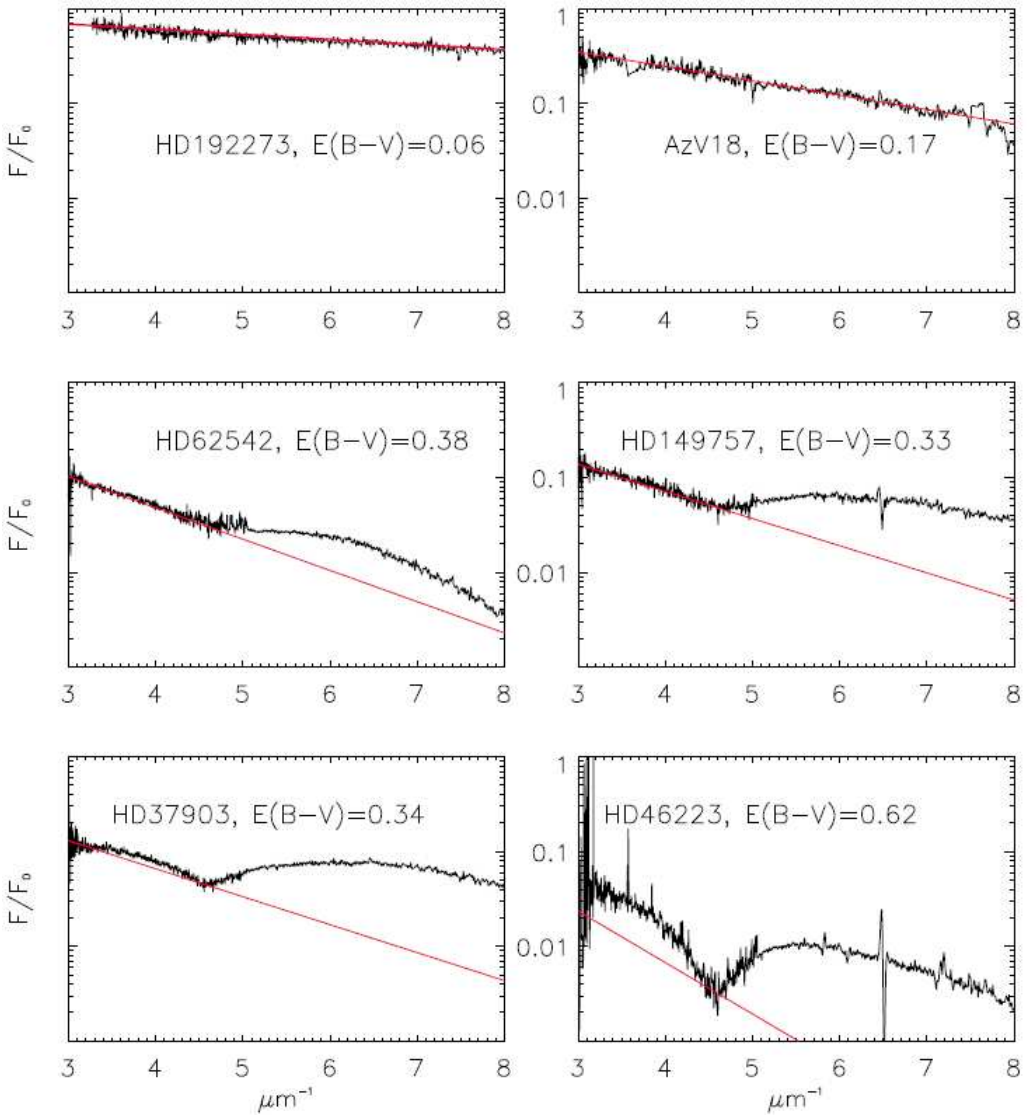

Figure 5.1: The three types of observed interstellar extinction.
The two upper F/F_0 curves (linear extinction laws, no bump) are found in low column density directions. First occurrences of departure from linearity (middle spectra) arise in the far-UV, at slightly higher reddening on average.
Bottom spectra correspond to bump-like (CCM), most currently observed, extinction curves. The observations of any reddened star in the Galaxy or in the Magellanic Clouds will fall into one of these three categories.
No fixed threshold of reddening separates one type of curve from the other.
The spectra have arbitrarily been normalized in such a way that the exponentials (red lines) are 1 at $1/\lambda = 0$. Y-axis are logarithmic.
Figure from [Zag13], pag.2.

5.1 Introduction

Early studies of interstellar extinction ([Whi58], [Nan64]) soon made it clear that the linearity of the visible extinction curve breaks towards the UV, near 4300 Å (the so-called *Nandy's knee*).
The break is such that extinction in the near-UV is less than expected from the continuation of the visible extinction curve.

After 1970, observations from outside the atmosphere (especially those taken with the **I**nternational **U**ltra-**V**iolet **E**xplorer telescope) completed the curve and revealed an even more complex UV extinction. Particularly spectacular is the absorption-like feature centred at 2175 Å, the 2200 Å bump, which interrupts the continuum of the extinction curve approximately between 1800 Å and 2500 Å.

The 2200 Å bump, a central feature of interstellar extinction, has become a subject of research in its own right. The wideness of the bump suggests a vibrational absorption band of a complex molecule; nevertheless, no molecule has yet been formally identified as the bump carrier but several have been proposed (see subsec. 2.4.1 for a deeper analysis).
The key point here is to underline the fact that the variations of any two points on extinction curves with a 2200 Å bump, whether they are in the bump region itself or not, are correlated; this led Cardelli *et al.* to conclude that the shape of an extinction curve with a 2200 Å bump depends on the reddening $E(B-V)$ and on one additional parameter only.
But the nature of this key parameter, essential to the comprehension of interstellar extinction and of the bump, remains to be understood. In fact, according to Zagury's idea, the choice of the absolute V-band extinction to reddening ratio $R_V = A_V/E(B-V)$ as the free parameter in the CCM model, is unjustified ([Zag12], [TMB14]).

Some of the most sensitive incongruencies within CCM, in this sense, are displayed in fig. 5.1. Focusing on upper and middle plots, in particular, it is noteworthy the existence of directions with no bump for which the linear visible extinction continues below 4000 Å, down to the bump region or even in the far-UV. In the CCM framework no bump means no reddening, but this is not true in an absolute way: there exist several particular circumstances (e.g. low column density directions, interstellar matter close to the star... see subsec. 5.2.1 for details) under which the bump tends to disappear.

This is another challenge a standard extinction model struggles to explain: how can interstellar molecules which absorb at 2200 Å be absent in some interstellar clouds and why, in this case, does the extinction law become linear over the whole spectrum?
The nature of the 2200 Å bump will therefore not be fully understood unless its relationship to the continuum, and the absence of a bump in some observations, are clarified.

Beyond the "bump problem", the interpretation of the continuum of interstellar extinction curves is a source of conflict on its own:

1. The value of R_V is independent of direction according to some studies, while other studies argue that it varies even on small angular scales ([Zag12]);

2. As already seen in CCM, the existence of different types of interstellar particles (suggested by the different features of a UV extinction curve) is difficult to reconcile with a one-parameter fit. In fact, all interstellar dust models rely upon a minimum of six independent parameters (in addition to $E(B-V)$) instead of the single CCM one.

It is useful to review the large amount of data now available on interstellar extinction, in order to re-examine the observational constraints imposed on the bump and on the continuum and finally investigate the implications of these constraints.

5.2 The CCM fit of interstellar extinction

Cardelli *et al.* in 1989 showed that the spatial variations of the extinction at two different wavelengths (from the infrared to UV wavelength range) are correlated: plots of A_λ-A_V versus $E(B-V)$ in different directions exhibit a linear relationship at all λ.
CCM deduced that normalized extinction curves constitute a set of curves of $1/\lambda$ which depend on only one, direction-dependent, parameter: R_{CCM}.
They derived an analytical fit for the curves and assumed that R_V was the free parameter (i.e. $R_{CCM} = R_V$). We anticipate here that this is certainly not the case; the question of the nature of the free parameter of interstellar extinction is, indeed, still open.

The CCM fit of normalized extinction curves is a purely empirical relationship. It is not always accurate (see fig. 3.2) and further applies to most but not all observations. Two reasons explain its inaccuracy: the relationship the fit establishes between the bump and $E(B-V)$, and its incapacity to reproduce linear extinction curves.
CCM implicitly assumed that the shape of 2200 Å bump depends on $E(B-V)$ alone which can only be a first-order approximation; in addition, this relationship only reproduces the set of extinction curves with a bump (no bump means $E(B-V)=0$), while extinction curves with no bump also exist, in the Galaxy as well as in the Magellanic Clouds (see fig. 5.1).
These curves, with no exception, continue the linear visible extinction in the UV, at least down to the bump region. Many are linear over the visible-UV spectrum and markedly distinct from the mean Seaton Galactic extinction law ([Sea79]). Linear curves over the whole spectrum can be included in a generalization of the CCM fit which still depends upon a single parameter.

5.2.1 Linear extinction laws

The absence or a reduction in the expected size of the 2200 Å bump is found in two circumstances:

1. Low column density directions;

2. Stars close to the obscuring material (shell stars, planetary nebulae). Planetary nebulae have little or no bump, and when they do have a bump it is likely because of the presence of a foreground cloud on the line of sight.

These observational evidences also bring the fact that there is no specific absorption at 2200 Å in the UV regarding nebulae: the spectrum of a nebula deduces from the spectrum of its illuminating star by the same linear law of $1/\lambda$ over the whole UV spectrum (including the bump region) and must continue the scattering law that should be found in the visible.
When there is a bump in the spectrum of a nebula illuminated by a nearby star, the bump exists in the same proportion in the spectrum of the star and is due to foreground interstellar matter. Very low extinction directions also have a linear extinction over the whole visible-UV spectrum (top plots of fig. 5.1).
Those directions exist in the Milky Way as well as in other galaxies; they are observed at much larger reddenings in the Magellanic Clouds.

Extinction curves will nearly always be decomposed into a linear (over the whole spectrum) and a CCM-like (with a bump) components. The CCM part of the extinction curve and its free parameter are fixed by the size of the bump.
The bump is no more strictly related to the total reddening of the star, as requested by Savage's observations (see [Sav75]). This decomposition provides a more general and considerably improved version of the CCM fit which still relies on a single parameter (in addition to $E(B-V)$).

5.2.2 The three types of extinction

Fig. 5.1 is a summary of the three different types of UV extinctions which can be observed. The F/F_0 representation[2], which is what observation most directly affords, was preferred to the traditional extinction curve (A_λ or $E(\lambda - V)$, that is roughly $-2.5\,log(F/F_0)$) for reasons to be cleared in next sections.
The y-coordinate is logarithmic, so exponentials are straight lines.

The two top spectra are low column density directions, one in the Galaxy and the other in the Small Magellanic Cloud; the extinction curve is linear over all the visible-UV wavelength range (F/F_0 is exponential).
The bottom plots are traditional, most commonly observed curves with a bump. Between these two types, the two middle plots are observed in directions of intermediate reddening: the extinction remains linear down to the bump region, and diverges in the far-UV. Extinctions of this type also exist in the Magellanic Clouds. Any extinction curve will inevitably fall into one of the three categories represented in fig. 5.1: there is no fixed threshold of reddening above which extinction turns over from one type to the other, from linearity to bump-like.

Linear extinction curves are more easily found among very low column density directions, curves with a bump towards large reddening ones, but the amount of reddening alone does not determine the type of extinction curve. The star AzV18 in the SMC for instance, with a reddening of 0.17 mag., has no 2200 Å bump (fig. 5.1).

[2] F is the observed spectrum of the reddened star; F_0 is the spectrum the star would have if it was not reddened. In practice, only F_1 ($\propto F_0$), the spectrum of a non or slightly reddened star of the same spectral type, is available.
The F/F_0 spectrum can be normalized from $F/F_0(1/\lambda \to 0) = 1$ provided that p, the exponent of the quasi-linear law of the visible extinction, is known. For the figures it has been arbitrarily assumed that $p = 1$.

A similar reddening in the Galaxy would most certainly result in a significant bump. The transition from linear to bump-like extinction must be driven by a parameter other than $E(B-V)$, necessarily the free parameter of interstellar extinction.

5.3 Constraints on interstellar extinction theory

Following the previous sections, conservative requirements for a rational explanation of the observations on interstellar extinction would be that:

1. Interstellar extinction depends on the reddening along the line of sight and on one additional parameter which varies from direction to direction;
2. Extinction curves are linear (from the visible to the far-UV) for sufficiently low reddening;
3. Extinction curves are linear when the interstellar matter is close to the star.

The expressions *"sufficiently low"* in item 2 or *"close to"* in item 3 are vague; they must be fixed by the free, yet unknown, parameter of interstellar extinction. Existing dust models do not satisfy these conditions. Any dust model will suppose the existence of at least three types of particles (large grains, bump carriers, small molecules for the far-UV rise), each responsible for the extinction in a particular wavelength range. Since the weight of each of the near-UV, bump, and far-UV features varies with direction, the relative proportion of each type of particle also needs to vary with sight-line.
The size distribution of the large grains has to be truncated towards the small sizes, otherwise the UV extinction curve would continue the linear visible extinction law and there would be far more extinction in the UV than observed.
The threshold of the truncation cannot be the same whether the UV extinction curve is linear, partly linear, or bump-like. It thus depends on the direction.
It must also depend on reddening (second item above) and on distance from the stars (third item).

In practice the work of Fitzpatrick & Massa (1988, see [FM88]) proves that any attempt to consider interstellar extinction as the sum of three separate extinctions, which is what a dust model formally does, requires a minimum of five to six independent parameters in addition to $E(B-V)$, in contradiction with the first item above.

5.4 What alternative for the UV extinction curve?

When extinction begins to depart from linearity in the UV, either in the near-UV or in the far-UV (middle plots of fig. 5.1), the extinction curve F/F_0 systematically lays above the linear continuation of the visible extinction curve. This deficiency in extinction has been attributed to a modification of interstellar grain properties, a change in the dust-size distribution, and the apparition of two new kinds of molecules.
The other and unique alternative is that the linear extinction of the direct light remains unaltered, and that what we observe is an additional contribution which has not been accounted for yet. The cloud itself must provide this contribution. In the latter alternative, the direct light from the star should follow the visible

extinction law over the whole spectrum, and therefore scale as $e^{-2\,E(B-V)/\lambda}$ (λ in μm) ([Zag12]).

If light from the cloud, presumably scattered starlight, is added to the light from the star, the radiative transfer equation

$$\frac{F}{F_0} = e^{-\tau_\lambda} \tag{5.1}$$

which presides at extinction theory, is incomplete and does not apply anymore to the observation of reddened stars. Instead one must write

$$\frac{F}{F_0} = C_0\,(1 + f_s)\,e^{-\alpha_p\,E(B-V)/\lambda^p} \tag{5.2}$$

Parameter $\boldsymbol{\alpha_p}$ depends on p only and its expression can be found in [Zag12]; $\boldsymbol{C_0}$ should be 1 in the absence of grey extinction, < 1 otherwise. $\boldsymbol{f_s}$ represents the wavelength-dependent proportion of scattered starlight. It must increase, as extinction does, with $E(B-V)$ and wave-number.
Both direct and scattered light components follow similar paths and need to be extinguished by the same amount of interstellar dust (the $C_0\,e^{-\alpha_p\,E(B-V)/\lambda^p}$ factor). At very low reddening photons available for the scattering are scarce, scattered starlight is negligible and direct light from the star should dominate over f_s ($f_s \ll 1$). The extinction is then linear over the whole visible-UV wavelength range (upper plots of fig. 5.1).
When extinction increases, scattering will begin to show up in the far-UV first, as observed (middle plots of fig. 5.1). Increasing the extinction even more will lead to the merging of scattered starlight in the near-UV, and also, but to a lesser extent, in the visible.

The free parameter of interstellar extinction determines the departure from the linearity of extinction curves. It fixes the proportion of scattered light in the observed spectrum of a reddened star and must be included in the expression of f_s. Since 2200 Å bumps always appear with scattered starlight, f_s also contains all the information on the bump. The hypothesis of a contribution of forward scattered starlight by the cloud to the spectrum of a reddened star explains the observations of fig. 5.1 and satisfies the two first items of sec. 5.3.

5.5 f_s's continuum

f_s increases with wave-number and reddening, contains the wavelength dependence of the bump, and depends upon a single parameter in addition to $E(B-V)$. Fig. 5.1 shows that f_s can be larger than 1 in the UV (the intensity of the scattered starlight is then larger than the intensity of the star, even corrected for reddening). For a star whose spectrum follows a linear extinction in the visible and has a large bump in the UV, one should find in the visible (where $f_s \ll 1$):

$$\left(\frac{F}{F_0}\right)_{VIS} \approx C_0\,e^{-\alpha_p\,E(B-V)/\lambda^p} \tag{5.3}$$

In the far-UV we have $f_s \gg 1$, therefore:

$$\left(\frac{F}{F_0}\right)_{UV} \approx C_0\,f_s\,e^{-\alpha_p\,E(B-V)/\lambda^p} \tag{5.4}$$

$E(B-V)$ can be estimated from the visible part of F/F_0 and from eq. (5.3).

The wavelength dependence of f_s in the far-UV will then be found from eq. (5.4):

$$f_s \propto \left(\frac{F}{F_0}\right)_{UV} e^{\alpha_p\, E(B-V)/\lambda^p} \tag{5.5}$$

This method was applied to star HD 46223 with HD 269698 as reference, two stars of same spectral type (for details about data and method, see [Zag01]). With $p \approx 1$ ($\alpha_p \approx 2$ with λ in μm), it was found that outside the bump region the ratio of the two spectra is correctly represented by the following expression:

$$\frac{F}{F_0} \approx C_0 \left(1 + \frac{c_s}{\lambda^4}\right) e^{-2\,E(B-V)/\lambda} \tag{5.6}$$

Fig. 5.2 shows the visual representation of eq. (5.6).

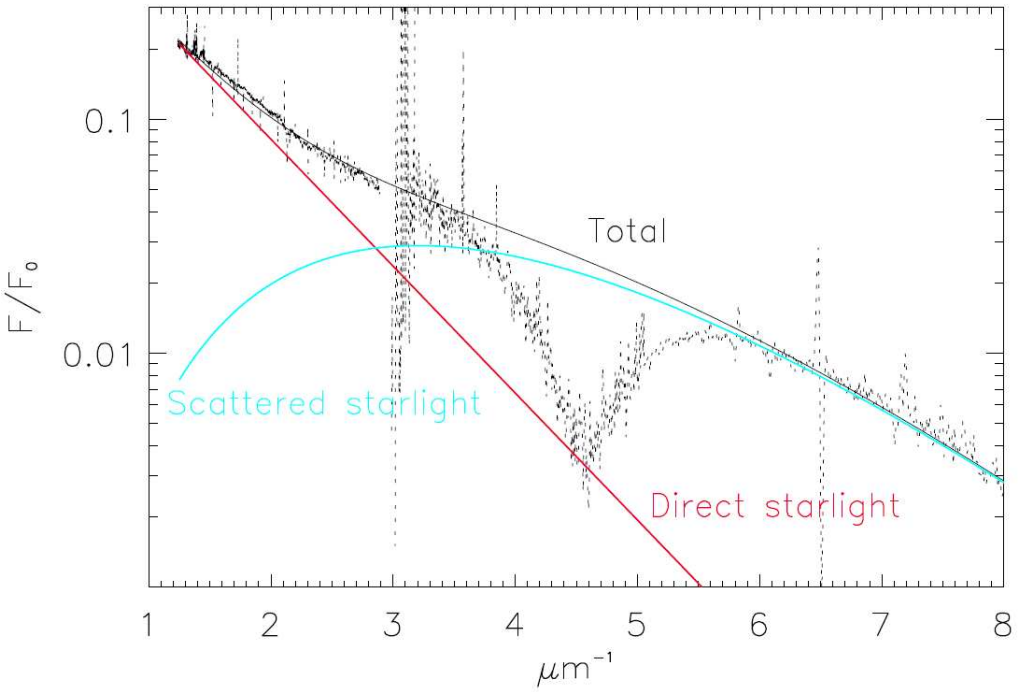

Figure 5.2: Tentative decomposition of F/F_0 for HD 46223 into its components of direct ($e^{-2\,E(B-V)}$), with $p = 1$, $C_0 = 1$ and scattered starlight ($\propto e^{-2\,E(B-V)}/\lambda^4$, the bump region is omitted). Figure from [Zag13], pag.6.

In the far-UV, f_s can be approximated by a $1/\lambda^4$ power law. The function c_s depends weakly on wavelength in the visible and in the far-UV, sharply in the bump region. This $1/\lambda^4$ dependence of f_s can be checked in the far-UV from any data set of stars with a bump. Since from eq. (5.6)

$$\lambda^4 \left(\frac{F}{F_0}\right)_{far-UV} \propto e^{-2\,E(B-V)/\lambda} \tag{5.7}$$

The product of λ^4 times F/F_0 for any star with a bump should be close to an exponential of $-1/\lambda$, $e^{-2\,E_{UV}/\lambda}$, in the far-UV. It is indeed observationally verified that $\lambda^4 \times F/F_0$ follows an exponential with, as expected, $E_{UV} \approx E(B-V)$.

The $1/\lambda^4$ dependence of f_s rules out forward scattering by dust (scattering by dust would vary as $1/\lambda^p$, $p \approx 1$). It implies Rayleigh scattering by particles small compared to the wavelength, presumably hydrogen which represents over 90% of interstellar clouds.
Theory shows that a slab of gas in between a star and an observer will, provided that distances are large, act as a lens and considerably enhance the apparent irradiance of the star itself. The coherence of the forward scattered starlight and the size of the Fresnel zones on astronomical distances are the two reasons which account for the importance of the light scattered by the slab.

5.6 The free parameter of interstellar extinction

Zagury's paper ([Zag12]) shows that, in order for scattering by gas to be significant, distances need to be large. Coherent scattered starlight vanishes when the gas is close to the star, as required by the third and last item of sec. 5.3.
It is this dependence on distances that c_s should include and which will determine the proportion of scattered starlight in the observed spectrum of a star.

The free parameter of the extinction curve must therefore be related to distances, presumably to the ratio of the distances from the star to the cloud and the cloud to the observer. The function c_s should also be proportional to the square of H-atoms column density, that is to $E(B-V)^2$.

Extinction in the direction of stars in the Magellanic Clouds (M.C.) can be separated into a linear and a CCM-like (with a bump) parts.
The linear extinction is due to the reddening within the Magellanic Clouds, since dust in the Clouds is very close to the stars (compared to the Sun-M.C. distance).
The CCM bump-like extinction, on the other hand, arises from Galactic cirrus on the line of sight: the scattered light component reaches a maximum when the star is infinitely far away ([Zag12]).

5.7 The 2200 Å bump

Fig. 5.1 shows that the bump is associated to the departure of extinction from linearity, thus to the presence of scattered starlight. It was therefore noted at the end of sec. 5.4 that the analytical expression of the 2200 Å bump had to be included in f_s (or in c_s). In fig. 5.2 the bump is indeed no deeper than the exponential decrease of the direct light from the star, as if only the scattered starlight, and all of it, was extinguished. Absorption by a molecule would not discern between the scattered and direct lights from the star; the bump is very unlikely to result from absorption, even by a complex molecule.
According to Zagury's proposal, there are two possible explanations for the feature:

- A minimum in the scattering cross-section of hydrogen;
- An interference/diffraction effect.

Noteworthy, the first known diffuse interstellar band, the broad $\lambda = 4430$ Å band, is close to twice the central wavelength of the bump (the ratio is ~ 2.03).

The DIB, if it was a second interruption of the scattered starlight, should be a few to over 10% of the light of a reddened star[3], which is the order of magnitude observation suggests.

5.8 Final considerations

A major obstacle to the understanding of interstellar extinction lies in the difficulty of establishing good resolution extinction curves over the whole infrared to UV wavelength range. Studies on interstellar extinction are for practical reasons compartmentalized between the infrared, the visible and the UV.
Data for the three domains are of uneven quality and have little overlap.
In the UV the IUE database provides good-resolution spectra for hundreds of stars, in all regions of the sky, but no such effort was made for the visible and the infrared: in these last two cases, data consist of a few data points that sample the spectrum. Observations are also made from the ground and suffer from the difficulty of removing atmospheric extinction (which furthermore mimics interstellar extinction in the visible).
In the infrared, interstellar extinction is low and uncertainties (or calibration problems) are probably often underestimated. The cross-section of interstellar grains shows a $1/\lambda^p$ ($p \approx 1$) dependence in the visible ([Zag12]); this extinction law probably extends to the infrared. In some directions, linear extinction curves are also observed in the UV and must continue the linear curve in the visible.

The determination of p is an issue on which depends the value of R_V, so of remarkable interest. If, as observation indicates, linear extinction curves depend on the reddening $E(B-V)$ alone, p and R_V must be the same constants in all directions. Their determination is up to date hampered by the absence of continuous extinction curves over a sufficiently large wavelength range.

The ultra-violet region, although the best documented, is also the most complex one. Observed UV extinction curves usually do not continue to be linear. New features appear and $E(B-V)$ is no longer sufficient to fix the shape of an extinction curve. Empirical works ([CCM89] above all) have established that an additional parameter is enough to reproduce all extinction curves.
This parameter cannot be R_V, according to Zagury's paper ([Zag13]) and lately confirmed by Turner's work ([TMB14]). Observation also shows that the transition of an extinction curve from its linear to non-linear regimes, whether it happens in the visible/near-UV (see [Nan64]) or in the far-UV (middle plots of fig. 5.1), always appears as less extinction than would be expected.

The possible new alternative vision about interstellar extinction (proposed by Zagury and endorsed by Turner) tries to reconcile these observational constraints with analytical models: the basic idea is that the light received from the direction of a reddened star, when its extinction curve has a 2200 Å bump, is not direct light from the star alone but contains a proportion of starlight scattered by the cloud on the line of sight.
An extinction curve then depends on the reddening and on the proportion of scattered starlight, that is on two parameters, as observation requires.

[3]With a $1/\lambda^4$ dependence of the scattered light, the depths of the bump (h_B) and of the DIB (h_D) would be related by $h_D \sim 0.06\, h_B/(1-h_B)$.

Since scattering, as extinction, increases with wave-number (in the present case it behaves as $1/\lambda^4$) it is less perceptible in the visible and even less in the infrared: extinction in these wavelength domains remains close to linearity and depends on $E(B-V)$ alone.
If the reddening is low enough, scattered starlight is negligible: the extinction curve is linear from the infrared to the far-UV. When extinction increases, scattered starlight will show up in the far-UV first, as observed.

Theory about the physics of ISM (see, for instance, [HH81]) does predict that a large proportion of scattered starlight should be mixed with direct starlight if the distances between the cloud, the star and the observer are large.
The free parameter of interstellar extinction is linked to these distances.
The last requirement suggested by observation (sec. 5.3), that the extinction becomes linear when the interstellar matter is close to a star, is then justified. The bump observed in the extinction curves of stars in the Magellanic Clouds, for instance, may come from cirrus[4] in the Milky Way and not from interstellar matter in the Clouds. The bump appears with the scattered light component only and does not extinguish more than the scattered starlight. It is therefore very unlikely to be the result of absorption by some kind of yet unknown molecule.
The free parameter of the extinction curve thus has nothing to do with interstellar grain properties.

The continuum of interstellar extinction does not contain any information on the composition of the particles which extinguish starlight. It does not teach us anything about interstellar chemistry: observations of interstellar extinction which diverge from linearity in the UV are a problem of optics, not of the chemistry of the interstellar medium.
Three main reasons have contributed to the non-recognition of the presence of scattered starlight in the spectrum of reddened stars.
The first reason is the standard representation of extinction curves (roughly $-2.5\,log(F/F_0) \approx \tau_\lambda$ adopted from the very beginning: scattered starlight is far more easily identified on a F/F_0 plot -as in fig. 5.1- than from the negative of its logarithm (as extinction curves are usually represented); furthermore, this is what observation directly provides.
The second reason is that the magnitude of the scattering is also unexpected and counter-intuitive: it implies that more light can be received from the direction of a star when it is observed behind a cloud of hydrogen than there would be without the cloud.
The last reason is the lack of a reliable database of spectra in the visible, free from atmospheric extinction. Plots of F/F_0 curves over the whole visible-UV spectrum could have highlighted the relationship between the exponential decrease of interstellar extinction in the visible and its divergence with observation in the UV.

[4] **Cirrus** (also known as **Galactic cirrus** or **infrared cirrus** are galactic filamentary structures seen in space over most of the sky that emit far-infrared light. The name is due to the fact that, in appearance, these structures are cloud-like.

This alternative description of the nature of the interstellar extinction can be summarized as follows[5]:

- The exact interstellar extinction law is linear over all the visible-UV spectrum. It is the same law for all directions, including directions in the Magellanic Clouds and presumably for all galaxies;
- Observations of the spectrum of reddened stars depend on two parameters:
  1. The quantity of interstellar matter, measured by the reddening $E(B-V)$ (extinction depends on $E(B-V)$ and scattered starlight on $E(B-V)^2$);
  2. The distances of the cloud to the star and to the observer. The ratio of these distances fixes the importance of starlight scattered by the gas in the observed spectrum of a reddened star.

  Interstellar extinction observations thus contain some (though probably loose) information on distances;
- R_V is likely a constant. It is related to the best power law that describes linear extinction curves. Spectral observations covering a large wavelength range will likely determine its value;
- The bump is not an absorption feature. It corresponds to an interruption of the scattered light component in the spectrum of reddened stars. It may be related to some of the diffuse interstellar bands;
- Neither the continuum of the extinction curve nor the 2200 Å bump can be used to constrain the chemistry or the molecular composition of the interstellar medium

The exact, physically meaningful, fit of interstellar extinction curves remains to be established.

[5] Another consequence, i.e. the implication of a scattered starlight component in the spectrum of reddened stars for distance estimates, would need further investigations. Scattered starlight attenuates the impression of reddening: photometric distances to reddened celestial objects may then be overestimated

Chapter 6

Conclusions

After decades of research and despite a now well-established set of observations, studies on interstellar extinction still lack a firm and internally consistent theoretical framework.
In particular, there are three major features under the spotlight:

1. The departure of the continuum from linearity in extinction curves;
2. The UV bump;
3. The DIBs.

For instance, the nature of the particles that would explain the 2200 Å bump (and the far-UV rise, as well) remains controversial; in the visible wavelength range, the carrier(s) of the diffuse interstellar bands have still not been identified.
It is taken for granted in interstellar extinction studies that an observer sees the direct light from reddened stars dimmed by different types of interstellar particles in the line of sight (see sec. 4.3), however this assumption can lead to several contradictions between theory and observations at UV wavelengths (see sec. 6.1).

A possible alternative, as already mentioned by Turner (subsec. 3.3.2), is represented by Zagury's idea that a large amount of scattered starlight is mixed with the direct light we receive from reddened stars ([Zag13], chapter 5).
Although this shift in perspective could bring many benefits in terms of parametrization and tension-solving between observed features and theoretical explanations, it is itself not free from difficulties. For instance:

- If light received from a reddened star decomposes into direct and scattered light components, the latter can overwhelm the former;
- At UV wavelengths a star would appear much brighter if it could be observed through an interstellar cloud of pure gas (no dust) than would be the case without the cloud in the line of sight;

- The cloud (with no dust) would amplify the signal from the background star and act more like a lens[1] than as an extinction medium.

Nevertheless, if we assume as plausible the idea that interstellar extinction is indeed an optical phenomenon through forward scattering, it is possible to use different equations. For instance, it is remarkable to mention the van de Hulst's formula -derived by H.C. van de Hulst in the 1950s for the irradiance of the forward scattering by a slab of identical particles:

$$\frac{I_S}{I_0} = \left(\frac{4\,\pi^2\,\alpha_X\,N_X}{\lambda} \right)^2 = \frac{3}{8\,\pi} N_X^2\,\lambda^2\,\sigma_X$$

where N_X is the column density of the particles, $\alpha_X \sim \frac{9}{2}a^3$ their polarizability, a their mean size; cross section σ_X is related to the polarizability by $\sigma_X = \frac{8}{3}\pi\,k^4\,\alpha_X^2$ (for details see [HH81]).
This equation, by the way, seems to anticipate the lensing effect of interstellar clouds, but it also predicts ratios of the scattered to the direct starlight intensities that are much too high (with respect to the observations).
In addition, if we try to describe interstellar extinction through forward scattering, there is the particularity of an impressive size (a few thousand kilometres wide) that Fresnel zones can reach on astronomical scales; it is the combination of complete forward scattering, large Fresnel zones and identical particles (atomic and/or molecular hydrogen) that could explain the very large proportion of scattered starlight in the spectrum of reddened stars and why observed extinction curves depart from linearity in the ultraviolet spectrum.
This shift in perspective would reframe our understanding of the two major issues cited above: the 2200 Å bump and the DIBs.

On the other hand, the "standard" view of interstellar extinction seems to still have quite advantageous points by its side.
In fact, if this phenomenon is seen as firmly correlated to the physical properties of the interstellar dust population in the ISM, the modelling appears more consistent and it does not need to inconvenience laws of optics *ad hoc*.
Data from several missions (e.g. Planck collaboration, GAIA satellite) could justify the R_V parameter and CCM model as a starting point; however, as for Zagury's theory, in this case, too, there are unwanted consequences on multiple astronomical scales (from photometry to cosmology).

Very recent studies ([Sie23], [Sie+23], [SC23]) focus on the fact that our understanding of the stellar distribution in the Galaxy might be biased, which reflects in a severe work of re-thinking the structure of Milky Way (in particular in the inner bulge) as reference in this field; sec. 6.4 provides further details.

In the future, a total tomography of the Galactic plane could reveal hints of what is missing up to now. What is clear is that the issue is on a theoretical level and it is our approach to the observational data which has to be changed.

[1] According to Zagury ([Zag17]), on observed extinction curves this effect is masked by the exponential extinction $e^{-\tau_\lambda}$ ($\tau_\lambda \propto 1$, $p \sim 1$). It is recovered when the latter is removed (see fig. 6.2).

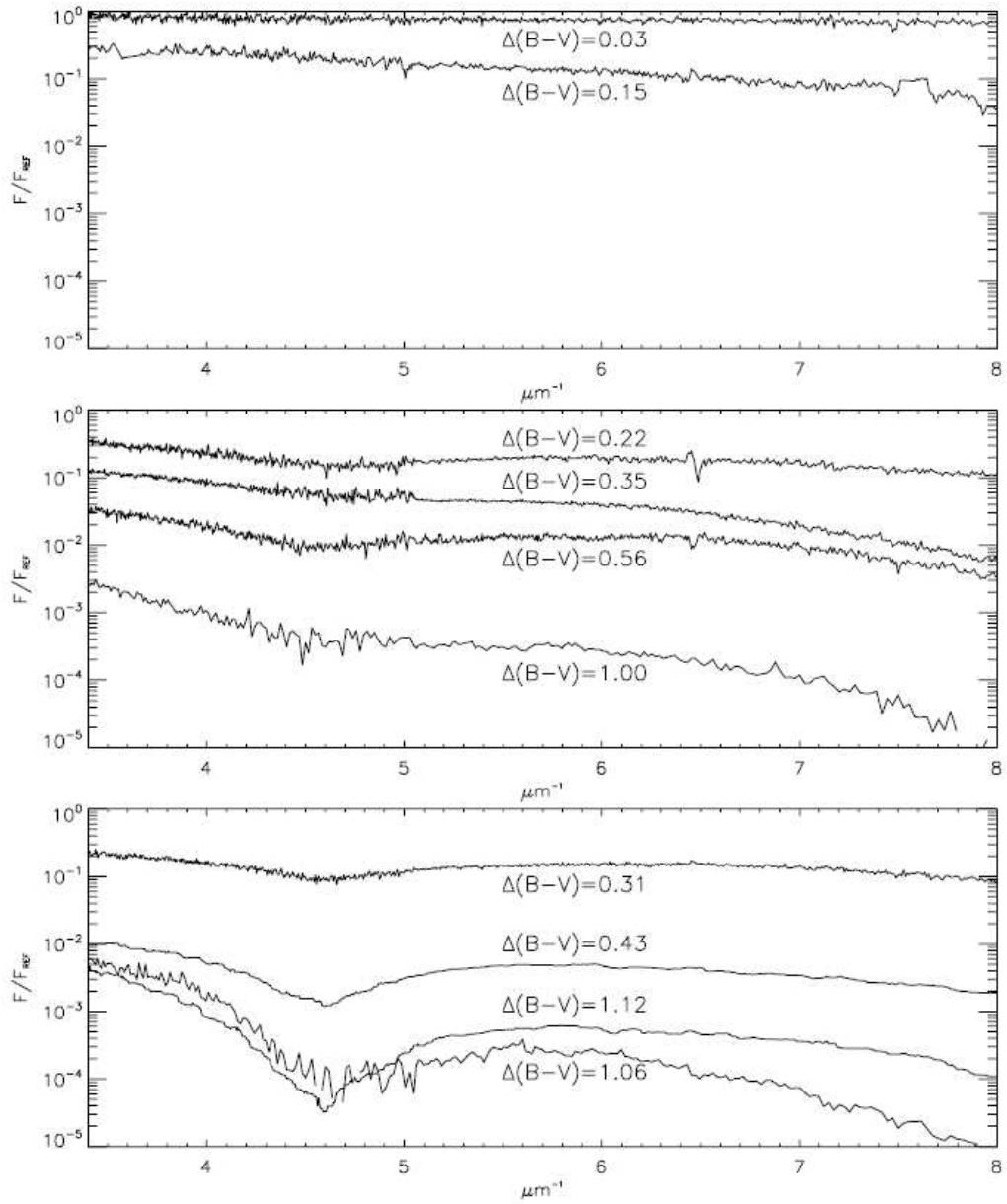

Figure 6.1: The three types of observed interstellar extinction curves: traditional bump-like extinction curves (bottom plot); extinction curves that deviate from linearity in the far-UV spectrum only (after the bump region, middle plot); linear over the whole visible/ultraviolet spectrum extinction curves (top plot). Each spectrum is the ratio of the spectrum of a reddened star to the spectrum of a reference star of low reddening and of the same spectral type. The spectra were normalized using the reddening difference $\Delta(B-V)$ between reddened and reference stars. Any extinction curve, in the Galaxy or in the Magellanic Clouds, falls into one of the three categories. It is clear from the figure that (i) $E(B-V)$ alone is not enough to fix the shape of an extinction curve, (ii) extinction curves with a 2200 Å bump and linear extinction curves anticorrelate.
Figure from [Zag17], pag.5.

6.1 Extinction as an optical phenomenon

For a star infinitely far away, the region of the interstellar cloud that should contribute most to the scattered starlight at the observer position corresponds to an area of order λ L (where λ is the mean free path of incident starlight and L is the length-scale of the cloud). This area is subtended by a very small angle ($\sim \sqrt{\lambda/L}$, see [Zag17]), by far much smaller than the resolution a telescope can reach: therefore, varying the size of the telescope will not modify the proportion of scattered starlight.
Generally speaking, this means that even if we embrace extinction as a physical phenomenon and not an optical one (so if we assume as valid the standard structure of Cardelli *et al.*), the outcome would not change because of an instrumental bias: the key is most likely on a theoretical level instead of an observational approach.

Recent works ([Sch+17]) seem to suggest that the mean observed Galactic R_V value depends on, and increases with, the distance of interstellar clouds; so the distance has to be taken from the Galactic center. Deviations from the average ratio of the size of the 2200 Å bump to $E(B-V)$ within a Galactic region, on the other hand, are more likely due to variations of star distances or to an additional extinction (e.g. circumstellar extinction) in the line of sight.
A peculiar situation is needed for Magellanic Clouds. Magellanic stars have low column density Galactic cirrus (for which the stars are infinitely far away) in the line of sight. That DIBs are observed at the Magellanic Clouds redshift indicates that the 2200 Å bump and the scattered starlight component of Magellanic extinction curves should be attributed to Magellanic interstellar clouds rather than to Galactic cirrus. It follows that the reason why bumps and DIBs are weaker in observations of Magellanic stars is that Galactic cirrus in the line of sight are too light to give appreciable scattered starlight.

In the end, the free parameter of interstellar extinction curves might be the size of the first Fresnel zone; it must be remarked that the parallelism between interstellar extinction as a scattering phenomenon and wave theory is just a suggestion: abnormally large Fresnel zones, as found on astronomical scales, raise a problem for wave theory, the solution of which should help the analytical treatment of interstellar extinction curves.

6.2 Scattered light in the spectrum of reddened stars

Several logical deductions can be drawn from interstellar extinction observations. Interpretations of interstellar extinction curves based on the assumption that we observe the extinction of the direct light from stars will hardly comport with these conclusions. Standard three-component models for interstellar extinction face the following difficulties:

- A three-component model is incompatible with the dependency of extinction curves on reddening and on an additional parameter alone;
- The free parameter (in addition to $E(B-V)$) of interstellar extinction cannot be R_V, which must be a constant;
- The non-linearity of an extinction curve is intimately linked to the presence of the 2200 Å bump and vice versa. In other words, when (and only when)

there is no bump, interstellar dust tends to recover a linear extinction law over the whole spectrum;

- The extinction cross-section of interstellar dust in nebulae does not have the near-UV break predicted by three-component models: the extinction law found in nebulae is continuous and linear over the whole spectrum (see [Zag00]).

In addition, the bump tends to disappear (and the extinction curve becomes linear) when there is very low reddening or when the star is close to the obscuring cloud. Besides reddening, the only parameter that is seen to impact the shape of an extinction curve is the distance between the star and the interstellar matter obscuring it, a conclusion that does not make sense if extinction is the only process at work. This conclusion does make sense, however, if -and this is the sole alternative to standard explanations of interstellar extinction- what is observed is not only the direct light from the reddened stars, but also a non-negligible amount of scattered starlight.

6.2.1 What type of scattering?

Two types of scattering are commonly found in nature, whose characterization is based on the ratio between the incident wavelength λ and the averaged size a of encountered particles; in fact:

1. If $a \gtrsim \lambda$, it is called **Mie scattering**: the phenomenon varies as $1/\lambda^p$, with $p \sim 1$. Scattering by aerosols is the associated obvious example;

2. If $a \ll \lambda$, it is called **Rayleigh scattering**: the phenomenon varies as $1/\lambda^4$ and it is nearly isotropic.

Dust particles interact with starlight via scattering according to Mie's theory, so Rayleigh extinction is far less efficient in this sense.
IUE ultraviolet observations of nebulae prove that light scattered by nebulae in near-forward directions behaves as $1/\lambda^p$ with $p \sim 1$ ([Zag00]).
The scattering can safely be attributed to interstellar dust grains and suggests that their linear extinction law at visible wavelengths extends into the ultraviolet. This result is not compatible with standard extinction models, which all suppose a modification of the size distribution of interstellar dust's extinction law at ultraviolet wavelengths. Nebulae IUE observations show no trace of Rayleigh scattering.
However, there is no way to decompose an extinction curve into the sum of a component of direct starlight ($\propto e^{-a/\lambda^p}$, $p \sim 1$) and a component of light scattered by dust grains ($\propto 1/\lambda^p\, e^{-a/\lambda^p}$, $p \sim 1$). Forward scattering by dust in the UV cannot explain the contamination by scattered starlight of the light received from the reddened stars. The analysis of a complete extinction curve F/F_0 of star HD 46223 (see fig. 5.2 of sec. 5.5 for a reminder), re-constructed from the near-infrared to the far-ultraviolet, shows that the spectral signature of its scattered light component varies as $1/\lambda^p$, with $p \sim 4$. Therefore, the scattering is of Rayleigh type, due to gas along the line of sight.
Fig. 6.2 plots the ratio f_s (dashed line) of scattered to direct light intensities found for HD 46223.

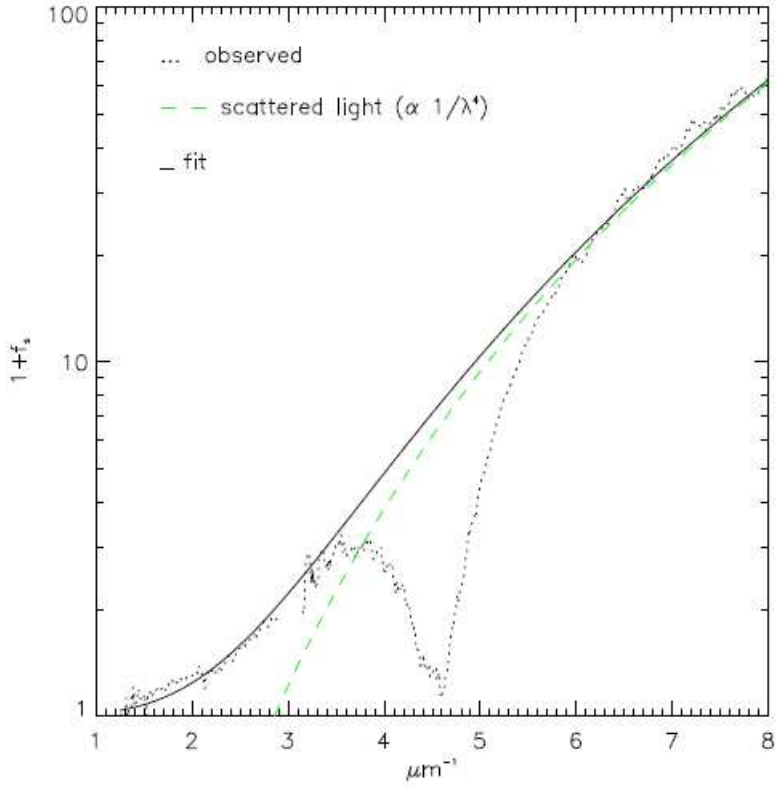

Figure 6.2: The ratio f_s of scattered to direct starlight fluxes for HD 46223. The extinction curve of the same star, corrected for the exponential extinction by dust, is in dots. The solid black line ($1 + a/\lambda^4$, $a \sim 0.015$ if λ is expressed in μm) fits the curve. The green dashed line represents the continuum of scattered starlight, $f_s = a/\lambda^4$. Figure from [Zag17], pag.9.

6.2.2 Amount of scattered starlight

The magnitude of the scattered light component in the UV spectrum can be estimated by the gap between the observed extinction curve and the continuation of the linear extinction law at visible wavelengths.
The scattered light intensity, expressed in proportion to the direct light from the star, estimated for HD 46223 (fig. 6.2), is of the order of $0.015/\lambda_\mu^4$ (λ in μm). Both components must be equally extinguished by interstellar dust extinction. At near-infrared wavelengths, scattered starlight is 2% of HD 46223's flux.
The ratio grows to 16% in the V band and to 30% in the B band. In the far-ultraviolet part of the spectrum, scattered starlight overwhelms the star's flux by nearly two orders of magnitude. The scattering component can thus be much larger than direct starlight would be without hydrogen in the line of sight.

6.3 Connection between DIBs and the 2200 Å bump

The fact that the 2200 Å bump and the diffuse interstellar bands concern different wavelength domains and that the bump is a far more prominent feature has encouraged the tendency to treat them independently.
However, observations seem to suggest some kind of correlation between these two important features within extinction: for instance, Friedman *et al.* (2011, see [Fri+10]) pointed out that when the DIBs are observed the bump is observed as well -and vice versa. When one is substantially weakened, the other is weakened, too. These correlations hold for the Galaxy as well as for the Magellanic Clouds.

6.3.1 H_2 absorption lines and the DIBs

It is since the 1970s that many diffuse interstellar bands match allowed transitions from electronically excited states of H_2; the finding was independently made in more recent years and extended by Sorokin and Glownia (2000 and 2013). These reveal an absorption spectrum of H_2 having topological resemblance with observed DIB profiles and coincidences between DIBs and H_2 resonances from ground state levels populated at low temperatures. If the molecular hydrogen is massively involved in the production of DIBs, this might be through a process of two-photon absorption of coherent light ([SG06]).
The bump's energy, centred close to 5.7 eV, is about half the energy needed to photo-dissociate molecular hydrogen; a two-photon absorption, enabled by the coherence of the scattered light along the star-observer direction, could explain the bump, leaving unaffected the direct light from the star and providing the H_2 excited state needed for the absorptions at the DIB wavelengths.
However, major difficulties would remain in finding the exact selection rules, therefore in an attempt to unify theory, hypothesis and observations.

6.4 'Standard' extinction: photometry as litmus paper

Interstellar extinction is strongly coupled with reddening; this 'bond' is a key aspect in the photometric evaluation of distances within astronomical scales.
This might have cascading catastrophic consequences if there is an unmatched evaluation of R_V, for instance.

Generally speaking, it seems that standard extinction models tend to **underestimate** extinction itself: e.g. a reddened star would appear brighter than what it truly is and its observed apparent V-magnitude m_V is less than it would have been (m_V^0). In the end, the star's distance moduli is overall underestimated, which implies an underestimation of the star's distance.
This aspect, even if it is moderate, can lead to photometric distances that can be considerably overestimated[2]; one possible solution is described as follows.
If A_V^0 is the exact visual extinction, one can write:

$$A_V - A_V^0 = m_V - m_V^0 \tag{6.1}$$

[2]Recalling the definition of R_V (see eq. (2.17)), if reddening is underestimated (i.e. if $E(B-V)$ has a lower value) then the ratio of total-to-selective extinction parameter is overestimated.

Therefore, the exact distance moduli for a reddened star of absolute V magnitude M_V is

$$m_V^0 - M_V = 5\,log\left(\frac{d}{10\,\mathrm{pc}}\right) + A_V^0 \tag{6.2}$$

which can be rewritten as:

$$\begin{aligned} m_V - M_V &= 5\,log\left(\frac{d}{10\,\mathrm{pc}}\right) + A_V^0 + (m_V - m_V^0) \\ &= 5\,log\left(\frac{d}{10\,\mathrm{pc}}\right) + A_V \end{aligned} \tag{6.3}$$

Eq. (6.3) shows that the relative error $\Delta d/d$ is of order $E(B-V)\,\Delta R_V/5$. Empirical methods for the determination of A_V and R_V have been used, resulting in impressively large error margins for photometric distances; Turner (2012, see [Tur12]), for instance, re-considering previous values of R_V, has found distances that are cut down by a factor of two. It can be assumed that, since $R_V = 3.1$ is generally accepted to be canonical, photometric distances are more likely to be overestimated.

6.5 Parallax and luminosity distance with GAIA

The distance measurement to stars has long intrigued astronomers and, by previous sections, it can be seen how important can be a precise measure of scales in the universe. Another approach is closer to the standard view of interstellar extinction, i.e. linked to dust grain population properties rather than optical phenomena (such as scattering).

There exist several techniques to compute distances on an astronomical level; parallax, based on geometric principles, provides a straightforward approach but is limited to nearby stars whereas luminosity distance D_L estimates enable the assessment of distances of several kpc. However, the extinction by dust diminishes the apparent brightness of stars and requires a precise determination.
Siebenmorgen and Chini ([SC23]) in 2023 examined 47 prominent OB stars within a distance of 2.5 kpc with the most superior sample of reddening curves currently accessible. These stars have undergone precise spectral classifications and their accurate distances have been obtained using the unprecedented precision of the GAIA[3] parallax at $\sigma < 0.1$ mas. It can be anticipated here that one of the most shocking results is a substantial inconsistency between both classical derivations of stellar distances.

Since the introduction of dust grain population in the ISM domain ([Tru30]), it was speculated that an additional non-selective or grey extinction term in the form of very large grains -at that time called *meteoritic bodies*- might exist. For a few stars it was hypothesized that incorporating such an additional dust component could reconcile the disparity between distance estimates; however, this remained unverified due to the lack of a physical dust model. It might be the case now, in light of the new observative evidence, to add new dust grains properties in the computation of reddening (hence of interstellar extinction).

[3] **G.A.I.A.** (**G**lobal **A**strometric **I**nterferometer for **A**strophysics) is an ESA mission devoted to create a 3D map of stellar distribution within Milky Way and beyond. For more details, see https://www.esa.int/Science_Exploration/Space_Science/Gaia.

6.5.1 Dark dust model

The addition to the "standard" dust model is needed to align theory with current observational constraints of dust in diffuse ISM of the Milky Way.
In a reviewed structure, it is possible to consider three dust populations:

1. nanoparticles of graphite, silicate and polycyclic aromatic hydrocarbons (PAH);

2. submicrometre-sized spheroidal grains of amorphous carbon and silicate, using the latest optical constants for amorphous silicates;

3. micrometre-sized dust particles.

The latter dust component is better known as **dark dust**: it is primarily composed of a composite of porous amorphous carbon and silicate particles.
These particles have been detected in scattering light haloes around X-ray sources from the submillimeter emission of evolved giants. This hidden dust component appears in sightlines that are connected to the cold ISM.

Micrometre-sized grains absorb a fraction of the interstellar radiation field; because these grains are large, they are cold and will emit at long wavelengths. Originally, very cold (10 K) dust emission was detected in our Galaxy towards high-density regions and in non-active galaxies.

6.5.2 Distance discrepancy

Fig. 6.3 displays the result of Siebenmorgen & Chini sampling, where a discrepancy between the distances obtained from luminosity and from parallax is evident: D_L generally overpredicts the distance D_{GAIA} derived from the GAIA parallax. A dependency of D_L on the stars' spectral types and luminosity classes is not observed.
The (sub)millimetre excess emission observed in the Milky Way has gained explanation only recently; in alternative models, this phenomenon is attributed to the adjustment of grain emissivity at these wavelengths. This vision, however, fails to resolve the distance discrepancy observed in [SC23] towards individual stars.

6.5.3 Reddening and extinction with dark dust

Galactic extinction studies derive the typical wavelength dependence of interstellar reddening. Such curves are commonly used, in particular in extra-galactic research, as the standard for dereddening the observed flux of objects for which there is no specific knowledge about the dust.
Although averaging a sufficiently large number of clouds and sightlines leads to similar mean parameters, they likely do not reflect the true nature of the dust. The degree to which mean Galactic extinction curves can be taken as typical shall always be put in question.

The shape of the average Galactic extinction for a sample of 243 stars with $2.4 \leq R_V \leq 3.6$ at $\lambda^{-1} \leq 8.6\,\mu\mathrm{m}^{-1}$ has been presented by Fitzpatrick & Massa (2007, see [FM07]): their mean curve has $R_V = 3.1$ as derived earlier and recent studies have found a similar value of $R_V = 3.16$. Siebenmorgen *et al.* ([Sie+23]) used a high-quality sample of hot stars (tab.4 in their cited paper) to compute average Milky Way reddening curves. Their work distinguishes between sightlines

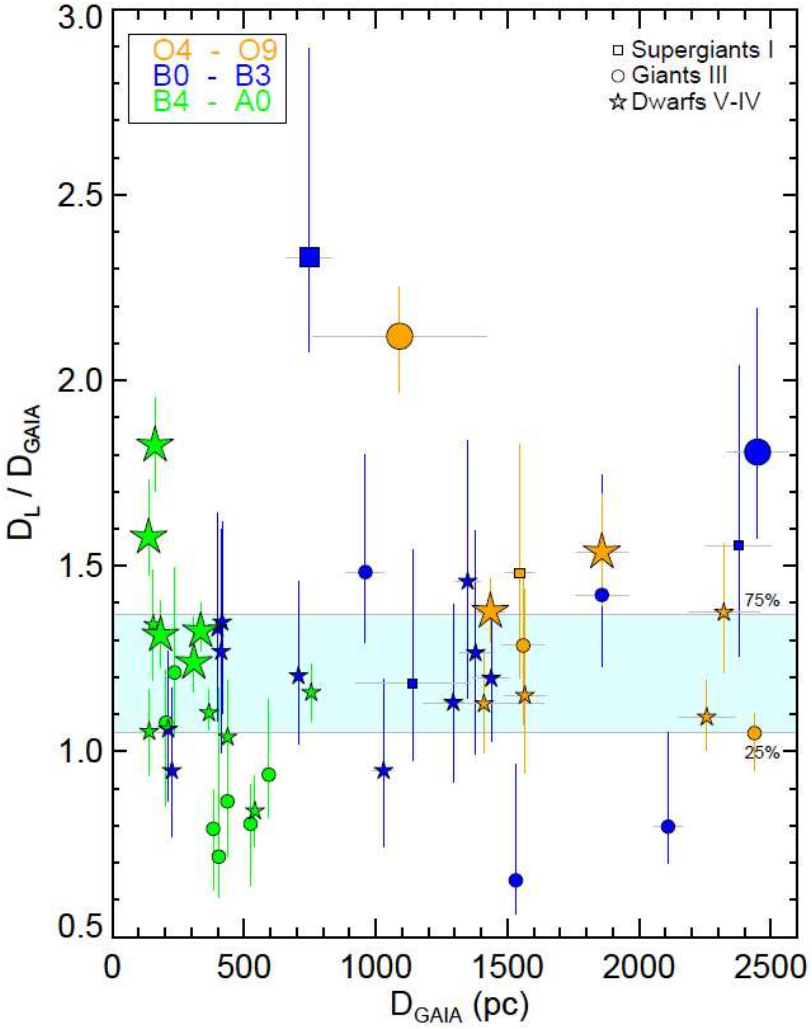

Figure 6.3: The distance discrepancy. The distance ratios D_L/D_{GAIA} vs D_{GAIA} for the sample of 47 stars with the most accurate reddening curves. The distance ratios range between 0.65 and 2.33 and a 1σ scatter of 0.33 at a median of 1.2. The area between the bottom and top quartiles at 1.05 and 1.35 is shown in cyan and underlines the overprediction in D_L. The error bars in D_L primarily arise from systematic uncertainties in the M_V determination. Different symbols and colours are used to visually represent the various spectral types and luminosity classes as labelled. Stars with a deviation in the distance ratios from unity that are below 3σ are shown by small and the other 10 stars with confidence above 3σ by large symbols, respectively. There are no stars with a distance ratio below $D_L/D_{GAIA} < 1.2$ detected at high 3σ confidence. Figure from [SC23], pag.4.

of translucent clouds at $1 < \tau_V \lesssim 2.2$ and single-cloud sightlines of the diffuse ISM at $\tau_V \lesssim 1$; fig. 6.4 shows the results.

The average curve of the translucent clouds in the sample has a peak-to-peak scatter, mean, and 1σ error of $2.7 \lesssim R_V = 3.3 \pm 0.4 \lesssim 4.1$ at a median of $R_V = 3.16$; that of the single-cloud diffuse ISM sightlines has $2.3 \lesssim R_V = 3.0 \pm 0.3 \lesssim 3.6$ at a median of $R_V = 3.1$, respectively. Driven *de facto* by the same R_V, a nearly perfect match from optical to longer wavelengths is found; noticeable is the large diversity of the reddening curves and agreement of the various mean

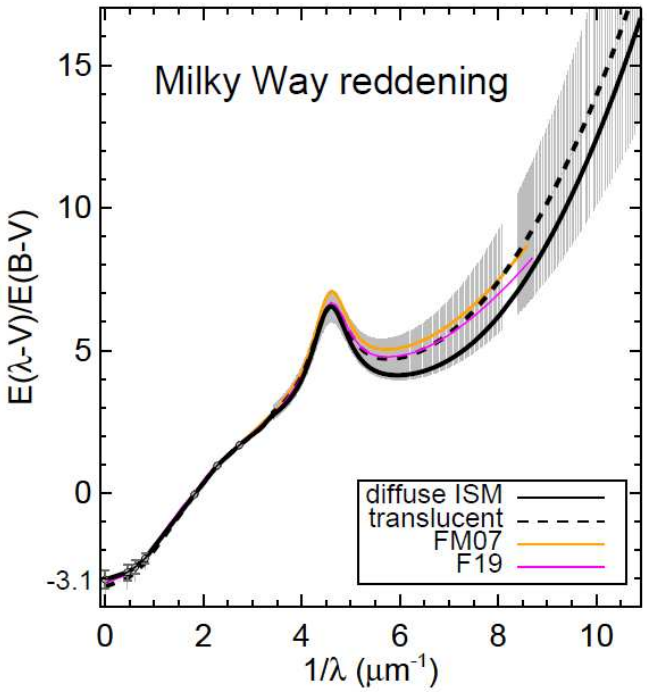

Figure 6.4: The Milky Way reddening derived from the high-quality sample for translucent clouds (see table 4 of [Sie+23]) -dashed with 1σ error bars- and for single-cloud sightlines of the diffuse ISM. The average Galactic reddening derived by Fitzpatrick & Massa (2007, [FM07]) and Fitzpatrick *et al.* (2019, [Fit+19]) are shown for comparison. Figure from [Sie+23], pag.12.

Milky Way reddening curves within $\sigma(R_V) = 0.4$.

Similarly, it is possible to compute a survey for the diffuse ISM; taking advantage of the dark dust model (see table 1 in [Sie23]), the observational results are displayed in fig. 6.5. As for the Milky Way, here $R_V = 3.1$ is adopted. In the diagram, the reddening curve of the star HD 046202 is shown (it is a very well-known comparative star): the behaviour of this reddened object perfectly matches the mean curve derived from IUE. Reddening in spectral regions close to wind lines at 6.5 and 7.1 μm^{-1} and Ly-α at 8 μm$^{-1} \leq$ x $\leq$ 8.45 μm^{-1}, or with apparent instrumental noise at x $\lesssim$ 3.6 μm^{-1} shall be ignored. Overall a typical error in the derived reddening is $\sim$ 10%.

The key role of the dust grain population, in particular of the 'new' dark dust component, in reddening and interstellar extinction can be emphasized through the diffuse emission spectrum of the ISM. Fig. 6.6 displays this spectrum. The dust emission of the diffuse ISM is not uniform across the sky and there is evidence that the properties of the dust as well as the spectral distribution and strength of the interstellar radiation field that heats the dust vary. Observations of this component for high galactic latitude ($|b| \gtrsim 25°$) from the Cosmic Background Explorer data are given by the Planck Collaboration (2015, [Col+15]).
A colour-corrected composite spectrum with error estimates is tabulated.

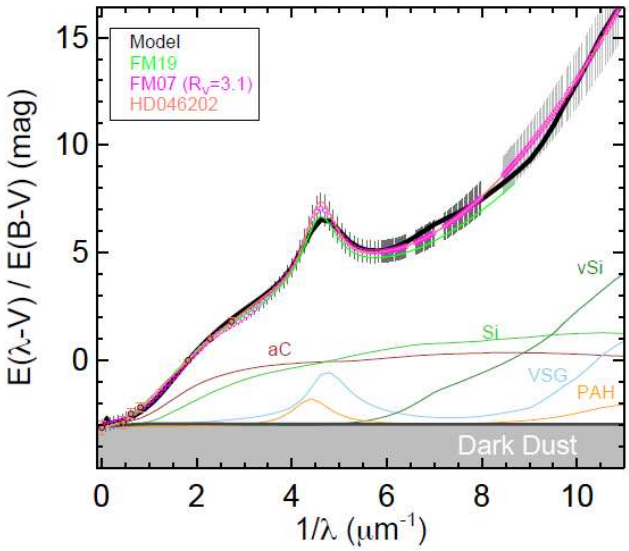

Figure 6.5: Extinction of the diffuse ISM according to some previous works in literature (e.g. [FM07], [Fit+19]). Model (black) with $r^{+}_{Dark} = 1\,\mu$m and individual dust components as labelled. The area in grey shows the contribution of dark dust. Figure from [Sie23], pag.4.

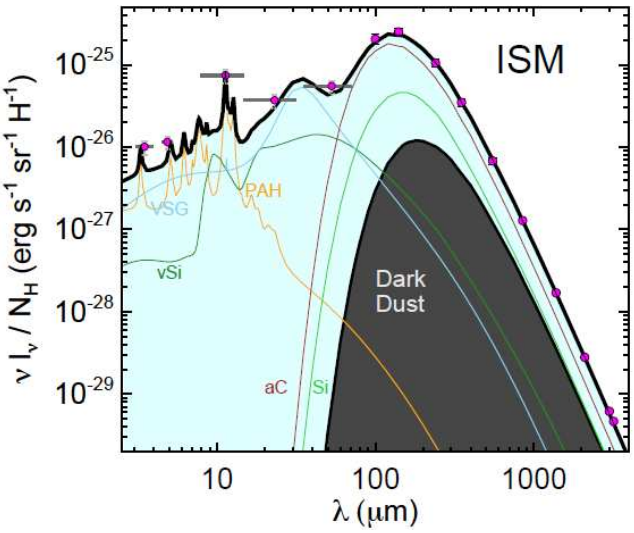

Figure 6.6: Dust emission of the diffuse ISM observed at high galactic latitudes and normalised per H atom ([Col+15]). Model (black) with $r^{+}_{Dark} = 1\,\mu$m and individual dust components as labelled. The area in grey shows the contribution of dark dust. Figure from [Sie23], pag.5.

Bibliography

[Her85] William Herschel. "XII. On the construction of the heavens". In: *Philosophical Transactions of the Royal Society of London* 75 (1785), pp. 213–266.

[Kap09] Jacob Cornelis Kapteyn. "On the absorption of light in space". In: *Astrophysical Journal, vol. 29, p. 46* 29 (1909), p. 46.

[Tru30] Robert J Trumpler. "Absorption of light in the galactic system". In: *Publications of the Astronomical Society of the Pacific* 42.248 (1930), pp. 214–227.

[Mer34] Paul W Merrill. "Unidentified interstellar lines". In: *Publications of the Astronomical Society of the Pacific, Vol. 46, No. 272, p. 206-207* 46 (1934), pp. 206–207.

[BM37] W Baade and R Minkowski. "Spectrophotometric Investigations of Some o-and B-Type Stars Connected with the Orion Nebula". In: *Astrophysical Journal, vol. 86, p. 123* 86 (1937), p. 123.

[Whi58] AE Whitford. "The law of interstellar reddening." In: *Astronomical Journal, Vol. 63, p. 201-207 (1958)* 63 (1958), pp. 201–207.

[Nan64] K Nandy. "Observations of interstellar reddening I. Results for Region in Cygnus". In: *Publications of the Royal Observatory, Edinburgh; v. 3, no. 6, Edinburgh: HMSO, 1964., p. 142-180: ill.; 31 cm.* 3 (1964), pp. 142–180.

[Sav75] Blair D Savage. "Ultraviolet photometry from the Orbiting Astronomical Observatory. XX-The ultraviolet extinction bump". In: *Astrophysical Journal, vol. 199, July 1, 1975, pt. 1, p. 92-109.* 199 (1975), pp. 92–109.

[Sak+77] A Sakata et al. "Spectroscopic evidence for interstellar grain clumps in meteoritic inclusions". In: *Nature* 266.5599 (1977), pp. 241–241.

[Spi78] L Spitzer Jr. *1978, Physical Processes in the Interstellar Medium.* 1978.

[SM79] Blair D Savage and John S Mathis. "Observed properties of interstellar dust". In: *Annual review of astronomy and astrophysics* 17.1 (1979), pp. 73–111.

[Sea79] MJ Seaton. "Interstellar extinction in the UV". In: *Monthly Notices of the Royal Astronomical Society* 187.1 (1979), 73P–76P.

[HH81] Hendrik Christoffel Hulst and Hendrik C van de Hulst. *Light scattering by small particles.* Courier Corporation, 1981.

[Zim82] H Zimmermann. "The interstellar band at λ 4430 Å and the abundance of interstellar iron, titanium, and molecular hydrogen". In: *Astrophysics and Space Science* 84 (1982), pp. 505–517.

[BH83] Craig F. Bohren and Donald R. Huffman. *Absorption and scattering of light by small particles*. 1983.

[Sak+83] Akira Sakata et al. "Does a 2,200 Å hump observed in an artificial carbonaceous composite account for UV interstellar extinction?" In: *Nature* 301.5900 (1983), pp. 493–494.

[Pre+84] ML Prevot et al. "The typical interstellar extinction in the Small Magellanic Cloud". In: *Astronomy and Astrophysics (ISSN 0004-6361), vol. 132, no. 2, March 1984, p. 389-392.* 132 (1984), pp. 389–392.

[FM86] Edward L Fitzpatrick and Derck Massa. "An analysis on the shapes of ultraviolet extinction curves. I-The 2175 A bump". In: *Astrophysical Journal, Part 1 (ISSN 0004-637X), vol. 307, Aug. 1, 1986, p. 286-294.* 307 (1986), pp. 286–294.

[FM88] Edward L Fitzpatrick and Derck Massa. "An analysis of the shapes of ultraviolet extinction curves. II-The far-UV extinction". In: *Astrophysical Journal, Part 1 (ISSN 0004-637X), vol. 328, May 15, 1988, p. 734-746.* 328 (1988), pp. 734–746.

[Whi88] DCB Whittet. *Dust in the Universe, ed. Bailey, ME & Williams, DA*. 1988.

[CCM89] Jason A Cardelli, Geoffrey C Clayton, and John S Mathis. "The relationship between infrared, optical, and ultraviolet extinction". In: *Astrophysical Journal, Part 1 (ISSN 0004-637X), vol. 345, Oct. 1, 1989, p. 245-256.* 345 (1989), pp. 245–256.

[FM90] Edward L Fitzpatrick and Derck Massa. "An analysis of the shapes of ultraviolet extinction curves. III-an atlas of ultraviolet extinction curves". In: *Astrophysical Journal Supplement Series (ISSN 0067-0049), vol. 72, Jan. 1990, p. 163-189.* 72 (1990), pp. 163–189.

[MW90] PG Martin and DCB Whittet. "Interstellar extinction and polarization in the infrared". In: *Astrophysical Journal, Part 1 (ISSN 0004-637X), vol. 357, July 1, 1990, p. 113-124. Research supported by NSERC and SERC.* 357 (1990), pp. 113–124.

[Ful+93] J Fulara et al. "Laboratory evidence for highly unsaturated hydrocarbons as carriers of some of the diffuse interstellar bands". In: *Nature* 366.6454 (1993), pp. 439–441.

[ODo94] James E O'Donnell. "Rnu-dependent optical and near-ultraviolet extinction". In: *Astrophysical Journal, Part 1 (ISSN 0004-637X), vol. 422, no. 1, p. 158-163* 422 (1994), pp. 158–163.

[SW95] Theodore P Snow and Adolf N Witt. "The interstellar carbon budget and the role of carbon in dust and large molecules". In: *Science* 270.5241 (1995), pp. 1455–1460.

[GCW97] Karl D Gordon, Daniela Calzetti, and Adolf N Witt. "Dust in starburst galaxies". In: *The Astrophysical Journal* 487.2 (1997), p. 625.

[SFD98] David J Schlegel, Douglas P Finkbeiner, and Marc Davis. "Maps of dust infrared emission for use in estimation of reddening and cosmic microwave background radiation foregrounds". In: *The Astrophysical Journal* 500.2 (1998), p. 525.

[Fit99] Edward L Fitzpatrick. "Correcting for the effects of interstellar extinction". In: *Publications of the Astronomical Society of the Pacific* 111.755 (1999), p. 63.

[Tua+00] Seathrún Ó Tuairisg et al. "A deep echelle survey and new analysis of diffuse interstellar bands". In: *Astronomy and Astrophysics Supplement Series* 142.2 (2000), pp. 225–238.

[Zag00] Frédéric Zagury. "The UV spectrum of nebulae". In: *New Astronomy* 5.4 (2000), pp. 211–222.

[Zag01] Frédéric Zagury. "The spectrum of HD46223". In: *New Astronomy* 6.7 (2001), pp. 403–413.

[SG06] Peter P Sorokin and James H Glownia. "Two-Photon Absorption by Hydrogen Molecules: Origin of the 2175 Angstrom Astronomical Band?" In: *arXiv preprint astro-ph/0608092* (2006).

[FM07] EL Fitzpatrick and D Massa. "An analysis of the shapes of interstellar extinction curves. V. The IR-through-UV curve morphology". In: *The Astrophysical Journal* 663.1 (2007), p. 320.

[Goo08] Ariel Goobar. "Low RV from circumstellar dust around supernovae". In: *The Astrophysical Journal* 686.2 (2008), p. L103.

[Dra10] Bruce T Draine. *Physics of the interstellar and intergalactic medium*. Vol. 19. Princeton University Press, 2010.

[Fri+10] Scott D Friedman et al. "Studies of diffuse interstellar bands V. Pairwise correlations of eight strong DIBs and neutral hydrogen, molecular hydrogen, and color excess". In: *The Astrophysical Journal* 727.1 (2010), p. 33.

[Tur12] David G Turner. "WR 38/38a and the ratio of total-to-selective extinction in Carina". In: *Astrophysics and Space Science* 337 (2012), pp. 303–312.

[Zag12] Frederic Zagury. "The extinction curve in the visible and the value of RV". In: *Astronomische Nachrichten* 333.2 (2012), pp. 160–165.

[Zag13] F Zagury. "The 2200 Å bump and the interstellar extinction curve". In: *Astronomische Nachrichten* 334.10 (2013), pp. 1107–1114.

[Abe+14] Ade Abergel et al. "Planck 2013 results. XI. All-sky model of thermal dust emission". In: *Astronomy & Astrophysics* 571 (2014), A11.

[Sch+14] EF Schlafly et al. "A Map of Dust Reddening to 4.5 kpc from Pan-STARRS1". In: *The Astrophysical Journal* 789.1 (2014), p. 15.

[TMB14] David G Turner, Daniel J Majaess, and David D Balam. "Testing new ideas regarding the nature of interstellar extinction". In: *Canadian Journal of Physics* 92.12 (2014), pp. 1696–1702.

[Col+15] Planck Collaboration et al. "Planck 2015 results. XXVI. The Second Planck Catalogue of Compact Sources". In: (2015).

[Gre+15] Gregory M Green et al. "A three-dimensional map of Milky Way dust". In: *The Astrophysical Journal* 810.1 (2015), p. 25.

[Sch+17] EF Schlafly et al. "Mapping the extinction curve in 3D: structure on kiloparsec scales". In: *The Astrophysical Journal* 838.1 (2017), p. 36.

[Zag17] Frederic Zagury. "On the relationship between the continuum of interstellar extinction curves, the 2200 Å bump, and the diffuse interstellar bands". In: *Astronomische Nachrichten* 338.7 (2017), pp. 807–822.

[Whi18] Doug CB Whittet. *Dust in the galactic environment*. CRC press, 2018.

[Fit+19] Edward L Fitzpatrick et al. "An analysis of the shapes of interstellar extinction curves. VII. Milky Way spectrophotometric optical-through-ultraviolet extinction and its R-dependence". In: *The Astrophysical Journal* 886.2 (2019), p. 108.

[Car+21] Giovanni Carraro et al. *Astrophysics of the interstellar medium*. Springer, 2021.

[Sie+23] R Siebenmorgen et al. "Dark dust-III. The high-quality single-cloud reddening curve sample: Scrutinizing extinction curves in the Milky Way". In: *Astronomy & Astrophysics* 676 (2023), A132.

[Sie23] Ralf Siebenmorgen. "Dark dust-II. Properties in the general field of the diffuse ISM". In: *Astronomy & Astrophysics* 670 (2023), A115.

[SC23] Ralf Siebenmorgen and Rolf Chini. "The Distance to the Stars". In: *arXiv preprint arXiv:2311.03310* (2023).

Acknowledgements

I would like to thank my supervisor for allowing me to focus on this project, as well as his availability concerning any questions, issues along the path of writing the present work or suggestions about managing this type of matter.

I would like to thank my external supervisor, Dr./Prof. Sergio Ortolani, with whom I already had the opportunity to work on my bachelor thesis project. His contribution during the final (and therefore critical) stages has been very helpful.

I would like to thank Dr. Zagury for the help, the suggestions and -above all- the availability he showed me during our personal e-mail correspondence about his alternative theory on interstellar extinction nature.

I would like to thank my family, i.e. my parents and my brother, for allowing me to reach this achievement through their support and emotional closeness.

I would like to thank every person who, in various ways, has been part of my journey for better or for worse: I have grown up and I have become mature despite them or alongside them.